**DEAFFERENTATION-INDUCED NEUROPLASTICITY IN CHICK AUDITORY NEURONS: A MATTER OF LIFE OR DEATH**

BY

Hope Elizabeth Karnes
B.S. Biomedical Engineering, Washington University in St. Louis, 2004

Submitted to the Graduate Degree Program in the Department of Anatomy and Cell Biology and the Graduate Faculty of the University of Kansas Medical Center in partial fulfillment of the requirements for the degree of Doctor of Philosophy

Dianne Durham, Ph.D.; Committee Chairperson

Thomas Imig, Ph.D.; Committee Member

Hiroshi Nishimune, Ph.D.; Committee Member

John Robertson, Ph.D.; Committee Member

Hinrich Staecker, M.D., Ph.D.; Committee Member

Doug Wright, Ph.D.; Committee Member

Date of Dissertation Defense: June 2, 2009

The Dissertation Committee for Hope Elizabeth Karnes certifies that this is the approved version of the following dissertation:

**DEAFFERENTATION-INDUCED NEUROPLASTICITY IN CHICK AUDITORY NEURONS: A MATTER OF LIFE OR DEATH**

Committee:

Dianne Durham, Ph.D.; Committee Chairperson

Thomas Imig, Ph.D.; Committee Member

Hiroshi Nishimune, Ph.D.; Committee Member

John Robertson, Ph.D.; Committee Member

Hinrich Staecker, M.D., Ph.D.; Committee Member

Doug Wright, Ph.D.; Committee Member

Date approved: _____

**Abstract**

Forty percent of elderly Americans suffer from hearing loss. Hearing loss is a significant public health concern, associated with social withdrawal, communication delays, and reduced comprehension, that is growing in magnitude as the population ages. It is a frustrating disorder, which is expensive and difficult to treat. Hearing loss occurs as a consequence of damage to inner ear or central nervous system (CNS) structures. Current technologies to restore hearing, like hearing aids and cochlear implants, have broadened the therapeutic options to treat this disorder, but these therapies solely target inner ear structures. The CNS component is equally as important in preserving auditory function, but little is known about the process of auditory neuronal damage and recovery. In this series of studies, the avian auditory system is used as a model in which to evaluate the CNS response to disruptions in auditory signaling.

Neurons in the chick cochlear nucleus, nucleus magnocellularis (NM), receive excitatory input exclusively from the ipsilateral cochlea. Cochlea removal permanently abolishes this input, and NM neurons undergo rapid morphologic and functional changes, including calcium dysregulation, mitochondrial and ribosomal compromise, and oxidative metabolic stress. Ultimately, a subset (30-50%) of deafferented NM neurons dies. To better characterize the cellular factors that influence whether a deafferented NM neuron dies or survives, auditory brainstems from unilaterally deafened

hatchling chicks were examined using a variety of immunocytochemical, histochemical, and molecular approaches.

Compared to contralateral NM neurons with intact afferent support, NM neurons ipsilateral to cochlea removal undergo activation of apoptotic mediators, functional impairment of mitochondrial inner membrane constituents, and alterations in the expression levels of certain genes. Specific differences in mitochondrial nucleic acid integrity and ATP coupling state, as well as in the expression of genes related to calcium signaling, glutamate receptor signaling, GABA receptor signaling, and phospholipid degradation, distinguish deafferented NM neurons that die from deafferented NM neurons that will survive. These results suggest that molecular signaling pathways involving mitochondrial function and calcium regulation play pivotal roles in cell fate determination of chick brainstem auditory neurons following peripheral deafferentation (i.e. deafness).

## DEDICATION

To my parents Bob and Mary Beth Karnes, for their many years of love, support, and encouragement to “use my head” and follow my heart

and

To my husband Will, for his support, reassurance, and commitment to me, and for his patience with my many early morning and late night trips to the lab

## ACKNOWLEDGEMENTS

I would like to thank my research adviser, Dianne Durham, PhD, for her support throughout my graduate studies. The knowledge and skills acquired under her tutelage will undoubtedly shape my career as a researcher.

I also thank Hinrich Staecker, MD, PhD, for his expertise, ingenuity, and insight in helping me plan and carry out my experiments, and for his support and patience when I encountered glitches in data acquisition and analysis.

Special thanks go out to all of those with whom I worked in the Auditory and Vestibular Neuroscience Laboratory, including: Susanna Pfannenstiel, MD, Peter Gochee, MD, PhD, Christina Schlecker, MD, Matt Rendel, MD, Shannon Kraft, MD, Kate Swisher, MD, Jennifer Brantley, Jennifer Thompson, Pete Scaletty, and John Tanksley. I am especially indebted to Peter Gochee, MD, PhD, whose advice and insight have contributed immeasurably to my professional development. I am, likewise, thankful to Christina Kaiser, PhD, for her advice and support throughout my graduate studies.

I owe debts of gratitude to all those individuals who offered me their technical expertise and insight; the success of many of my experiments is directly

related to their generous contributions of knowledge. Special thanks go out to Don Warn, PhD, for his assistance and patience with laser capture microdissection, as well as for his help with histochemical data imaging, collection, and analysis. I am indebted to Clark Bloomer, Yafen Niu, and the other members of the KUMC Microarray Core Facility for their assistance with RNA handling and microarray GeneChip analyses. I thank Stan Svojanovsky, PhD, and Sumedha Gunewardena, PhD, of the KUMC Bioinformatics Core, for their expertise in microarray statistical analyses. I owe many thanks to Lane Christenson, PhD, as well as to two members of his laboratory: Lacey Luense and Martha Carletti, for their assistance with quantitative RT-PCR protocols and data analysis. Their patience, support, and dedication to my work will not be forgotten. I also thank Peter Smith, PhD, for use of his light microscope, and Russell Swerdlow, MD, for many discussions about mitochondrial analyses. I thank Jing Huang, PhD, Phil Shafer, and Eric Grimes for their technical assistance with many tasks throughout my graduate studies, and for their kind and friendly spirits.

I would like to thank Doug Girod, MD, Mike Edwards, Kaelen Van Cura, and the other members of the ENT Department for their administrative, professional, and personal support. It was an honor to work in their company.

I would also like to thank George Vielhauer, PharmD, PhD, and Mercedes Amado, MD, for their kind and generous support during my graduate studies. I was lucky to have been mentored by such gifted individuals. I will emulate their ways in my future career.

Thank you to the members of my dissertation committee: Dianne Durham, PhD, Tom Imig, PhD, Hiroshi Nishimune, PhD, John Robertson, PhD, Hinrich Staecker, MD, PhD, and Doug Wright, PhD. I appreciate the advice, support, patience, and critical feedback provided throughout the course of my graduate studies.

I would like to thank the MD/PhD Program, as well as the members of the Executive Board, for allowing me the opportunity to pursue my simultaneous interests in clinical medicine and basic science research. In particular, I would like to thank Joseph Bast, PhD, for his commitment to students. He is a role model, an advocate, an invaluable resource, and best of all, a good friend. His advice, support, and encouragement throughout the years kept my studies and my spirits in line. Thank you, Dr. Bast, for everything.

I would also like to thank the members of the Kansas Intellectual and Developmental Disabilities Research Center (KIDDRC), who were instrumental in the administration and maintenance of our laboratory core

equipment and resources: Beth Van Luchene, MHSA, Tina Darrow, and Doug Brownyard.

I owe many thanks to my friends and colleagues here at KUMC, with whom I consider myself lucky to have worked: Karra Muller, PhD, Elizabeth Taglauer, PhD, Melinda Arnett, PhD, Megan Johnson, PhD, Janelle Ryals, Susan Smittkamp, PhD, Sarah Tague, Megan Dunn, and Eva Selfridge.

I cannot express enough gratitude towards my family. My parents, Bob and Mary Beth Karnes, have endured many cycles of excitement, frustration, and exhaustion during my 21 years of schooling, yet their support and encouragement remains constant. Likewise, my husband, Will, has provided a stable and encouraging source of support throughout my graduate studies. I love you and appreciate your commitment to me.

## Table of Contents

## Table of Contents (cont'd)

## Table of Contents (cont'd)

## LIST OF FIGURES

**Figure** **Page**

**Chapter I**

**Chapter II**

**Chapter III**

**Chapter IV**

## LIST OF TABLES

**Table** **Page**

**Chapter IV**

## LIST OF ABBREVIATIONS

| | |
|---|---|
| $\Delta\Psi_m$ | Mitochondrial membrane potential |
| AAA | ATPase associated to various cellular activities |
| AMPA | α-amino-3-hydroxy-5-methyl-4-isoxazolepropionic acid |
| ANOVA | Analysis of variance |
| Apaf-1 | Apoptotic protease activating factor 1 |
| ATP | Adenosine Triphosphate |
| ATPase | ATP synthase |
| AVCN | Anteroventral cochlear nucleus |
| BDNF | Brain-derived Neurotrophic Factor |
| CAMK | Calcium/calmodulin-dependent protein kinase |
| CASP | Caspase |
| CASQ2 | Calsequestrin 2 |
| CMXRos | Chloromethyl-X-rosamine |
| CNS | Central nervous system |
| CO | Cytochrome oxidase |
| cRNA | Complementary ribonucleic acid |
| DAB | 3,3'-diaminobenzidine tetrahydrochloride |
| DMSO | Dimethyl sulfoxide |
| DNA | Deoxyribonucleic acid |
| DPX | Dibutyl phthalate xylene |

| | |
|---|---|
| EDTA | Ethylenediaminetetraacetic acid |
| ER | Endoplasmic reticulum |
| ETC | Electron transport chain |
| FC | Fold change |
| GABA | γ-aminobutyric acid |
| GCOS | Gene Chip Operating Software |
| GRID1 | Glutamate receptor delta 1 |
| GRIK1 | Glutamate receptor 5 kainate receptor |
| IACUC | Institutional Animal Care and Use Committee |
| IPA | Ingenuity Pathways Analysis |
| IP3R | Inositol triphosphate receptor |
| IR | Infrared |
| IVT | *In vitro* transcription |
| KIDDRC | Kansas Intellectual and Developmental Disabilities Research Center |
| LCM | Laser Capture Microdissection |
| MM | Mismatch |
| mRNA | Messenger Ribonucleic Acid |
| NIDCD | National Institute on Deafness and Other Communication Disorders |
| NIH | National Institutes of Health |
| NM | Nucleus magnocellularis |

| | |
|---|---|
| NMDA | *N*-methyl-D-aspartate |
| NetAffx | Affymetrix website |
| NOS | Nitric oxide synthase |
| NSF | *N*-ethylmaleimide-sensitive factor |
| $O_2$ | molecular oxygen |
| OD | Optical density |
| PARP | poly (ADP-ribose) polymerase |
| PBS | Phosphate buffered saline |
| PCR | Polymerase Chain Reaction |
| PI | Propidium Iodide |
| PLSD | Protected least significant difference |
| PM | Perfect match |
| PMCA | Plasma membrane calcium ATPase |
| PTEN | Phosphatase and Tensin homologue |
| RIN | RNA Integrity Number |
| RMA | Robust multi-array Analysis |
| RNA | Ribonucleic Acid |
| ROS | Reactive oxygen species |
| RT-PCR | Reverse Transcriptase Polymerase Chain Reaction |
| SDH | Succinate dehydrogenase |
| SSC | Sodium chloride, sodium citrate |
| TBS | Tris Buffered Saline |

| | |
|---|---|
| TCA | Tricarboxylic Acid |
| TM | Tympanic membrane |
| TrkA | Tropomyosin-related Kinase A |
| TTX | Tetrodotoxin |
| TUNEL | Terminal deoxynucleotidyl transferase-mediated dUTP Nick-End Labeling |
| UV | Ultraviolet |

# CHAPTER I

# INTRODUCTION

## The auditory system

Human experience is enriched by specialized sensory systems, which make unique contributions towards one's perception of his/her surroundings. The auditory system, composed of peripheral organs of hearing (external, middle, and inner ear structures) and central nervous system (CNS) pathways, is intricately refined to detect and translate mechanical vibrations in the environment into sound cues meaningful to the brain (see Figure 1). The cochlea, housed peripherally within the temporal bone of humans, contains the primary sensory receptors of the auditory system (Bess and Humes, 2003) (Figure 1A, B). Each human cochlea contains approximately 16,000 sensory hair cells (Kandel et al., 2000). These hair cells are arranged topographically by frequency, such that mechanical air current oscillations ranging from 20-20,000Hz may be discriminated and transmitted to the brain as precise electrical inputs (Squire et al., 2003). Brainstem neurons are also arranged tonotopically to process frequency-specific inputs and transmit sound intensity and localization parameters to higher-order auditory centers (Squire et al., 2003) (Figure 1C). Higher-order auditory neurons integrate complex sound cues from brainstem nuclei on both sides of the brain, and

from them, derive meaning and significance (i.e. interpret language) (Kandel et al., 2000).

Hair cells within each cochlea are innervated by peripheral processes of spiral ganglion neurons, whose central processes form the eighth nerve and carry afferent information to brainstem auditory neurons (Squire et al., 2003) (Figure 1, C). Continuity of this system is essential for normal hearing. Hearing loss may occur from damage to cochlear hair cells (due to noise exposure, ototoxic drugs, or genetic predisposition) or from degeneration of eighth nerve afferent fibers (sensorineural hearing loss) (Bess and Humes, 2003). In 2008, the National Institute on Deafness and Other Communication Disorders (NIDCD) estimated hearing loss to affect more than 36 million Americans. It is a significant public health concern that is growing in magnitude as the population ages (Boyle et al., 1994, Crews and Campbell, 2004, Someya et al., 2006).

Hearing loss is a debilitating disorder associated with social withdrawal, communication delays, and reduced comprehension (Bess and Humes, 2003). Our current methods to restore hearing, like hearing aids and cochlear implants, target solely the peripheral, cochlear structures of the auditory system. However, successful restoration of hearing requires that both cochlear *and* CNS components remain functionally intact. Therefore, an understanding of the CNS response to cochlear damage is essential to

advance the therapeutic options to treat hearing loss and to ameliorate the symptom severity associated with this widespread public health concern.

**The avian auditory system as a model for hearing loss**

The avian auditory system is an exceptional model in which to study the CNS response to hearing loss (Rubel and Parks, 1988). Interestingly, the chick auditory system, unlike its mammalian counterpart, has the unique ability to regenerate cochlear hair cells and stimulate structural and functional recovery of brainstem auditory neurons following exposure to damaging stimuli (Cotanche, 1987, Cruz et al., 1987, Corwin and Cotanche, 1988, Ryals and Rubel, 1988).

The chick cochlea (basilar papilla) is a flat, curvelinear membrane with an epithelial layer of sensory hair cells arranged tonotopically from base to apex (Ryals and Rubel, 1982). Avian cochlear hair cells are innervated by peripheral processes of cochlear ganglion neurons, whose central processes send afferent projections with the eighth nerve to a homogeneous population of brainstem auditory neurons within nucleus magnocellularis (n. magnocelluaris, NM). High-frequency hair cells at the base of the chick cochlea send afferent projections to NM neurons within the rostro-medial region of the nucleus, whereas low-frequency hair cells located at the apical end of the cochlea send afferents to the caudo-lateral region of NM (Lippe and Rubel, 1985) (see Figure 2). Since the frequency axis is maintained

between cochlear hair cells and NM neurons, disruption of the cochlea at specific sites along its length produces corresponding, tonotopic alterations in function in NM. Noise damage, ototoxic drugs, and complete cochlea removal interrupt afferent signals to the brainstem in pathologically distinct manners. Noise damage injures cochlear hair cells in a frequency-dependent fashion and destroys cochlear support structures and the tectorial membrane (Cotanche, 1987, Girod et al., 1989, Saunders et al., 1992, Ryals et al., 1995, Durham et al., 2000). Ototoxic drugs like gentamicin injure hair cells in a basal to apical progression with increasing exposure to the drug or increasing dose (Girod et al., 1991, Hashino et al., 1991, Janas et al., 1995, Girod et al., 2000). The tectorial membrane remains intact (Epstein and Cotanche, 1995), and support structures in the cochlea are mildly or undamaged. Cochlea removal permanently abolishes afferent input to NM by disrupting peripheral processes of cochlear ganglion cells, without compromising cell body integrity (Born et al., 1991). Cochlea removal, unlike noise and gentamicin administration, creates a permanent severance between cochlea and brainstem structures (Rubel et al., 1990), effectively eliminating avian hair cell regenerative potential and any spontaneous auditory recovery. It is, therefore, the method of choice used to model human CNS responses to unilateral sensorineural hearing loss.

**Deafferentation-induced neuroplasticity**

Interruption of afferent projections from the periphery produces drastic changes within corresponding regions of the CNS (Linden, 1994, Rubel and Fritzsch, 2002, Syka, 2002). In the chick auditory system, the homogeneous population of second-order auditory neurons within brainstem NM receives excitatory input exclusively from ipsilateral cochlear ganglion neurons (Rubel et al., 1990). Cochlea removal permanently deprives NM neurons of afferent input (Parks and Rubel, 1978) and triggers a series of changes across the ipsilateral auditory nucleus, which ultimately produces death in 30-50% of deafferented neurons (Born et al., 1991).

Within minutes of cochlea removal, all deafferented NM neurons undergo cessation of electrical activity (Born et al., 1991), reduced glucose utilization (Heil and Scheich, 1986), and diminished blood flow (Richardson and Durham, 1990). Within hours, protein synthesis declines (Steward and Rubel, 1985, Kelley et al., 1997, Lu et al., 2004), and intraneuronal calcium levels rise across the nucleus (Lachica et al., 1995, Zirpel and Rubel, 1996).

As early as 6 hours following cochlea removal, two populations of neurons emerge within deafferented NM: approximately 70% of deafferented neurons nearly recover their ability to synthesize proteins, while approximately 30% of cells remains largely deficient in protein production (Steward and Rubel, 1985). This protein-deficient subpopulation of neurons soon shows signs of ribosomal disassembly (Rubel et al., 1991), mitochondrial vacuolization (Hyde

and Durham, 1994), oxidative metabolic stress (Durham and Rubel, 1985, Hyde and Durham, 1990, Durham et al., 1993), calcium dysregulation (Zirpel and Rubel, 1996), and activation of the apoptotic caspase cascade (Wilkinson et al., 2003, Karnes et al., 2009), and eventually dies. Two to 5 days following deafferentation, NM neurons destined to die show signs of more permanent, irreversible damage, including depletion of oxidative enzymes (Born and Rubel, 1985, Durham and Rubel, 1985, Hyde and Durham, 1990).

The molecular determinants that influence whether an NM neuron will die or survive following deafferentation are not well defined. However, the seemingly cell-specific pattern of compromise and subsequent death in 30% of deafferented neurons strongly suggests activation of an apoptotic or apoptotic-like cell-suicide cascade (Wilkinson et al., 2002, Wilkinson et al., 2003, Karnes et al., 2009).

**Neuronal survival and the apoptotic pathway**

Selective death of CNS neurons occurs under a variety of circumstances. Normal developmental pruning of neural circuits and matching of target populations with neuronal number are highly regulated processes that require activation of physiologic apoptotic cascades (Oppenheim, 1991, Johnson et al., 1996). This form of programmed cell death engages active cellular processes, including neurotrophic factor targeting of cells destined to survive (Truman, 1984, Johnson et al., 1989,

Yuan and Horvitz, 1990, Raff et al., 1993, Fuentes-Prior and Salvesen, 2004). Pathologic apoptotic cascades are triggered independent of development by traumatic or injurious stimuli, and the evoked response is mediated by pro-apoptotic, death-promoting factors (Sun et al., 1999). In contrast to necrotic cell death, which is generally a widespread, uncontrolled process, apoptotic cell death is a highly regulated, energy-dependent cell disassembly process (Denecker et al., 2001).

In the auditory system, apoptotic indicators have been identified within damaged cochlear structures (Hu et al., 2000, Wilkins et al., 2001, Hu et al., 2002, Mangiardi et al., 2004, Kaiser et al., 2008), as well as within mammalian auditory (anteroventral cochlear nucleus, AVCN) neurons during development (Harris et al., 2005). Preliminary examination of chick NM after cochlea removal suggests that apoptotic mechanisms underlie the cell-specific degradation of 30% of neurons; however, molecular details remain ambiguous.

Typically, detection of apoptotic markers is limited to cells that will die. In the intrinsic, mitochondrial-mediated apoptosis scheme (see Figure 3), leakage of cytochrome *c* from mitochondria is the first sign of cellular distress (Kluck et al., 1997, Denecker et al., 2001). As cytochrome *c* accumulates in the cytoplasm, it binds the cytoplasmic protein, apoptotic protease activating factor-1 (Apaf-1), and the protein complex activates caspase-9 (Slee et al., 1999, Jiang and Wang, 2000, Bratton et al., 2001). Caspase-9 is an initiator

caspase, which activates downstream effector caspases, including caspase-3 (Bratton et al., 2000, Bratton et al., 2001). Caspase-3 has a myriad of cellular substrates and activates the cellular endonuclease responsible for migrating to the nucleus and degrading genomic DNA (Liu et al., 1997, Enari et al., 1998, Liu et al., 1999). A late step in apoptosis, DNA degradation is an imminent sign of cell death.

In deafferented NM, cytochrome *c* and active caspase-9 have been observed as early as 6 and 3 hours, respectively, following cochlea removal (Wilkinson et al., 2003), clearly implicating apoptosis in the mechanism of cell death. However, caspase-9 was detected pan-neuronally in both dying and surviving neurons, and cytochrome *c* was not definitively traceable as having been released from mitochondria (Wilkinson et al., 2003). Further investigation of mitochondrial function and the pivotal role of these organelles in regulating apoptotic cell death may elucidate the mechanism underlying deafferentation-induced death in NM.

**Mitochondrial dysfunction**

Mitochondria are primitive organelles acquired evolutionarily by endosymbiotic engulfment of a prokaryote (Embley et al., 2003a, Embley et al., 2003b, Tovar et al., 2003, van der Giezen and Tovar, 2005, Embley and Martin, 2006, Poole and Penny, 2007). Mitochondria are responsible for a wide range of biochemical reactions within the cell, including oxidation,

electron transport, and ATP generation (Scheffler, 2001, van der Giezen and Tovar, 2005), and defects in mitochondrial integrity have been associated with a number of neurological disorders (Scheffler, 2001, Zeviani, 2004), including deafness (Fischel-Ghodsian, 1999, Kokotas et al., 2007). In addition to their essential roles in energy metabolism and maintenance of life, mitochondria are also critically involved in active cell death processes (Orrenius et al., 2007). Many of these processes are evolutionarily conserved and have been increasingly linked to damaging oxygen free radical agents as well as mutations in mitochondrial DNA (Orrenius et al., 2007).

The circular mitochondrial genome is remarkably conserved over time, and the same sets of mitochondrial-derived genes are found within most organisms (Scheffler, 2001). Many proteins involved in mitochondrial activities are derived from nuclear DNA and imported to mitochondrial compartments following synthesis in the cell cytoplasm; however, certain protein subunits involved in oxidative metabolism originate from mitochondrial DNA (Tzagoloff and Myers, 1986, Attardi and Schatz, 1988, Nicholson and Neupert, 1988, Hartl and Neupert, 1990). Cytochrome oxidase (CO), for example, is derived from both nuclear- and mitochondrial-encoded subunits but is assembled by mitochondrial protein synthetic machinery (Hoppeler et al., 1981, Nelson, 1987, Ozawa et al., 1987). Mitochondrial function, therefore, may be influenced by a multitude of factors, including nuclear-

encoded genes, mitochondrial-encoded genes, as well as integrity of protein synthetic machinery and cellular energy status.

Functionally, mitochondria synthesize cellular ATP through a series of coordinated oxidation-reduction reactions within the mitochondrial inner membrane (Stryer, 1995, Scheffler, 2001). Electrons liberated from glycolytic and Tricarboxylic Acid cycle (TCA) intermediates (NADH and $FADH_2$) are passed through four enzyme complexes to molecular oxygen ($O_2$) (Saraste, 1999, Scheffler, 2001). Energy generated by three of these electron transport chain (ETC) enzymes (NADH dehydrogenase, cytochrome reductase, and cytochrome oxidase) is used to establish an electrochemical gradient of protons ($H^+$) across the mitochondrial inner membrane (Scheffler, 2001). The electrochemical gradient is required by ATP synthase, which uses the energy stored in the gradient to synthesize ATP (Mitchell, 1961, Scheffler, 2001, Fukui and Moraes, 2008).

In deafferented NM, mitochondria rapidly proliferate within hours of cochlea removal (Hyde and Durham, 1994) and exhibit transient increases in oxidative enzymes (Durham and Rubel, 1985, Hyde and Durham, 1990, Durham et al., 1993). Interestingly, a subset of deafferented neurons, presumably those that will die, show ultrastructurally-vacuolated mitochondria (Hyde and Durham, 1994). It seems likely that mitochondrial functional impairment accompanies the structural changes observed within deafferented NM neurons destined to die.

**Molecular genetic approaches**

Molecular approaches to study the auditory system have been hindered by the limited quantity of auditory sensory tissue available per animal. Unlike the visual or olfactory systems, the number of sensory cells, as well as the number of molecular sensory transducers (eg. ion channels) reside in much fewer numbers in auditory tissue (Steel and Kros, 2001). The recent development of laser capture microdissection (LCM), however, has allowed researchers to circumvent this obstacle.

LCM allows individual cells to be microdissected from heterogeneous tissue sections without compromising genomic or proteomic integrities (Emmert-Buck et al., 1996, Luo et al., 1999, Roberts et al., 2004). Two different classes of LCM have been developed based on the type of laser employed by the system: infrared (IR) capture systems separate individual cells from complex tissue specimens by forming a polymer-cell composite between the polymer-coated capture cap and the cells of interest (Emmert-Buck et al., 1996, Bonner et al., 1997), whereas ultraviolet (UV) cutting systems photo-volatilize the cells surrounding a pre-selected area of interest (Schutze et al., 1997, Schutze et al., 1998, Kolble, 2000, Micke et al., 2005). The former system has been commercially developed by Arcturus/Molecular Devices (Espina et al., 2006), although the basic principles of both systems are the same (see Figure 4): (1) slide-mounted tissue sections are visualized using standard microscopic techniques; (2) cells of interest are targeted for

selection; (3) a thermolabile cap is centered above the targeted cells and placed directly atop the tissue section; (4) the laser is pulsed, and energy is transferred to adhere cells to the cap and separate them from the tissue (Espina et al., 2006).

LCM can be applied to the chick auditory system to evaluate molecular differences between deafferented NM neurons that die and deafferented NM neurons that survive cochlea removal. In combination with microarray GeneChip technology and quantitative Real-Time PCR (RT-PCR), specific genomic differences in gene expression can be assessed and quantified across samples to provide greater insight into the molecular mechanism underlying cell fate determination in NM.

**Purpose of this study**

The purpose of the experiments described in this dissertation is to better characterize the mechanism underlying cell-specific death of chick NM auditory neurons after deafferentation by peripheral damage to the cochlea. Several strategies were undertaken to elucidate factors with differential influences on neuronal fate. In Chapter II, we utilized immunofluorescent techniques to evaluate the activity of known apoptotic mediators involved in the mitochondrially-mediated apoptotic pathway. Specifically, we examined late-stage markers of intrinsic apoptosis: active caspase-3 and TdT-mediated dUTP Nick-End labeling (TUNEL) of degraded DNA. In Chapter III, we

investigated the mitochondrial functional contributions to cell fate. Histochemical evaluations of enzymatic reaction products, as well as a fluorescent detector of mitochondrial membrane potential reversal, were used to identify differences in mitochondrial functional status between deafferented NM neurons that die versus survive. In Chapter IV, we utilized LCM to selectively separate subpopulations of NM neurons based on their ribosomal integrities using Thionin staining of Nissl substance. We microdissected Thionin-negative “ghost neurons” ipsilateral to cochlea removal, which are known to undergo cell death (Karnes et al., 2009), from Thionin-positive neurons destined to survive deafferentation. We also microdissected a population of Thionin-positive, control neurons from contralateral NM. We utilized Affymetrix microarray GeneChips and RT-PCR to identify differentially expressed genes across groups. The results from these studies may help identify factors that either confer susceptibility to deafferentation-induced neuronal cell death or prevent death in the CNS following disruption of primary afferent input. The potential benefit derived from these results has widespread applicability to other neurodegenerative and neuropathic disorders including loss of vision, smell, and sensation (diabetic neuropathy), as well as stroke.

**Figure 1**

Schematics illustrating the anatomy of the human auditory system. Mechanical vibrations in the air (20-20,000Hz) are collected by the pinna and transmitted through the external auditory canal towards the tympanic membrane (TM) or eardrum. The TM oscillates, activating three middle ear ossicles, and transmitting mechanical vibrations to the cochlea, a snail-like structure housed within the inner ear (A). The cochlea contains a sensory epithelium, lined with specialized hair cells, whose deflection in response to sound activates spiral ganglion neurons, and transduces mechanical sound waves into electrical signals interpretable by auditory neurons in the brain (B). Brainstem auditory neurons process timing and spatial aspects of sound, while higher-order auditory neurons interpret meaning (C). Images adapted from *Netter's Atlas of Human Anatomy*.

A

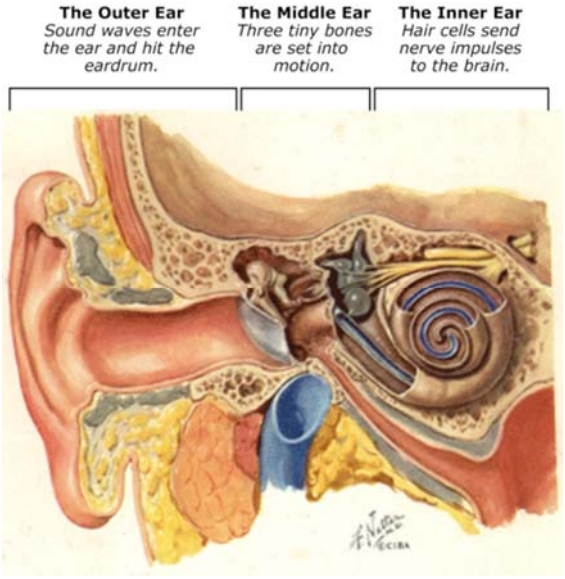
The Outer Ear
Sound waves enter the ear and hit the eardrum.
The Middle Ear
Three tiny bones are set into motion.
The Inner Ear
Hair cells send nerve impulses to the brain.

B

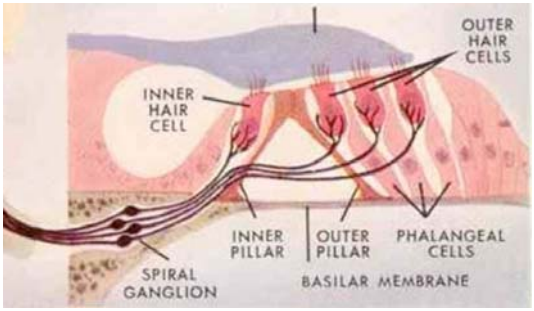
OUTER HAIR CELLS
INNER HAIR CELL
INNER PILLAR
OUTER PILLAR
PHALANGEAL CELLS
SPIRAL GANGLION
BASILAR MEMBRANE

C

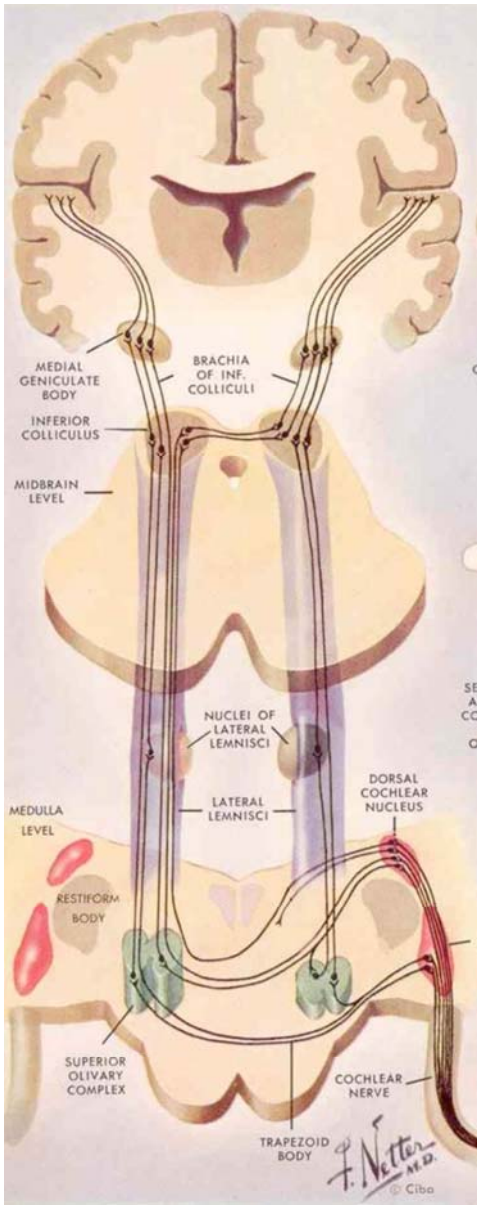
MEDIAL GENICULATE BODY
BRACHIA OF INF. COLLICULI
INFERIOR COLLICULUS
MIDBRAIN LEVEL
NUCLEI OF LATERAL LEMNISCI
LATERAL LEMNISCI
DORSAL COCHLEAR NUCLEUS
MEDULLA LEVEL
RESTIFORM BODY
SUPERIOR OLIVARY COMPLEX
COCHLEAR NERVE
TRAPEZOID BODY
F. Netter M.D.
© Ciba

**Figure 2**

A schematic illustrating the preservation of frequency topography throughout the chick auditory system. The chick cochlea (basilar papilla) is a relatively flat curvelinear membrane that contains an epithelial layer of sensory hair cells specialized for the transduction of sound from the ear to the brain. As illustrated by the color-code, high-frequency hair cells at the base of the cochlea send afferent projections to neurons within rostro-medial NM, while low-frequency hair cells at the apex of the cochlea send afferent projections to the caudo-lateral region of the nucleus. Figure adapted from Park et al 1999.

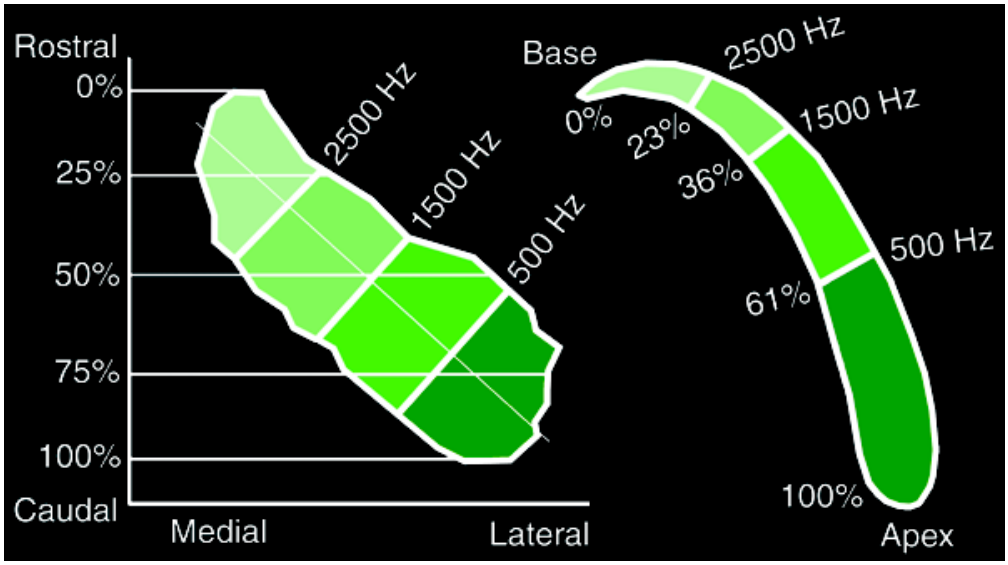


**NUCLEUS MAGNOCELLULARIS** **COCHLEA**

**Figure 3**

A schematic illustrating the intrinsic, mitochondrially-mediated apoptotic cascade. Intrinsic cellular stress causes mitochondria to extrude cytochrome *c* from the intermembrane space into the cell cytoplasm. Cytochrome *c* binds to the circulating cytoplasmic protein apoptotic protease activating factor1 (Apaf1), the action of which cleaves and activates caspase-9. Active caspase-9 is an initiator caspase, which subsequently, cleaves and activates caspase-3, an effector caspase. Active caspase-3 has a host of cellular substrates involved in the structured dismantling of cellular machinery. Active caspase-3 is required for the activation of an endogenous endonuclease, which migrates to the nucleus and degrades genomic DNA.

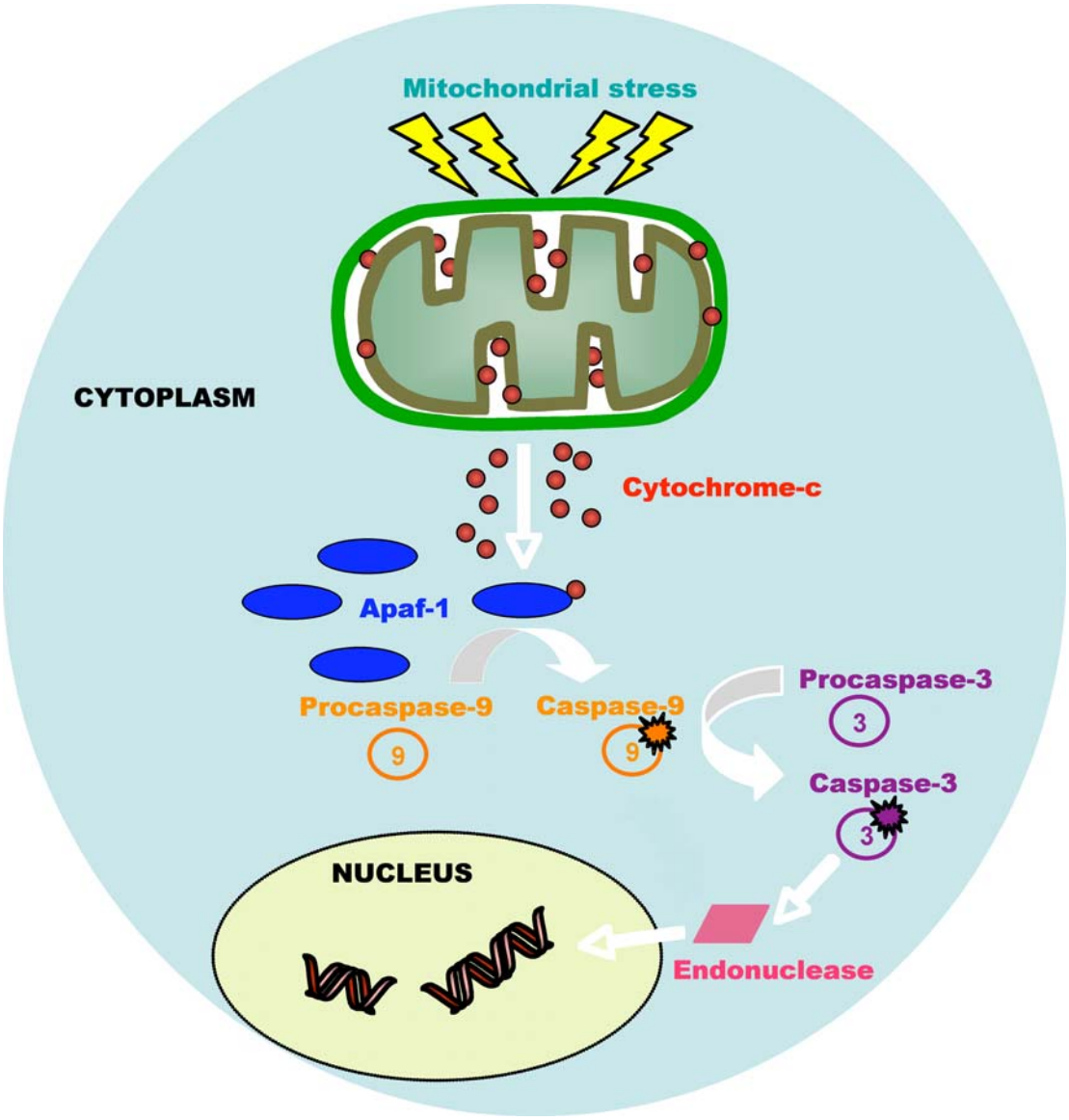
Mitochondrial stress
CYTOPLASM
Cytochrome-c
Apaf-1
Procaspase-9
9
Caspase-9
9
Procaspase-3
3
Caspase-3
3
NUCLEUS
Endonuclease

**Figure 4**

A schematic illustrating the methodology underlying laser capture microdissection (LCM). (1) Individual cells of interest (beige), embedded within complex tissue sections, are visualized under microscopy. (2) A cap (blue), equipped with a thermolabile polymer film, is placed directly above the cells of interest and lowered onto the tissue section. (3) Cells are targeted for microdissection using the LCM software. (4) An infrared (IR) laser is pulsed (gray) in the targeted area, melting the thermolabile polymer film to the cells of interest and forming a polymer-cell composite. (5) The polymer-cell composite is lifted from the slide, effectively microdissecting individual cells from a heterogeneous tissue section. RNA, DNA, or protein can be extracted from microdissected cells for use in downstream applications.

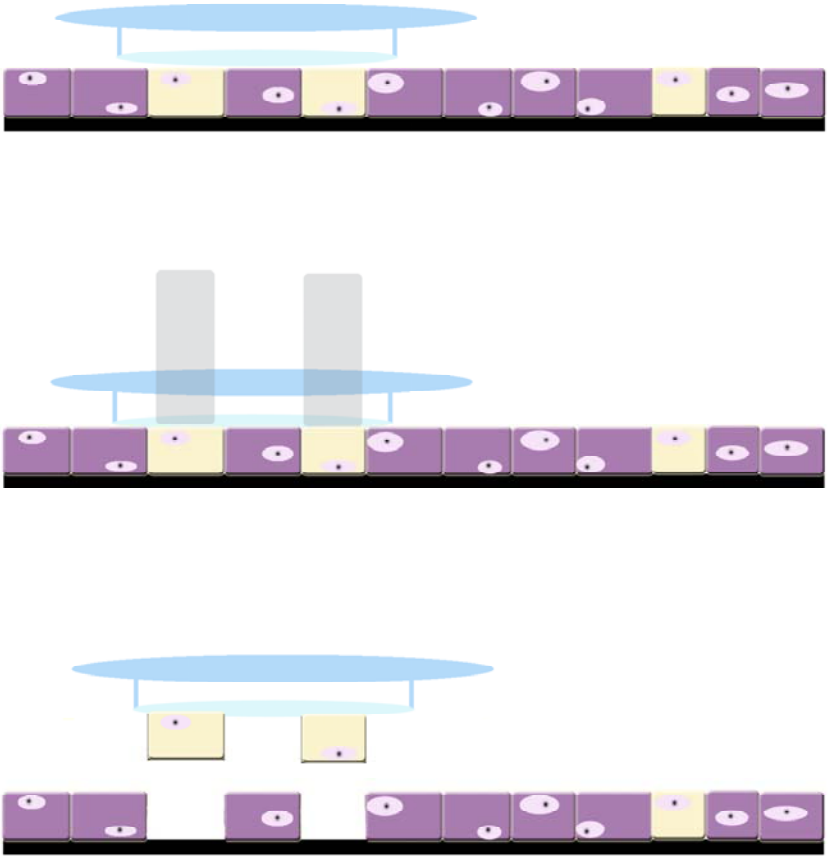

# CHAPTER II

# DEAFFERENTATION-INDUCED CASPASE-3 ACTIVATION AND DNA FRAGMENTATION IN CHICK COCHLEAR NUCLEUS NEURONS

## Introduction

Neurons exposed to afferent disruption undergo a series of post-synaptic cellular changes in an effort to adapt to their new environment. In the auditory system, deafferentation-induced changes in sensory neurons have been examined following cochlear manipulation (Rubel and Parks, 1988, Rubel et al., 1990, Rubel and Fritzsch, 2002). Chick nucleus magnocellularis (NM) neurons receive their excitatory input exclusively from eighth nerve afferents from the ipsilateral cochlea (Parks and Rubel, 1978). Cochlea removal permanently severs the connections between cochlea and brainstem structures (Rubel et al., 1990) and produces rapid neuroplastic changes in NM, including reduced metabolic (Durham and Rubel, 1985, Heil and Scheich, 1986, Hyde and Durham, 1990), electrical (Born et al., 1991), and protein synthetic capabilities (Steward and Rubel, 1985, Garden et al., 1994, Kelley et al., 1997). Approximately 20-40% percent of cells ultimately die (Born and Rubel, 1985, Edmonds et al., 1999, Smittkamp et al., 2005).

Previous studies showed a marked correlation between loss of ribosomal integrity and cell death (Rubel et al., 1991, Hyde and Durham, 1994, Hartlage-Rubsamen and Rubel, 1996). As a consequence, Thionin

staining of ribosomal Nissl substance in deafferented NM has been used to distinguish cells that will die from cells that will survive (Born and Rubel, 1985). Cells staining poorly with Thionin are devoid of functional ribosomes and are thought to approximate the subset of neurons susceptible to deafferentation-induced cell death. These Thionin-negative NM neurons have characteristic hollowed appearances under light microscopy and are consequently termed “ghost” neurons (Born and Rubel, 1985).

Studies of cell death in deafferented NM suggest activation of the intrinsic or mitochondrial apoptotic cascade (Wilkinson et al., 2002, Wilkinson et al., 2003, Danial and Korsmeyer, 2004), which initiates with leakage of cytochrome *c* from damaged mitochondria (Kluck et al., 1997, Denecker et al., 2001). As cytochrome *c* accumulates in the cytoplasm, it binds the cytoplasmic protein, apoptotic protease activating factor-1 (Apaf-1), and this protein complex activates a series of cysteine proteases, known as caspases. Caspase-9 becomes activated first, by binding to the cytochrome-c/Apaf-1 apoptosome complex (Slee et al., 1999, Bratton et al., 2000, Jiang and Wang, 2000, Fuentes-Prior and Salvesen, 2004). Caspase-9 is an initiator caspase, which activates the downstream effector caspase, caspase-3 (Bratton et al., 2000, Bratton et al., 2001). Caspase-3 has a host of cellular substrates and is important for the activation of Caspase-activated DNAse (CAD) (Enari et al., 1998) or DNA fragmentation factor (DFF) (Liu et al., 1997, Liu et al., 1999), which, upon activation, migrates to the nucleus and degrades genomic

DNA (Bratton et al., 2000, Jiang and Wang, 2000, Yuan and Yankner, 2000).

Cytochrome *c* and active caspase-9 have been observed in deafferented NM neurons (Wilkinson et al., 2003), however the source of the cytochrome *c* could not be attributed to leaky mitochondria. In addition, active caspase-9 was observed unexpectedly in both surviving and dying deafferented NM neurons (Wilkinson et al., 2003). Here we evaluated two late markers of apoptosis, active caspase-3 and TUNEL, in deafferented NM neurons. In addition, we describe a novel relationship between these late markers of apoptosis and the established histochemical techniques used to describe cell death in NM.

## Materials and Methods

Animal preparation and surgery

Broiler chickens (Avian x Peterson) were obtained as fertilized eggs from a commercial supplier (Pilgrim's Pride, Batesville, AR). The eggs were hatched in a forced draft incubator, and hatchlings were housed in communal brooders with *ad libitum* access to food and water. Ten- to 15-day post-hatch chicks were anesthetized with intramuscular injections of Ketamine HCl (35mg/kg; Phoenix Pharmaceutical, Inc., St. Joseph, MO) and Xylazine (2mg/kg; Lloyd Laboratories, Shenandoah, IA) and subjected to unilateral cochlea (basilar papilla) removal, as described previously (Born and Rubel, 1985, Hyde and Durham, 1990). Briefly, the left tympanic membrane was punctured and the columella extracted. The cochlea was removed in its entirety from the oval window aperture using Dumont forceps. Cochlea removal severs the peripheral processes of cochlear ganglion neurons, but leaves cell bodies intact. The cochlear duct was aspirated following surgery, and animals were allowed to recover. Contralateral cochleae remained intact, and contralateral NM neurons maintained their afferent input, allowing them to serve as within-animal controls. In addition, control brains from anesthetized, unoperated animals (n=3) were included in the study. All experimental protocols were approved by the University of Kansas Medical Center Institutional Animal Care and Use Committee (IACUC).

Tissue preparation

Following cochlea removal, animals were given intraperitoneal injections of Beuthanasia-D (Schering-Plough, Union, NJ) and sacrificed at 1 (n=4), 6 (n=5), 12 (n=10), 24 (n=5), 48 (n=4) or 168 (n=10) hours to examine active caspase-3 activity, and at 12 (n=7), 18 (n=5), 24 (n=5), 36 (n=6), 48 (n=5) or 168 (n=6) hours to examine fragmented DNA with TUNEL labeling. For active caspase-3 staining, animals were systemically perfused with 0.1M phosphate buffered saline (PBS, pH 7.4) containing heparin (1U/mL) for 1 minute, immediately followed by perfusion with 10% phosphate buffered formalin for 5 minutes. Brains were post-fixed for one hour, cryoprotected by sinking in sucrose (10%, 20%, 30% in PBS), frozen in heptane cooled by dry ice, and stored at -80C until sectioning. For TUNEL staining, animals were systemically perfused with Avian Ringer's solution (2M NaCl, 2M KCl, 2M $MgCl_2$, and 100mM EDTA), and brains were removed, post-fixed for six hours in modified Carnoy's fixative (containing ethanol, chloroform, Avian Ringer's solution, and glacial acetic acid), stored overnight in 70% ethanol, and embedded in paraffin (Lurie and Durham, 2000).

Active caspase-3 immunofluorescence

Coronal 25μm sections through NM were cut on a cryostat, and a 1-in-4 series was thaw-mounted on Superfrost/Plus slides (Fisher Scientific, Pittsburgh, PA). Sections were rinsed three times in PBS and permeabilized

in 1% Triton X-100. Sections were then blocked in 10% normal goat serum in PBS and incubated for two hours in primary antibody (rabbit anti-cleaved caspase-3 [Asp175] antibody; Cell Signaling Technologies, Beverly, MA) diluted 1:200, in PBS. Additional caspase-3 antibody dilutions (1:500 and 1:1,000) were also examined and showed labeling patterns indistinguishable from those seen with the 1:200 dilution. Sections were incubated in secondary antibody solution (AlexaFluor 488 goat-anti-rabbit IgG; Invitrogen/Molecular Probes, Eugene, OR) 1:1000 in PBS for two hours at room temperature and rinsed three times in PBS before coverslipping with Vectashield antifade mounting medium (Vector Laboratories, Burlingame, CA). Additional controls with no primary antibody, no secondary antibody, and neither antibody were also included. No labeling was seen in these control tissues. For evaluation of NM neuronal number, an adjacent 1-in-4 series of sections mounted on Superfrost/Plus slides was stained for cytochrome oxidase (CO) histochemistry (Hyde and Durham, 1990). Sections were immersed in a solution containing 0.05% diaminobenzidine, 0.02% Type III cytochrome c, and 4% sucrose in PBS (Sigma Chemical, St. Louis, MO). Sections were incubated at 40°C for two hours, washed in PBS, and dehydrated through graded ethanols and xylenes before coverslipping with DPX mounting medium (VWR International Ltd., Poole, UK).

TUNEL, Nissl, and Propidium Iodide staining

Coronal paraffin sections through NM were cut at 10-14μm and saved as ribbons. To evaluate the presence of Nissl substance, a 1-in-4 series of sections throughout the anterior to posterior extent of NM was deparaffinized in xylenes and hydrated through graded ethanols to distilled water. Sections were immersed in 1% Thionin stain, rinsed in distilled water, dehydrated briefly through graded ethanols, and stored in xylenes before coverslipping with DPX mounting medium. To evaluate TUNEL labeling, a 1-in-4 series of sections in the first (high frequency) and third (low frequency) quartiles of NM, adjacent to Nissl-stained sections, was mounted on silane-coated slides (Scientific Device Laboratory, Des Plaines, IL). Sections were reacted for TUNEL using Promega's DeadEnd Fluorometric TUNEL System (Promega Corporation, Madison, WI) according to the manufacturer's instructions. Briefly, sections were deparaffinized through xylenes and rehydrated through graded ethanols. Sections were washed in 0.85% NaCl followed by PBS, and fixed in 4% paraformaldehyde. Cells were permeabilized with 20g/ml Proteinase K, washed in PBS, and equilibrated in the kit's Equilibration Buffer. Sections were incubated with rTdT enzyme, nucleotide mix, and Equilibration Buffer in a humidity chamber in the dark for one hour. Following incubation, sections were immersed in 1x SSC (150mM NaCl and 15mM sodium citrate) buffer and washed in PBS. Sections were counterstained with 1g/ml propidium iodide (PI) and washed in distilled water, then coverslipped with

Vectashield antifade mounting medium (Vector Laboratories, Burlingame, CA).

Analysis of neuron number

TUNEL and PI staining were evaluated as a function of the tonotopic organization of NM; therefore, neuron number in Thionin-stained paraffin sections was evaluated as a function of location within NM. Sections were divided into quartiles along the anterior to posterior extent of NM. Nucleolar profiles in the first (high frequency) and third (low frequency) quartiles were counted using a 40X objective under brightfield illumination. The fourth quartile was not chosen as a representative low frequency region as these neurons are functionally heterogeneous (Rubel and Parks, 1975). Neurons displaying a stained cytoplasm, a clear, intact nucleus, and visible nucleoli were counted. Total neuron number in each quartile was estimated by multiplying profile counts by four, as one-in-four sections were counted. Since nucleolar size can affect the accuracy of profile counts for estimating absolute number (Clarke and Oppenheim, 1995), we measured the diameter of the nucleolus in the first (rostral) quartile and third (caudal) quartiles of both deafferented and contralateral NM in two randomly-selected animals from each time point. In each animal, a section at the midpoint of each quartile was examined with a 40X dry objective under brightfield microscopy. Nucleolar diameters were measured in at least 10 neurons per section. The

values were averaged and used to derive Abercrombie correction factors for both deafferented and contralateral neurons in each quartile over time (Abercrombie, 1946). All measurements were conducted by an individual blind to the treatment and duration of survival.

Percent cell survival was calculated in the first and third quartiles at 12-hour, 24-hour, 48-hour, and 7-day survival times using the corrected profile counts. Percent cell survival was calculated as [1-(total neuron number in contralateral NM-total neuron number in ipsilateral NM)/ total neuron number in contralateral NM)] x 100%. Contralateral NM neurons maintain normal afferent input, thereby serving as within-animal controls.

Comparison of TUNEL and PI staining with Nissl staining

TUNEL-stained sections were examined using fluorescence microscopy. Representative sections in the first and third quartiles of NM were photographed digitally with a MagnaFire Camera to visualize TUNEL and PI staining separately. Photographs were analyzed using Photoshop (Adobe Systems Incorporated, San Jose, CA). For each image, brightness and contrast were optimized to visualize neurons, and a merged image was created by overlaying the photographs of PI- stained and TUNEL-stained images for each section (Figure 1A-C). NM neurons with various staining characteristics were then counted from the PI-stained, the TUNEL-stained, or the merged images. To estimate total neuron number, a neuron was counted

if a nuclear outline was clearly visible in the merged image (Figure 1C, arrowheads). A neuron was considered PI-positive if its cytoplasm stained red in the PI-stained image (Figure 1B, arrow). The number of PI-negative neurons was calculated by subtracting the number of PI-positive neurons from the total neuron number. A neuron was considered TUNEL-positive if its nucleus (Figure 1A, arrows), or its cytoplasm (Figure 1A, asterisks), or both stained green. Counts were performed on a computer monitor using a transparent overlay to mark neurons with various characteristics.

To assess the relationship between fluorescence staining and Nissl substance, Thionin-stained sections in the first and third quartiles adjacent to those evaluated for fluorescent staining were photographed. In each photograph, the number of Thionin-positive neurons and the number of Thionin-negative neurons were counted. A neuron was considered Thionin-positive if a clear, intact nucleus and dark nucleolus were visible, and the surrounding cytoplasm was darkly stained (Figure 1D, arrow). A neuron was considered Thionin-negative if its nucleus and cytoplasm were visible and intact but devoid of stain (Figure 1D, asterisks). Total neuron number for each section was calculated by adding values for Thionin-positive and Thionin-negative neurons.

To compare the prevalence of various neuronal types among animals, cell counts for each staining type were converted to a percentage of the total number of neurons in a given section. Three proportions were determined for

each image: (1) the number of neurons with a TUNEL-positive cytoplasm was divided by the total neuron number, (2) the number of PI-negative neurons was divided by the total neuron number, and (3) the number of Thionin-negative “ghost” neurons was divided by the total neuron number. Using these percentages, TUNEL-positive (cytoplasm and nucleus) and propidium iodide-negative neuron counts were independently compared to “ghost” neuron counts in adjacent, Thionin-stained sections to identify descriptive relationships between staining modalities.

Statistical analyses

Percent cell survival was calculated from Thionin-stained sections, and normalized counts per brain were plotted using SigmaPlot 10.0 (Systat Software, Inc., San Jose, CA). Paired t-tests were performed with Statview (SAS Institute, Inc., Cary, NC) to compare differences in cell survival in the rostral, first quartile (Q1) and caudal, third quartile (Q3) of NM.

Percentages of deafferented NM neurons positive for nuclear TUNEL labeling or cytoplasmic TUNEL labeling, and negative for cytoplasmic PI labeling were plotted independently against “ghost” neuron counts obtained from Thionin-stained images using SigmaPlot 10.0 (Systat Software, Inc., San Jose, CA), and Pearson product moment correlation coefficients (r) were derived using Microsoft Excel (Microsoft, Seattle, WA). Percentages were averaged per brain across all survival times (12, 24, and 48 hours) and

compared to the average percent cell survival observed at 7 days using a two-way analysis of variance (ANOVA) and Fisher's protected least significant difference (PLSD) post-hoc comparisons via Statview.

## Results

Active caspase-3 increases in deafferented NM neurons

Caspase-3 is activated late in the mitochondrial apoptotic pathway and relieves the inhibition of endogenous cellular endonucleases, thereby triggering degradation of genomic DNA (Liu et al., 1997, Enari et al., 1998, Sakahira et al., 1998, Liu et al., 1999, Fuentes-Prior and Salvesen, 2004). Immunocytochemistry using an antibody directed against active caspase-3 demonstrates no labeling in ipsilateral nucleus magnocellularis (NM) neurons of control birds and in birds at 1 or 6 hours after cochlea removal (data not shown). Twelve hours following deafferentation, some ipsilateral neurons show caspase-3 immunoreactivity; however, the number of labeled neurons is inconsistent across animals (data not shown). This inter-animal variability is not unexpected and probably marks the initiation of caspase-3 activation in deafferented NM neurons. By 24 hours, ipsilateral NM neurons show robust labeling for active caspase-3 in all animals (Figure 2D). Comparison to the adjacent cytochrome oxidase (CO)-stained sections (Figure 2B) demonstrates that all ipsilateral NM neurons are labeled. Increased CO staining is also seen in ipsilateral NM neurons, as has been described previously (Hyde and Durham, 1990). By 48 hours post-cochlea removal, ipsilateral neuronal cell loss is evident in CO-stained sections (Figure 3B vs. 3A). In the adjacent caspase-3-stained sections, labeled debris is detected in areas of cell loss as well as within the cytoplasm of intact NM neurons (Figure

3D). Evidence of active caspase-3 in ipsilateral, surviving NM neurons, as well as neuronal debris (Figure 4D versus Figure 4C), persists well after cell death is complete at 7 days (Born and Rubel, 1985, Rubel et al., 1990).

Time course of TUNEL labeling in deafferented NM neurons

Downstream effects of active caspase-3 were examined using a TdT-mediated dUTP Nick-End Labeling (TUNEL) assay. TUNEL identifies fragmented DNA, which is characteristic of apoptotic cells. TUNEL-labeled sections were counterstained with propidium iodide (PI) to asses the status of cellular DNA, and adjacent sections were stained with Thionin to estimate the proportion of "ghost" neurons in ipsilateral NM. No TUNEL labeling was seen in NM neurons of control brains.

Figure 5 shows sections through rostral NM from an animal sacrificed 12 hours after cochlea removal. In contralateral neurons, PI staining is seen both in the nucleus and the cytoplasm of NM neurons (Figure 5C). Cytoplasmic PI staining presumably identifies the prolific volume of mitochondrial DNA present in these neurons (Parks, 1981, Hyde and Durham, 1994, Hartlage-Rubsamen and Rubel, 1996). The nucleus and cytoplasm of healthy, contralateral neurons are clearly visible, also, by Thionin staining of Nissl substance (Figure 5A). In contrast, no TUNEL labeling is evident in contralateral NM neurons (Figure 5E). In ipsilateral NM, Thionin staining reveals the presence of numerous "ghost" neurons visible by

a stained nucleus surrounded by an unstained cytoplasm (Figure 5B, inset). In the adjacent fluorescently-stained section, a similar number of NM neurons with a PI-positive nucleus but no cytoplasmic PI staining is also apparent (Figure 5D). Nuclear TUNEL labeling of degraded genomic DNA is restricted to a subset of deafferented NM neurons (Figure 5F, inset). Neurons with nuclear TUNEL labeling do not stain with propidium iodide (Figure 1A, B, C). Quantitative comparisons between adjacent Thionin and fluorescently-labeled sections (see below) show that these same neurons do not stain with Thionin, indicating that neurons devoid of functional ribosomes are the same neurons undergoing apoptosis. It should be noted, however, that not all PI-negative neurons show nuclear TUNEL labeling (Figure 1A, B, C). Similar PI and TUNEL labeling patterns are seen 18 hours after cochlea removal (data not shown).

Twenty-four hours following cochlea removal, an unusual pattern of cytoplasmic TUNEL staining emerges in a subset of PI-negative, deafferented neurons (Figure 6). Robust cytoplasmic TUNEL staining is observed in ipsilateral NM neurons (Figure 6F) and coincides with the loss of cytoplasmic PI staining (Figure 6D). More intense, robust, cytoplasmic TUNEL staining is seen 48 hours after cochlea removal (Figure 7F). At both 24- and 48-hour survivals, the number of NM neurons with cytoplasmic TUNEL staining parallels the number of “ghost” neurons observed in adjacent Thionin-stained sections. Seven days following cochlea removal, no TUNEL labeling is seen

(Figure 8F), as deafferented neurons have been completely degraded and are no longer present. Likewise, neither “ghost” neurons in Thionin-stained tissue (Figure 8B) nor neurons lacking cytoplasmic PI staining (Figure 8D) are present in deafferented NM.

Relationship between molecular markers and neuronal cell death

Previous work in nucleus magnocellularis (NM) has established that ribosomal degradation is likely to occur only in those neurons ultimately destined to die as a consequence of cochlea removal (Rubel et al., 1991). Thus, the number of Thionin-negative “ghost” neurons observed in deafferented NM at early survival times should be an accurate quantitative predictor of the extent of cell death. We examined this premise by comparing the number of Thionin-positive neurons present 7 days after cochlea removal (after “ghost” neurons have been degraded and cell death is complete) (Born and Rubel, 1985, Rubel et al., 1990) to the number of Thionin-positive neurons observed at early survival times (when “ghost” neurons are present but are not counted due to lack of cytoplasmic Thionin staining). These results are shown in Figure 9A, which plots the percent of Thionin-positive neurons in the first (rostral, high frequency region) and third (caudal, low frequency region) quartiles of NM across survival times. Percentages of Thionin-positive neurons were calculated by dividing the total number of Thionin-positive ipsilateral neurons by the total number of Thionin-positive

contralateral neurons. Thionin-positive neuronal counts were consistently higher in the caudal, low frequency quartile (Q3) than in the rostral, high frequency quartile (Q1), suggesting a tonotopic pattern of cell loss following deafferentation. Paired t-tests between quartiles at 12-hour, 48-hour, and 7-day survival times showed significantly greater cell survival in Q3 ($p=0.0007$ at 12 hours, $p=0.0673$ at 24 hours, $p=0.0226$ at 48 hours, and $p=0.0477$ at 7 days). Two-way ANOVA analysis followed by Fisher's PLSD post-hoc tests of Thionin-positive neuronal counts of both quadrants and across all time points showed no differences in cell survival ($p=0.1891$). These results reaffirm that "ghost" neurons appearing 12-48 hours after cochlea removal accurately approximate the cell death that occurs by 7 days.

Given the quantitative relationship between Thionin-positive neurons and neuronal survival, we next compared the number of Thionin-negative "ghost" neurons to neurons exhibiting specific staining characteristics, as a means of identifying intracellular markers of cell death. Activation of caspase-3 initiates a number of proteolytic processes within a cell including fragmentation of nuclear genomic DNA by cellular endonucleases (Liu et al., 1997, Enari et al., 1998, Sakahira et al., 1998, Liu et al., 1999, Fuentes-Prior and Salvesen, 2004). Consequently, neurons destined to die following deafferentation are expected to show localized TUNEL labeling within their nuclei. In deafferented NM, however, nuclear TUNEL labeling poorly correlates with the number of "ghost" neurons present 12-48 hours following

deafferentation (r=0.20) (Figure 9B). This relationship indicates that many fewer neurons display nuclear TUNEL labeling than are Thionin-negative. Cytoplasmic TUNEL labeling better represents the “ghost ” neuron population (r=0.57), especially in the rostral, first quartile of NM (Figure 9C). Similarly, loss of cytoplasmic PI labeling correlates better (r=0.72) with “ghost” neurons throughout NM (Figure 9D). These results demonstrate that nucleic acid degradation in both the nucleus and cytoplasm modulate deafferentation-induced cell death in NM.

## Summary and Discussion

Cell specific loss of CNS neurons occurs under a variety of circumstances. Normal developmental pruning of neural circuits (Linden and Renteria, 1988, Jacobson et al., 1997, Lu and Trussell, 2007) and matching of target populations with neuronal number (Hamburger and Levi-Montalcini, 1949, Linden, 1994, Yuan and Yankner, 2000) involve activation of physiologic apoptotic cascades (Oppenheim, 1991, Johnson et al., 1996). Pathologic apoptotic cascades may be activated independent of development by traumatic or injurious stimuli and involve upregulation of pro-apoptotic factors. While the process of apoptosis is undoubtedly complex, two predominant signaling pathways are generally considered responsible for effecting apoptosis in most cells: the (1) intrinsic mitochondrially-mediated pathway involves release of apoptogenic factors into the cytoplasm and cleavage of procaspases, while the (2) extrinsic death receptor- mediated pathway activates Fas and tumor necrosis factor receptors (Danial and Korsmeyer, 2004, Zhang et al., 2004, Harris and Rubel, 2006).

The results presented here show activation of the intrinsic mitochondrially-mediated apoptotic pathway in deafferented NM neurons. Specifically, we demonstrate upregulation of two late apoptotic indicators. Active caspase-3 is observed in all deafferented NM neurons regardless of cell fate. TUNEL identifies fragmented nucleic acid in a subset of deafferented neurons, first arising within neuronal nuclei 12 hours following

cochlea removal and accumulating cytoplasmically by 24-48 hours. Cytoplasmic TUNEL labeling is accompanied by a loss of propidium iodide (PI) staining in the cytoplasm. This labeling pattern occurs in those neurons likely to die. In addition, we show a tonotopic pattern of cell loss that favors the rostral, high-frequency region of the auditory nucleus.

Changes in some traditional apoptotic markers have been described in the auditory system. For example, in the mouse auditory system, apoptotic genes are upregulated in anteroventral cochlear nucleus (AVCN) neurons during the developmental time period when deafferentation causes neuronal cell loss (Harris et al., 2005). Apoptotic gene expression thereafter is replaced by an upregulation of pro-survival genes (Harris et al., 2005). Examination of deafferented nucleus magnocellularis (NM) neurons in the chick reveals increased presence of pro-apoptotic proteins cytochrome *c* and active caspase-9 (Wilkinson et al., 2003). Our results are the first to demonstrate activation of late apoptotic indicators in NM, including caspase-3 and TUNEL. These apoptotic markers have previously been shown to play a role in cochlear hair cell death in the avian inner ear (Mangiardi et al., 2004, Duncan et al., 2006, Kaiser et al., 2008). Interestingly, in deafferented NM neurons, cytochrome *c* is not released from stressed mitochondria (Wilkinson et al., 2003). In addition, caspase-9 (Wilkinson et al., 2003) and caspase-3 (see Results section) are activated in all deafferented neurons regardless of cell fate. Also shown here, TUNEL labeling of degraded DNA is not restricted

to nuclei and emerges in the cellular cytoplasm of deafferented NM neurons as early as 24 hours following cochlea removal (see Results section). These unexpected and novel results suggest deviation from the traditional intrinsic mitochondrial apoptotic cascade. In contrast to the labeling for caspase-9 and caspase-3, however, TUNEL labeling occurs only in those neurons likely to die. Our discussion will address possible explanations for the molecular mechanism underlying cell death in deafferented NM neurons. In addition, we will speculate on the significance of the tonotopic cell loss we observe throughout the nucleus following cochlea removal.

Although caspase-3 activation is thought to be essential for apoptotic death (Yuan and Horvitz, 1990, Woo et al., 1998, Roth et al., 2000), its precise molecular involvement in the death process warrants further characterization. Several lines of evidence suggest a tissue-specific susceptibility to caspase-3-mediated death (Kuida et al., 1996, Woo et al., 1998). Specifically, caspase-3 deficiency suspended apoptosis in neurons but had no effect on other developing cell types (Kuida et al., 1996). Interestingly, activation of caspase-3 in cultured cells does not always trigger apoptosis (Boise and Thompson, 1997), nor does caspase inhibition prevent death in cells actively induced to undergo apoptosis (Xiang et al., 1996, McCarthy et al., 1997). These findings, as well as those reported here, suggest that caspase-3 is a primary regulator of mammalian apoptosis, rather than an irreversible executioner. Interestingly, murine cells deficient in

caspase-3 (Woo et al., 1998) exhibit early indications of apoptosis, including plasma membrane blebbing and cleavage of poly(ADP-ribose) polymerase (PARP), without signs of late-stage chromatin condensation and nuclear DNA degradation (Wyllie et al., 1980), suggesting that the nuclear events occurring late in the apoptotic pathway require caspase-3 and/or its downstream targets (Samejima et al., 1998). It is possible that caspase-3 upregulation in deafferented NM neurons permits DNA fragmentation, but alone, is not a prerequisite for death.

TUNEL labeling specifically identifies fragmented DNA characteristic of cells undergoing apoptosis by catalytically incorporating dUTP nucleotides into short (180-200bp) DNA fragments with exposed 3'OH ends (Gavrieli et al., 1992). Although evidence of DNA fragmentation has been described in mammalian auditory neurons following cochlea ablation (Mostafapour et al., 2000, Alam et al., 2007, Luoma and Zirpel, 2008), our TUNEL results in deafferented NM are novel, as was the unexpected subcellular distribution of TUNEL.

Nuclear TUNEL labeling, consistent with apoptotic degradation of genomic DNA, was observed initially in a subset of neurons 12 hours after cochlea removal, although the proportion of neurons with TUNEL-positive nuclei was smaller than and correlated poorly with the proportion of "ghost" neurons in adjacent Thionin-stained sections. Previous studies in avian species have shown similar underestimates of cell death by TUNEL labeling

(Torchinsky et al., 1999, Wilkins et al., 2001). These results imply that nuclear TUNEL labeling is a transient phenomenon, detectable during a brief and finite duration of the cell death process.

It should be noted that the cell death process is certainly not an all-or-none phenomenon; once activated, a number of checkpoints exist whereby cell death might be facilitated or reversed. In fact, reversible deafferentation via a single, local injection of tetrodotoxin (TTX) did not elicit cell death in NM at 24 hours (Born and Rubel, 1988), suggesting a reversibility of the neuronal death process if afferent activity is restored. Our perinuclear TUNEL labeling pattern emerged 24 hours following permanent deafferentation, correlated well with “ghost” neuron counts from Thionin-stained sections, and robustly persisted in deafferented NM 48 hours after deafferentation, effectively distinguishing those neurons going on to complete cell death.

Cytoplasmic TUNEL labeling has been described in other neurodegenerative disease pathologies and has been shown to identify abnormal mitochondria (de la Monte et al., 2000, Martin et al., 2006). De la Monte et al. (2000) performed TUNEL assays on cortical sections from human Alzheimer’s Disease (AD) patients. They observed clear cytoplasmic TUNEL labeling, with and without accompanying nuclear TUNEL labeling, in AD neurons and glia compared to non-AD control cells (de la Monte et al., 2000). They went on to show increased levels of mitochondrial DNA fragmentation in AD brains, as well as elevated intramitochondrial

accumulations of 8-oxo-7,8-dihydro-2'-deoxyguanosine (8-OHdG), a byproduct of reactive oxidative damage known to damage mitochondrial DNA (de la Monte et al., 2000). Martin et al. (2006) observed similar cytoplasmic distributions of TUNEL labeling in spinal motor neurons in mice overexpressing a human Parkinsonian $\alpha$-Synuclein gene (Martin et al., 2006). TUNEL-EM with colloidal gold affirmed that mitochondria with damaged DNA labeled positively with TUNEL (Martin et al., 2006).

It is likely that the cytoplasmic TUNEL staining we observe in subpopulations of deafferented NM is due to loss of mitochondrial integrity and/or activation of a non-traditional apoptotic cascade. Previous studies have shown that auditory deafferentation triggers a robust proliferation of mitochondria throughout all NM neurons, shortly followed by the degradation of mitochondrial morphology in a subset, presumably those destined to die (Hyde and Durham, 1994, Hartlage-Rubsamen and Rubel, 1996). Additional studies of metabolic oxidative enzyme activity in deafferented NM have shown a rapid upregulation early, in concert with mitochondrial proliferation, followed by a gradual loss of enzyme function in surviving deafferented neurons (Durham and Rubel, 1985, Hyde and Durham, 1990, Durham et al., 1993). The perinuclear pattern of TUNEL labeling we observed mimics the morphologic accumulations of mitochondria, likely identifying those neurons that accumulate abnormal mitochondria prior to dying.

Our novel propidium iodide (PI) labeling pattern reiterates a role for

mitochondrial DNA in mediating cell death. PI is a nucleic acid intercalation dye that is normally excluded from cells with intact membranes (Bevensee et al., 1995, Dengler et al., 1995). Accordingly, previous studies in NM slice preparations utilized PI *in vivo* to assess degeneration of NM neurons: PI uptake correlated with damaged membrane integrity and cell degeneration (Zirpel et al., 1998, Zirpel et al., 2000b). In our studies, PI was utilized as an *in vitro* DNA intercalation dye, as no precautions were undertaken to preserve RNA integrity. In our fixed tissue specimens, PI labeled all NM neurons because sections were permeabilized with Proteinase K. PI bound to DNA present in the cytoplasm and nucleus. Because ultrastructural studies have shown that NM neurons have prolific mitochondria, the cytoplasmic PI staining is presumed to be mitochondrial DNA. PI accompanied by TUNEL labeling is often used to distinguish live (PI-positive) from dying (TUNEL-positive) cells at the time of fixation. Loss of cytoplasmic PI staining 24-48 hours after cochlea removal correlated well with “ghost” neuronal counts in deafferented NM, implicating fragmentation of mitochondrial DNA in those cells destined to die.

Other evidence to support a non-traditional mechanism of apoptotic cell death in deafferented NM neurons includes (1) the activation of caspase-9 (Wilkinson et al., 2003) and caspase-3 in both dying and surviving neurons, as well as (2) the inability to detect release of cytochrome *c* from mitochondria (Wilkinson et al., 2003). Recent studies have demonstrated a novel apoptotic

pathway linked to endoplasmic reticulum (ER) stress that occurs in the absence of cytochrome *c* release (Nakagawa et al., 2000). In this pathway, ER stress activates an alternative initiator caspase, caspase-12, which directly transforms pro-caspase-9 into its active form and triggers downstream activation of caspase-3 (Morishima et al., 2002). Deafferented NM "ghost" neurons are devoid of polyribosomes (Born and Rubel, 1985) and deficient in protein synthesis (Born and Rubel, 1988, Rubel et al., 1990), suggesting that ER stress plays a role in mediating cell death, perhaps via activation of caspase-12. Future experiments in which caspase-3 or caspase-12 were perturbed would strengthen our understanding of the molecular mechanism underlying cell death in deafferented NM neurons.

Like the unusual *mechanism* of cell loss in deafferented NM, the *pattern* of cell loss in NM warrants further investigation. At early and late survival times, the number of neurons surviving deafferentation is statistically higher in the caudal, low frequency region of NM (see Figure 9), suggesting a tonotopic susceptibility to cell death. Previous studies in our laboratory showed a tonotopic gradient of glucose metabolism throughout the NM frequency axis in normal hatchling and adult birds; however, a tonotopic pattern of cell loss after cochlea removal is seen only in hatchling birds (Smittkamp et al., 2005). Although the details of tonotopic deafferentation-induced loss have not been elucidated, several mechanisms of neuronal susceptibility may be postulated. A single homogeneous population of

neurons exists in NM (Rubel and Parks, 1988, Kubke et al., 1999), but it is possible that neurons in caudal regions of NM may be more equipped to activate a protective glial response. Astrocytes are known to rapidly upregulate in deafferented NM, perhaps to increase nutrient supply to neurons or establish protective borders from dying neurons (Canady and Rubel, 1992). Alternatively, tonotopic differences in synaptic vesicle densities may predispose rostral, high frequency NM neurons to excitotoxic death (Crumling and Saunders, 2007). Perhaps neurons in caudal NM selectively receive additional inputs or differentially express pro-survival genes basally or in response to deafferentation. Further experimentation is necessary to elucidate the tonotopic susceptibility to death in deafferented NM neurons.

## Conclusions

In summary, we observe activation of caspase-3 throughout deafferented NM neurons as early as 24 hours following cochlea removal. We also describe a TUNEL labeling pattern in a subset of deafferented neurons that arises within nuclei at 12 hours and appears cytoplasmically at 24-48 hours. TUNEL labeling accompanies a loss of PI labeling and suggests involvement of mitochondrial DNA in deafferentation-induced cell death. The cell death that occurs in deafferented NM neurons suggests an atypical mechanism of apoptosis and tonotopic selectivity. In response to the loss of afferent support, NM neurons rapidly upregulate mitochondria. The subset whose mitochondria are morphologically dysfunctional likely corresponds to those with cytoplasmic TUNEL labeling, which may be actively undergoing caspase-12-mediated apoptosis. It remains unclear why caspase-9 and -3 are observed in surviving and dying populations of deafferented neurons. Analysis of a molecular mechanism may provide additional information to elucidate cell fate determination after loss of afferent support.

**Figure 1:** Photomicrographs of ipsilateral sections through nucleus magnocellularis (NM) from an animal sacrificed 12 hours after unilateral cochlea removal. Sections are double-labeled with TUNEL (**A**) and propidium iodide (PI) (**B**). A merged image was created for each section by overlaying TUNEL and PI images (**C**). Adjacent sections were stained with Thionin (**D**). Neurons were considered TUNEL-positive if nuclear (**A**, **arrows**) or cytoplasmic (**A**, **asterisks**) TUNEL labeling was observed in the TUNEL-stained image (**A**). Neurons were considered PI-positive if cytoplasmic PI labeling was observed in the PI-stained image (**B**, **arrow**). Total neuronal counts were determined by counting the number of neurons with visible nuclear outlines in the merged image (**C, arrowheads**). TUNEL- and PI-negative neuronal counts were calculated by subtracting the number of TUNEL- and PI-positive neurons, respectively, from the total neuronal count. Neurons were considered Thionin-positive if a clear, intact nucleus and dark nucleolus were surrounded by a darkly stained cytoplasm (**D**, **arrow**). Neurons were considered Thionin-negative “ghost” neurons if a nucleus and cytoplasm were visible and intact but devoid of stain (**D**, **asterisks**). Total neuronal number for Thionin-stained sections was calculated by adding Thionin-positive and Thionin-negative counts.

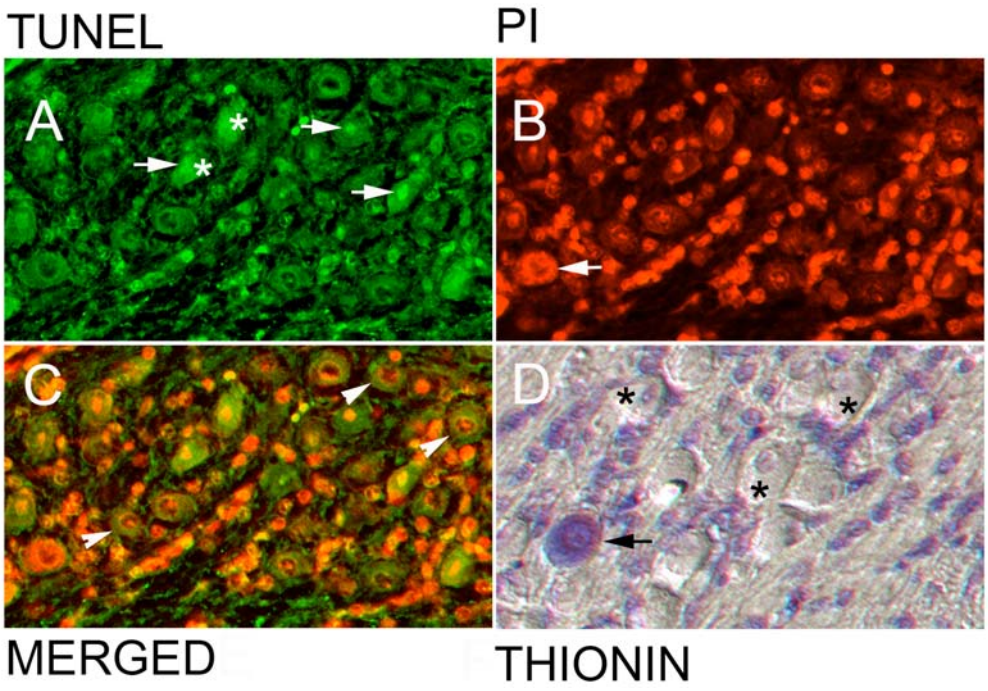
TUNEL
PI
A
B
C
D
MERGED
THIONIN

**Figure 2**: Photomicrographs of ipsilateral (**B, D**) and contralateral (**A, C**) sections through NM from an animal sacrificed 24 hours after unilateral cochlea removal. Adjacent sections are stained for cytochrome oxidase (CO) (**A,B**) and active caspase-3 (**C, D**). NM neurons ipsilateral to cochlea removal show intense CO staining throughout the nucleus (**B**) as well as a marked presence of active caspase-3 (**D**) compared to contralateral neurons (**A, C**). Scale bar = 200μm

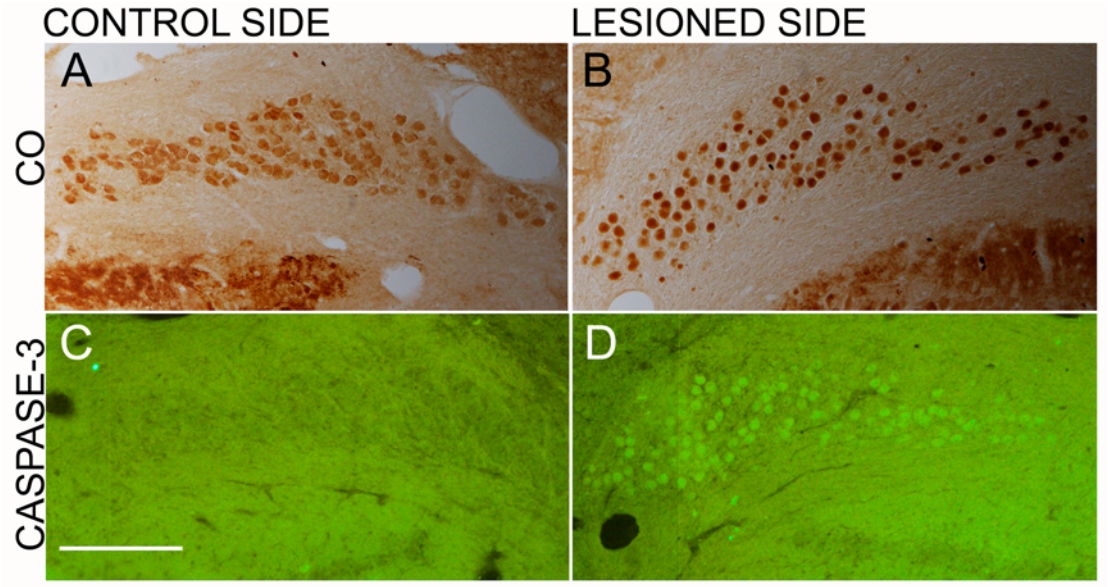
CONTROL SIDE
LESIONED SIDE
CO
CASPASE-3
A
B
C
D

**Figure 3:** Photomicrographs of ipsilateral (**B, D**) and contralateral (**A, C**) NM sections from an animal sacrificed 48 hours after unilateral cochlea removal. Adjacent sections are stained for cytochrome oxidase (CO) (**A,B**) and active caspase-3 (**C, D**). Particulate CO staining reveals degrading ipsilateral neurons in lateral NM (**B**) compared to contralateral neurons (**A**). Particulate active caspase-3 staining labels degrading ipsilateral neurons (**D**). Diffuse caspase-3 staining also labels surviving neurons in medial NM (**D**) with normal CO staining (**B**). Scale bar = 200μm

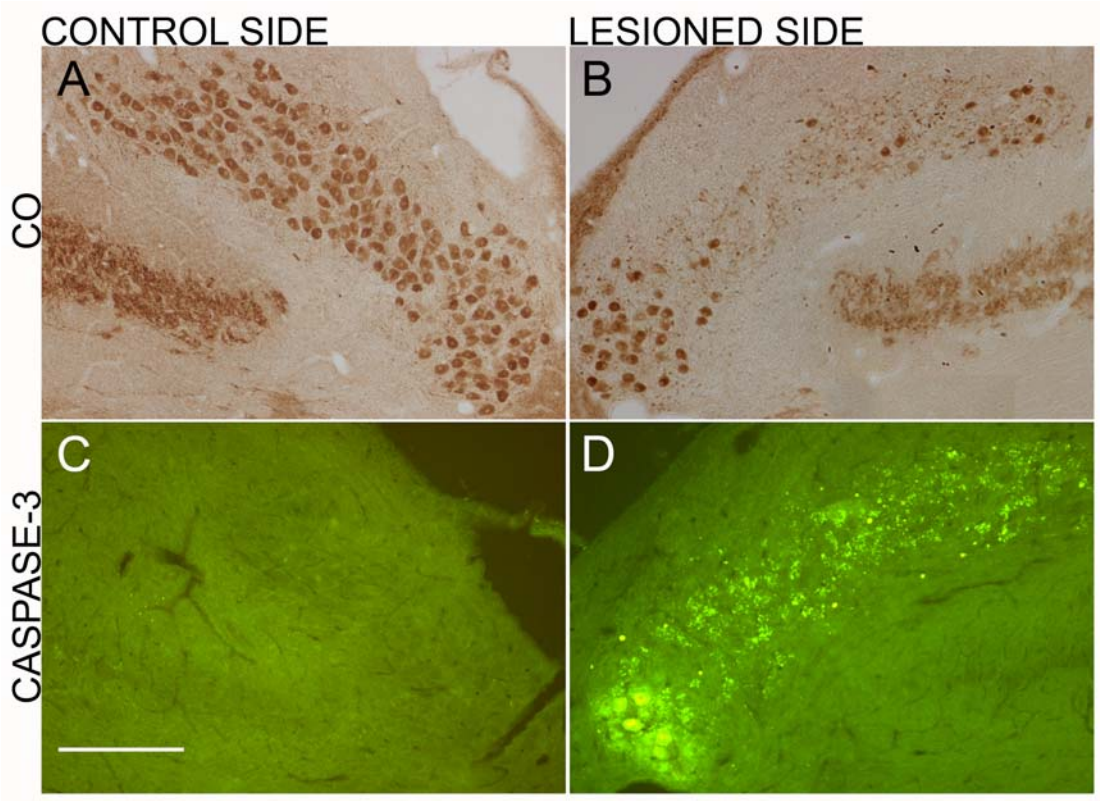
CONTROL SIDE
LESIONED SIDE
A
B
C
D
CO
CASPASE-3

**Figure 4:** Photomicrographs of ipsilateral (**B, D**) and contralateral (**A, C**) NM sections from an animal sacrificed 7 days after unilateral cochlea removal. Adjacent sections are stained for cytochrome oxidase (CO) (**A,B**) and active caspase-3 (**C, D**). Intense CO staining identifies only surviving ipsilateral neurons (**B**). All formerly degrading ipsilateral neurons have died by this point. Diffuse active caspase-3 staining persists in ipsilateral surviving neurons (**D**), but is completely absent from contralateral neurons (**C**). Scale bar = 200μm

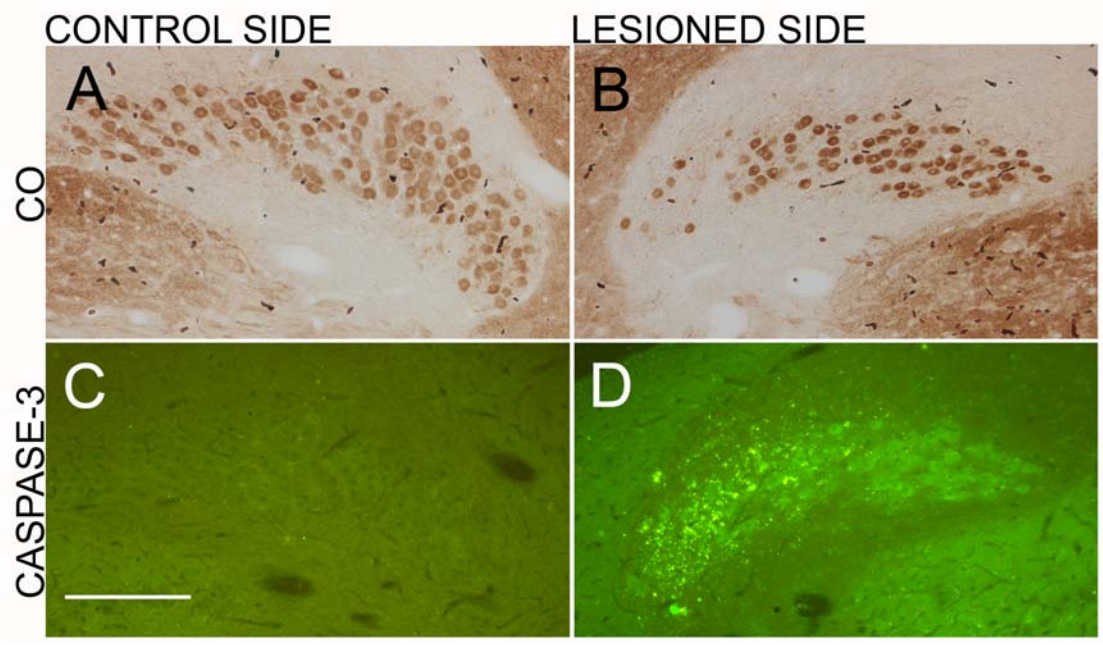
CONTROL SIDE
LESIONED SIDE
CO
CASPASE-3
A
B
C
D

**Figure 5:** Photomicrographs of ipsilateral (**B, D**, **F**) and contralateral (**A, C, E**) sections through rostral NM from an animal sacrificed 12 hours after unilateral cochlea removal. Adjacent sections are stained for Thionin (**A, B**) or PI (**C, D**) and TUNEL (**E, F**). "Ghost" neurons devoid of cytoplasmic Nissl substance show only nucleolar Thionin staining and demonstrate characteristic hollowed appearances under brightfield microscopy (**B, inset**) compared to contralateral neurons, which show intense cytoplasmic Thionin staining surrounding intact, visible nuclei (**A**). "Ghost" neurons do not stain with PI, while deafferented surviving neurons show intense PI staining (**D, inset**) similar to contralateral neurons (**C**). Some "ghost" neurons and glia show punctate TUNEL labeling within nuclei (**F, inset**). No TUNEL labeling is observed within contralateral neurons (**E**). Scale bar = 100$\mu$m

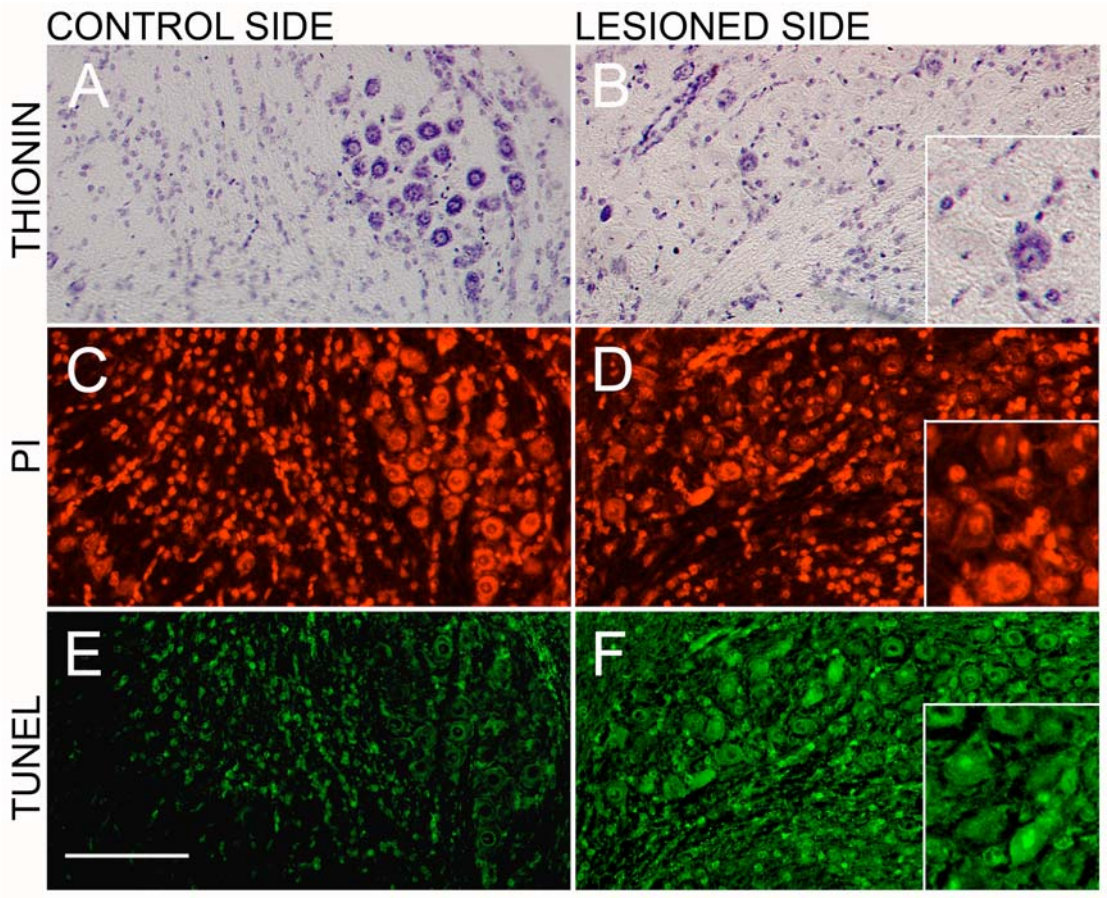
CONTROL SIDE
LESIONED SIDE
THIONIN
PI
TUNEL
A
B
C
D
E
F

**Figure 6:** Photomicrographs of ipsilateral (**B, D**, **F**) and contralateral (**A, C, E**) sections through rostral NM from an animal sacrificed 24 hours after unilateral cochlea removal. Adjacent sections are stained for Thionin (**A, B**) or PI (**C, D**) and TUNEL (**E, F**). Deafferented "ghost" neurons (**B**) do not stain with PI (**D**), but show diffuse cytoplasmic TUNEL labeling (**F**). Contralateral neurons stain intensely for Thionin (**A**) and PI (**C**) but do not stain for TUNEL (**E**). Scale bar = 100m

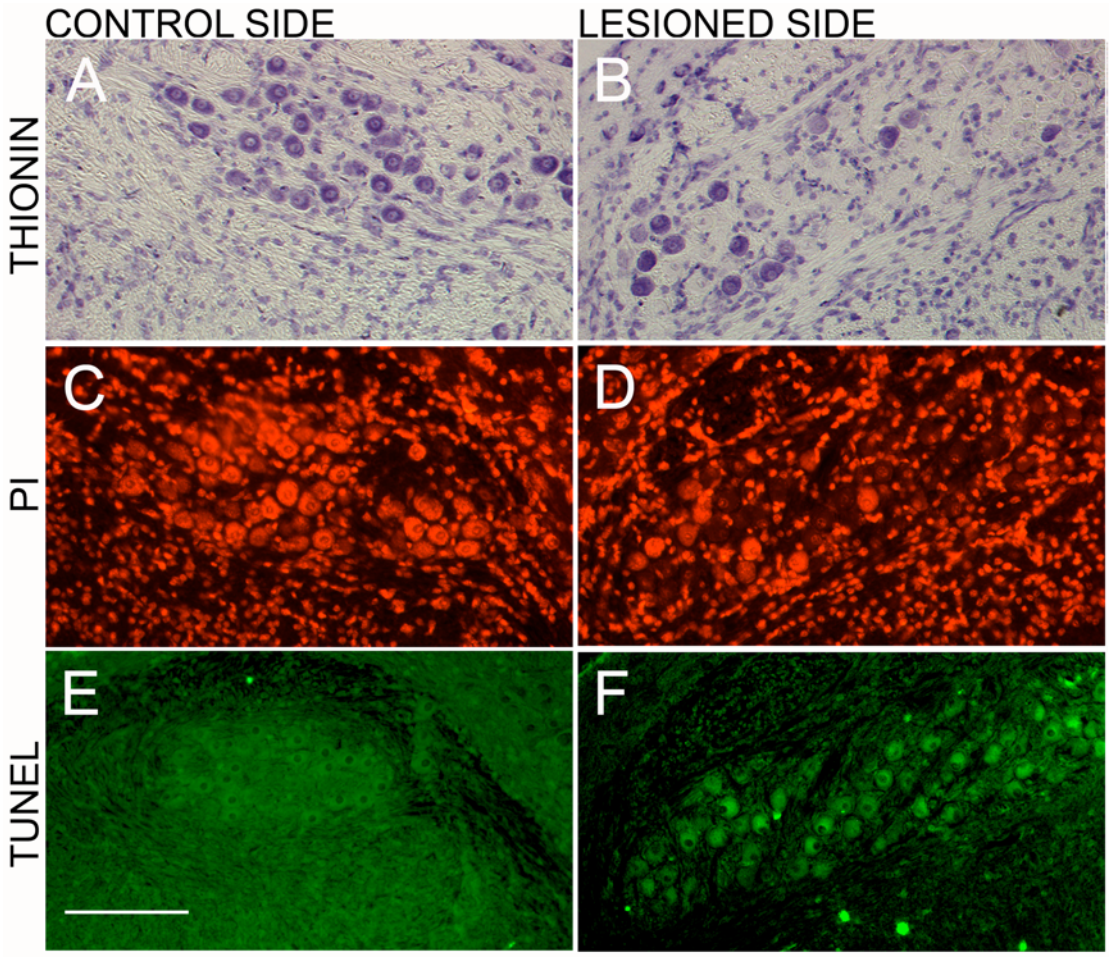
CONTROL SIDE
LESIONED SIDE
THIONIN
PI
TUNEL
A
B
C
D
E
F

**Figure 7:** Photomicrographs of ipsilateral (**B, D**, **F**) and contralateral (**A, C, E**) sections through rostral NM from an animal sacrificed 48 hours after unilateral cochlea removal. Adjacent sections are stained for Thionin (**A, B**) or PI (**C, D**) and TUNEL (**E, F**). Like the pattern observed at 24 hours, deafferented "ghost" neurons (**B**) do not stain with PI (**D**), but show robust TUNEL labeling throughout the cytoplasm (**F**). Contralateral neurons stain intensely for Thionin (**A**) and PI (**C**) but show no evidence of TUNEL labeling (**E**). Scale bar = 100μm

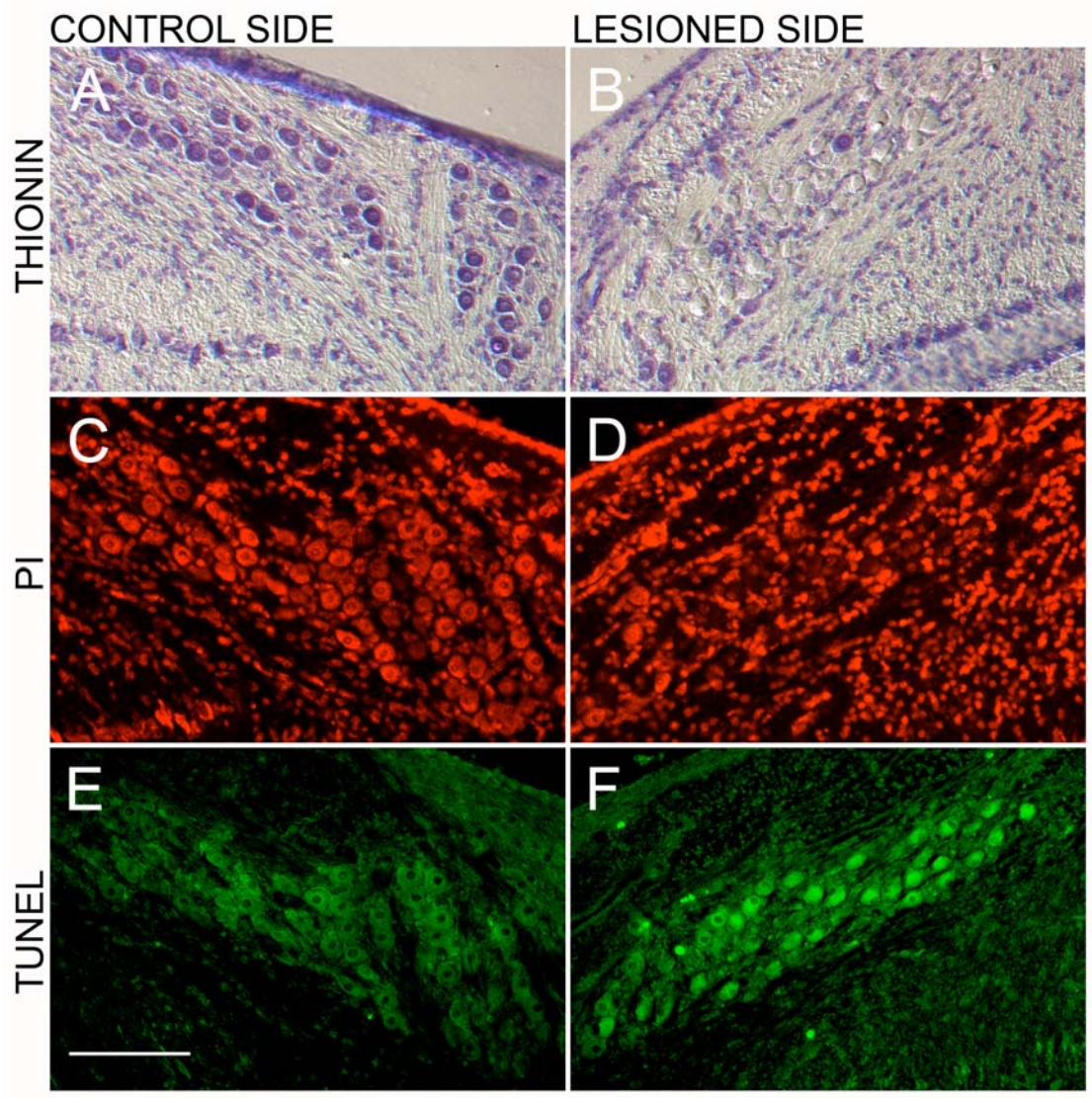
CONTROL SIDE
LESIONED SIDE
THIONIN
PI
TUNEL
A
B
C
D
E
F

**Figure 8:** Photomicrographs of ipsilateral (**B, D**, **F**) and contralateral (**A, C, E**) sections through rostral NM from an animal sacrificed 7 days after unilateral cochlea removal. Adjacent sections are stained for Thionin (**A, B**) or PI (**C, D**) and TUNEL (**E, F**). At this survival time, "ghost" neurons are no longer present in deafferented NM and only surviving neurons remain (**B**). Neurons that have survived deafferentation stain intensely with PI (**D**). TUNEL labeling persists only in some glial cells, but is absent from deafferented neurons (**F**). Scale bar = 100μm

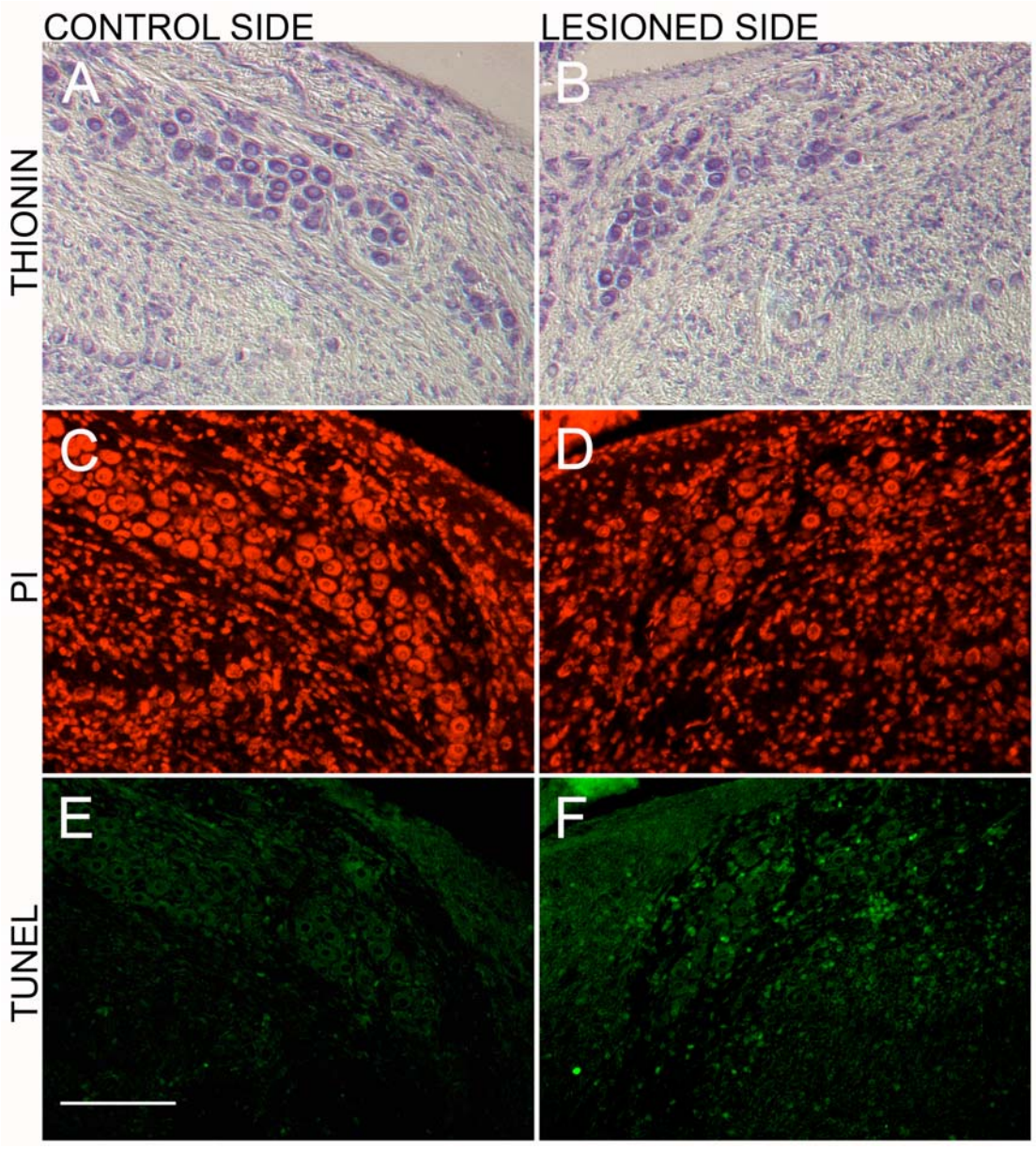
CONTROL SIDE
LESIONED SIDE
THIONIN
PI
TUNEL
A
B
C
D
E
F

**Figure 9:** Bar graph showing the average cell survival in the first quartile (Q1,black) and third quartile (Q3,gray) of NM as a function of Thionin-positivity across all survival times. Paired t-tests showed statistically higher cell survival in caudal NM (Q3) compared to rostral NM (Q1) at 12-hour ($p=0.0007$), 48-hour ($p=0.0226$), and 7-day ($p=0.0477$) survival times, suggesting a tonotopic pattern of cell loss that favors rostral NM. Two-way ANOVA and post-hoc analyses showed no differences in cell survival across survival times (Fisher's PLSD $p=0.1891$), suggesting that Thionin-negative "ghost" neurons appearing 12-48 hours following deafferentation accurately approximate the cell death that occurs by 7 days.

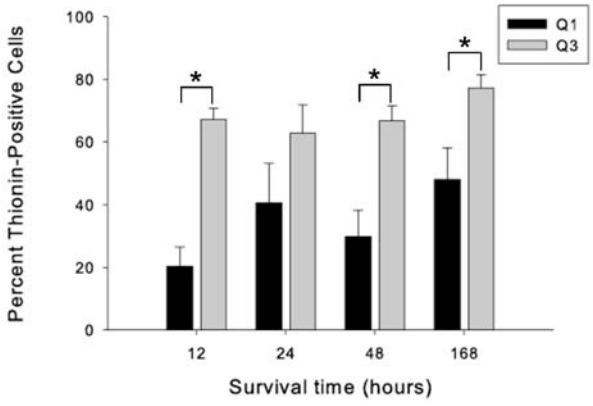
Percent Thionin-Positive Cells
100
80
60
40
20
0
Q1
Q3
*
*
*
12
24
48
168
Survival time (hours)

**Figure 10**

Graph correlating the percentage of neurons with nuclear TUNEL labeling to the percentage of “ghost” neurons in Thionin-stained sections in the rostral, first (Q1, open circles) and caudal, third (Q3, triangles) quartiles of NM. Throughout NM, more “ghost” neurons were present than were neurons with TUNEL-positive nuclei. r= 0.20,  line: y=x.

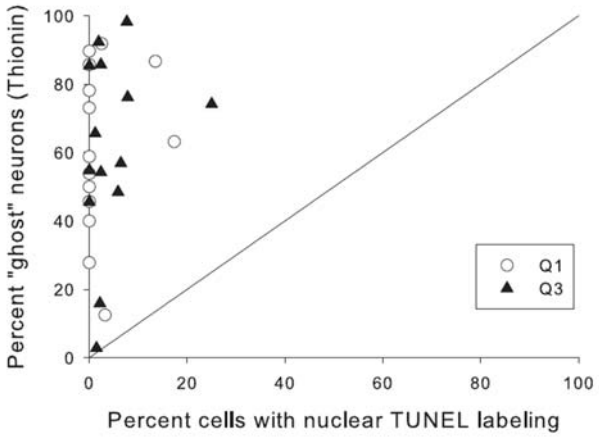
Percent "ghost" neurons (Thionin)
100
80
60
40
20
0
0
20
40
60
80
100
Percent cells with nuclear TUNEL labeling
Q1
Q3

**Figure 11**

Graph correlating the percentage of neurons with cytoplasmic TUNEL labeling to the percentage of “ghost” neurons in Thionin-stained sections in the first (Q1, open circles) and third (Q3, triangles) quartiles of NM. “Ghost ” neurons better correlated with cytoplasmic TUNEL labeling in neurons within rostral Q1 compared to caudal Q3. r= 0.57, line: y=x.

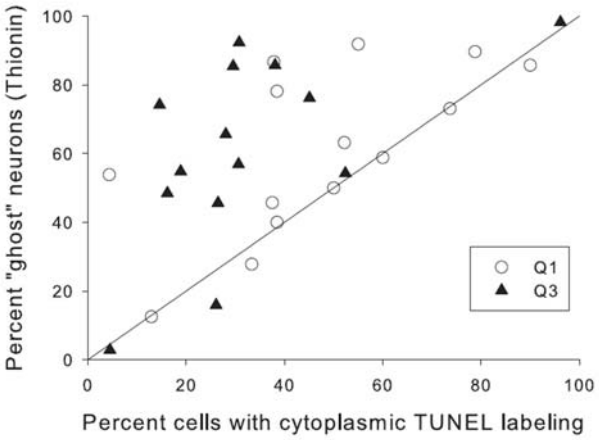
Percent "ghost" neurons (Thionin)
100
80
60
40
20
0
0
20
40
60
80
100
Percent cells with cytoplasmic TUNEL labeling
Q1
Q3

**Figure 12**

Graph correlating the percentage of neurons with loss of cytoplasmic propidium iodide (PI) labeling to the percentage of “ghost” neurons in Thionin-stained sections in the first (Q1, open circles) and third (Q3, triangles) quartiles of NM. Throughout NM, “ghost neurons” correlated relatively well with loss of PI labeling in neurons. r= 0.72, line: y=x

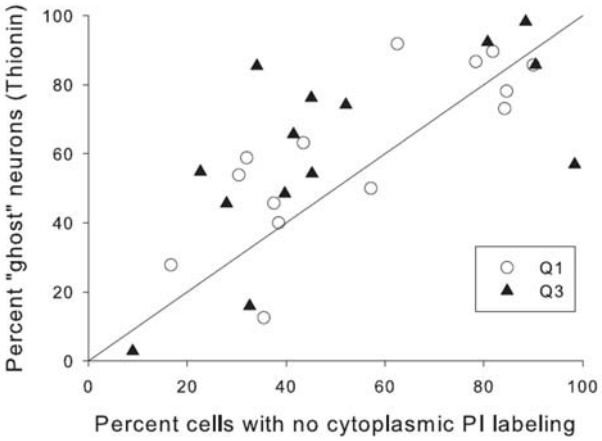
Percent "ghost" neurons (Thionin)
100
80
60
40
20
0
0
20
40
60
80
100
Percent cells with no cytoplasmic PI labeling
Q1
Q3

# CHAPTER III
# HISTOCHEMICAL AND FLUORESCENT ANALYSES OF MITOCHONDRIAL INTEGRITY IN CHICK AUDITORY NEURONS FOLLOWING DEAFFERENTATION

## Introduction

Determining mechanisms of cellular integrity is critical for understanding both physiologic and pathologic processes in living systems. In the nervous system, neuron number is rigorously regulated to ensure proper development and maintenance of neurologic function (Oppenheim, 1991). In response to traumatic or injurious stimuli, neurons, like most cells in the body, either rapidly adapt or undergo a program of self-destruction, the latter often producing devastating consequences (Honig and Rosenberg, 2000, Mattson, 2000, Martin, 2001, Friedlander, 2003, Vila and Przedborski, 2003). Elucidating the molecular events that modulate programmed neuronal death will provide valuable insight towards reversing or preventing the loss that accompanies neurological trauma or disease (Forman et al., 2004).

Second-order neurons in the chick auditory nucleus, nucleus magnocellularis (n. magnocellularis, NM), are exceptional models in which to study the cell death process (Rubel and Parks, 1988, Rubel et al., 1990, Rubel and Fritzsch, 2002). NM neurons represent a homogeneous population of sensory neurons (Rubel and Parks, 1975) whose sole source of excitatory input derives from eighth nerve afferents from the ipsilateral cochlea (avian basilar papilla) (Parks and Rubel, 1978). Cochlea removal

permanently disrupts the afferent signal to NM (Rubel et al., 1990, Born et al., 1991) and triggers a series of cellular perturbations across the entire population of deafferented neurons. Immediately following cochlea removal, electrical activity within NM ceases (Born et al., 1991). Within an hour, neuronal glucose utilization dramatically declines (Heil and Scheich, 1986, Born et al., 1991), and intracellular calcium levels rise (Zirpel et al., 1995, Zirpel and Rubel, 1996). By six hours, mitochondria proliferate across the deafferented nucleus (Hyde and Durham, 1994), perhaps as an attempt to offset rising calcium levels. At the same time, a subset of neurons develops signs of ultrastructural compromise, including vacuolization of mitochondria (Hyde and Durham, 1994), degradation of polyribosomes (Born and Rubel, 1985, Rubel et al., 1991), and loss of protein synthetic machinery (Steward and Rubel, 1985, Kelley et al., 1997, Lu et al., 2004). Two to five days later, the morphologically-compromised neurons (approximately 30-50% of the deafferented population) begin to degrade (Born and Rubel, 1985, Edmonds et al., 1999, Smittkamp et al., 2005, Karnes et al., 2009).

Although the entire population of NM neurons relies on excitatory, glutamatergic innervation from eighth nerve afferents, only a subset succumbs to death following afferent withdrawal. Cell-specific degradation of 30-50% of neurons is known to involve activation of the mitochondrially-mediated intrinsic apoptotic cascade: cytochrome *c*, active caspase-9 (Wilkinson et al., 2003), and active caspase-3 (Karnes et al., 2009) have been

detected in deafferented NM neurons. Interestingly, however, these apoptotic indicators are not specific to dying cells, a finding that suggests cell fate may ultimately be influenced by alternative pathways.

Recent work in our laboratory revealed the presence of fragmented DNA, via terminal deoxynucleotidyl transferase-mediated dUTP Nick-End Labeling (TUNEL), in deafferented NM neurons targeted to die (Karnes et al., 2009). Surprisingly, TUNEL accumulated in neuronal cytoplasm implicating fragmentation of mitochondrial DNA in the deafferentation-induced death process. Mitochondria are intimately involved in the neuronal response to deafferentation in NM (Durham and Rubel, 1985, Hyde and Durham, 1990, Garden et al., 1994, Hyde and Durham, 1994, Hartlage-Rubsamen and Rubel, 1996). It was our goal to further characterize how mitochondria influence neuronal fate in deafferented NM.

Here, we evaluated histochemical reaction products of three mitochondrial enzymes across deafferented NM: cytochrome oxidase (CO), succinate dehydrogenase (SDH), and ATP synthase (ATPase). Differential SDH and ATPase staining was observed across the deafferented nucleus, and preferentially increased levels of enzyme reaction products correlated well with neuronal death. In addition to measuring enzyme reaction product intensity, we utilized a marker of mitochondrial inner membrane potential ($\Delta\Psi_m$) to predict cell fate. $\Delta\Psi_m$ is directly linked to mitochondrial ATP production (Mitchell, 1961, Saraste, 1999, Scheffler, 2001). Consequently, an

irreversible loss of $\Delta\Psi_m$ has been shown to accompany apoptosis in several systems (Schinder et al., 1996, White and Reynolds, 1996, Wadia et al., 1998). We describe the loss of $\Delta\Psi_m$ within a subset of deafferented NM neurons undergoing mitochondrial DNA fragmentation and, subsequently, death.

## Materials and Methods

Animal preparation and surgery

Cornish Rock broiler chickens (Ross 308 x Ross 308) were obtained as day-old hatchlings from a commercial supplier (Welp Hatchery, Bancroft, IA) and were housed in communal brooders at the University of Kansas Medical Center Lab Animal Resources center with *ad libitum* access to food and water. Eight- (P8) to 12-day (P12) post-hatch chicks were anesthetized with intramuscular injections of Ketamine HCl (35mg/kg; Phoenix Pharmaceutical, Inc., St. Joseph, MO) and Xylazine (2mg/kg; Lloyd Laboratories, Shenandoah, IA) and subjected to unilateral cochlea (basilar papilla) removal, as described previously (Born and Rubel, 1985, Hyde and Durham, 1990). Briefly, the left tympanic membrane was punctured and the columella extracted. The cochlea was removed from the oval window aperture using fine forceps and was examined from base to apex under brightfield microscopy to ensure complete removal of the organ. Cochlea removal severs the peripheral processes of cochlear ganglion neurons, but leaves cell bodies intact (Born et al., 1991). The cochlear duct was aspirated following surgery, and animals were allowed to recover. Contralateral cochleae remained intact, and contralateral NM neurons served as within-animal controls.

To assess mitochondrial membrane potential ($\Delta\Psi_m$), unilaterally-operated birds were anesthetized as before 12 hours (n=6), 24 hours (n=9),

48 hours (n=6), or 7 days (n=4) following cochlea removal; treated topically with Lidocaine HCl (10mg/ml; Hospira, Inc., Lake Forest, IL) just above the odontoid process of the axis; and subjected to intrathecal injections of cold 0.5mM Mitotracker Red CMXRos (Molecular Probes, Eugene, OR) in dimethyl sulfoxide (DMSO) and 0.1M phosphate buffered saline (PBS, pH 7.4) containing 2.5% glycerol as described previously (Sekido and Lovell-Badge, 2007). Mitotracker Red is a positively-charged, fixable, fluorescent probe containing chloromethyl-X-rosamine (CMXRos) that is utilized to detect changes in $\Delta\Psi_m$ (Macho et al., 1996). Following intrathecal injection, animals were maintained under anesthesia for three hours at room temperature prior to sacrifice. All experimental protocols were approved by the University of Kansas Medical Center Institutional Animal Care and Use Committee (IACUC) and carried out in accordance with the National Institutes of Health Guide for the Care and Use of Laboratory Animals (NIH Publications No. 80-23). Every effort was made to minimize the number and suffering of all animal subjects.

Tissue preparation

Animals were sacrificed by intraperitoneal injections of Beuthanasia-D (Schering-Plough, Union, NJ) and decapitated 12 hours (n=8), 24 hours (n=7), 48 hours (n=10), and 168 hours (n=12) following cochlea removal for histochemical analyses, and 3 hours following intrathecal injections for

Mitotracker Red analyses. For histochemical evaluation of mitochondrial enzyme reaction product accumulation, brains were extracted and rapidly frozen in heptane cooled by dry ice. Brainstems were sectioned coronally through nucleus magnocellularis (n. magnocellularis, NM), and 20μm sections were mounted serially onto four series of slides, which were subsequently reacted for Thionin, succinate dehydrogenase (SDH), cytochrome oxidase (CO), or ATP synthase (ATPase), respectively. Slides were stored at -20°C or stained immediately. For Mitotracker Red analyses, animals were perfused intracardially with Avian Ringer's solution (2M NaCl, 2M KCl, 2M $MgCl_2$, and 100mM ethylenediaminetetraacetic acid (EDTA)) in PBS, and brains were removed, post-fixed for six hours in modified Carnoy's fixative (containing ethanol, chloroform, Avian Ringer's, and glacial acetic acid), stored overnight in 70% ethanol, and embedded in paraffin as previously described (Lurie and Durham, 2000).

Histologic examination of mitochondrial enzymes

*Thionin staining:* Frozen slide-mounted sections were defatted in xylenes, rehydrated through graded ethanols to 50% ethanol, and rinsed briefly in distilled water. Sections were then stained in 1% Thionin working solution, consisting of Thionin acetate (Sigma, St. Louis, MO), glacial acetic acid, and 1M NaOH. Stained sections were rinsed twice in distilled water, dehydrated through graded ethanols to 100% ethanol, washed in xylenes at least twice,

and coverslipped with DPX mounting medium (VWR International Ltd., Poole, UK).

*SDH staining:* Sections were reacted for SDH activity as described previously (Nachlas et al., 1957, Durham and Rubel, 1985). Briefly, sections were stained in a solution (per 25ml) of 0.05M phosphate buffer (pH 7.4), 0.338g succinic acid, and 10.2mg nitro blue tetrazolium (Sigma, St. Louis, MO) for 10 minutes at 37°C. Sections were then immersed in 10% buffered formalin for at least one hour, and dehydrated through graded ethanols and xylenes prior to coverslipping with DPX mounting medium.

*CO staining:* Sections were reacted for CO activity as described previously (Wong-Riley, 1979, Hyde and Durham, 1990). In brief, slide-mounted sections were immersed in a solution containing (per 100ml): 50mg 3,3'-diaminobenzidine tetrahydrochloride (DAB; Sigma, St. Louis, MO), 20mg cytochrome *c*, and 4g sucrose in 0.1M PBS (pH 7.4) for 40 minutes at 37°C. Sections were then washed three times in PBS, dehydrated through graded ethanols and xylenes, and coverslipped with DPX mounting medium.

*ATPase staining:* Sections were reacted for ATPase enzyme activity as described previously (Meijer and Vloedman, 1980). In brief, sections were immersed in cold (4°C) acetone for 5 minutes, then stained with freshly

prepared ATPase staining solution, containing (per 100ml): 50 mg adenosine triphosphate (ATP; Sigma, St. Louis, MO), 40ml 0.2M Tris maleate buffer (Tris maleate, Tris base, and 10N NaOH in distilled water, pH 7.4), 35.2mg dinitrophenol (Sigma, St. Louis, MO), 6ml 0.06M lead nitrate, and 10ml 0.05M magnesium chloride in distilled water for 10 minutes at 37°C. Sections were rinsed with Tris maleate buffer and immediately washed for one minute in 1% ammonium sulfide. Sections were then dehydrated through graded ethanols, washed three times in xylenes, and coverslipped with DPX mounting medium.

TUNEL labeling of fragmented DNA

To directly evaluate the relationship between $\Delta\Psi_m$ and cell death in deafferented NM, brainstem sections from animals injected with Mitotracker Red were co-labeled with TdT-mediated dUTP Nick-End Labeling (TUNEL). Double labeling with CMXRos-conjugated dyes and TUNEL has been successfully demonstrated elsewhere (Macho et al., 1996). TUNEL identifies fragmented DNA in cells undergoing apoptosis (Gavrieli et al., 1992). Coronal paraffin-embedded sections through NM were cut at 10μm on a microtome and saved as ribbons. Sections at the 50$^{th}$ percentile along the anterior to posterior extent of NM were reacted for TUNEL using Promega's DeadEnd Fluorometric TUNEL System (Promega Corporation, Madison, WI) as described previously (Karnes et al., 2009) according to the manufacturer's instructions. Briefly, sections were deparaffinized through xylenes and

rehydrated through graded ethanols. Sections were washed in 0.85% NaCl followed by PBS, and fixed in 4% paraformaldehyde. Neurons were permeabilized with 20μg/ml Proteinase K, washed in PBS, and equilibrated in the kit's Equilibration Buffer. Sections were incubated with rTdT enzyme, nucleotide mix, and Equilibration Buffer in a humidity chamber in the dark for one hour. Following incubation, sections were immersed in 1x SSC (150mM NaCl and 15mM sodium citrate) buffer and washed in PBS and distilled water prior to coverslipping with Vectashield antifade mounting medium (Vector Laboratories, Burlingame, CA).

Image Acquisition

SDH, CO, and ATPase are mitochondrial enzymes involved in oxidative metabolism and energy generation within the cell. Levels of these enzymes directly correlate with changes in cellular metabolic demand (Stryer, 1995). Consequently, changes in histologic staining intensities have been used to interpret the metabolic status of respiring cells (Wong-Riley, 1979, Meijer and Vloedman, 1980, Vladutiu and Heffner, 2000). Optical densities (OD) of SDH, CO, and ATPase reaction products were measured in individual NM neurons and compared across survival times using methods similar to those described elsewhere (Hyde and Durham, 1990, Smittkamp et al., 2003). Briefly, neurons within the 50$^{th}$ percentile along the anterior to posterior frequency axis of NM were visualized under brightfield Köhler

illumination at 40x magnification and photographed using a Nikon Digital Sight DS-Fi1 high-definition color camera (Nikon Instruments, Inc., Melville, NY) and NIS-Elements F-3.0 software (Nikon Instruments, Inc., Melville, NY). All photos were acquired using identical illumination parameters.

Tonotopic patterns of glucose metabolism and cell loss (Smittkamp et al., 2005, Karnes et al., 2009) have been previously described in NM; to avoid confounding our results, we restricted analyses to neurons within the 50$^{th}$ percentile of NM, where neuronal responses to deafferentation have been well characterized (Rubel and Parks, 1975). For each section from a given animal, photomicrographs on both sides of the brainstem were acquired from NM. All photomicrographs were collected by an individual blind to the treatment and duration of survival. Photomicrographs through each NM tissue section were merged to create montages of each auditory nucleus, and montaged images were magnified an additional 100x and analyzed using Photoshop CS3 Extended (Adobe, San Jose, CA), which is equipped with scientific and analytic image analysis software.

For analysis of TUNEL and Mitotracker Red staining, NM sections were visualized using a Nikon Digital Eclipse C1Si confocal microscope system (Nikon Instruments, Inc., Melville, NY) under 40x oil magnification. Photomicrographs were acquired using a Nikon Digital Sight DS-Fi1 high-definition color camera and NIS-Elements F-3.0 software.

Data analysis

*Analysis of histologic enzyme reaction product*

For each NM montage, OD measurements of ATPase, CO, and SDH reaction products were acquired in individual neurons (in a medial to lateral progression) until at least 50 neurons per nucleus were measured. A stylus connected to a Tablet PC computer was used to trace the outline of each neuronal cytoplasm (excluding the non-staining nucleus), and a mean grayscale value was measured for each neuron.

To convert mean grayscale values to OD measurements, a standard curve was generated. Eight optical standards of a calibrated step tablet (The Tiffen Company, Hauppauge, NY) were photographed using the same illumination parameters as those used to acquire NM images, and corresponding mean grayscale values were measured. These values were plotted against the known OD values for which they were calibrated, and a standard curve was generated using Microsoft Excel (Microsoft, Seattle, WA). A trend line was fitted to the standard curve, and the equation used to convert mean grayscale values from NM neurons to OD measurements.

To compare OD measurements from different animals at a given survival time, OD values were normalized. For each animal, the mean and standard deviation of OD values from contralateral NM neurons were calculated, and Z-scores were determined using the following formula:

Z = (OD - mean contralateral OD) / (standard deviation of contralateral OD)

Z-scores were generated for all ipsilateral and contralateral OD values from NM neurons. Z-scores for all animals at a given survival time were plotted as histograms using DeltaGraph 5 (Red Rock Software, Inc., Salt Lake City, UT), and the shapes of histograms were evaluated for differences in enzymatic activity as a function of survival time. All OD measurements were collected by an individual blind to the experimental manipulation and duration of survival.

*Neuronal counts*

To determine numbers of neurons within NM at seven days, neurons with visible and intact nuclei and with enzymatic reaction products present in the cytoplasm were quantified in contralateral and ipsilateral NM from the same tissue section using photo montages. Percentages of cell loss were derived using the following formula: ((# neurons in contralateral NM - # neurons in ipsilateral NM) / # neurons in contralateral NM) x 100%. The mean percentage of cell loss at seven days was calculated for each enzymatic stain using SigmaStat 3.5 (SYSTAT Software, Inc., San Jose, CA).

*Statistical analyses*

To compare differences in CO reaction product intensity between ipsilateral and contralateral brainstem nuclei, the mean OD value (from each CO-stained nucleus) at every survival time was calculated using Microsoft Excel (Microsoft, Seattle, WA). Unpaired *t*-tests were performed using SigmaStat 3.5 (SYSTAT Software, Inc., San Jose, CA) to compare mean OD values for CO activity per animal across survival times. Differences were deemed significant if p-value<0.05.

To compare differences in SDH and ATPase reaction product intensities in ipsilateral versus contralateral NM neurons, ipsilateral neurons were first categorized based on their Z-score OD value. For SDH and ATPase stains, ipsilateral neurons with a Z-score ≥ 2 were assigned to one group, while neurons with a Z-score < 2 were assigned to a second group. This arbitrary partition was determined by visually examining the distributions of OD histograms. OD values from each ipsilateral group, as well as OD values from contralateral NM, for both stains (SDH and ATPase) were compared using a Kruskal Wallis one-way analysis of variance (ANOVA) on ranks, followed by a series of pair-wise, post-hoc comparisons using Dunn's Method.

## Results

Deafferentation-induced changes in histochemical enzyme activities

Deafferentation by cochlea removal incites a cascade of events in auditory brainstem nucleus magnocellularis (NM) that ultimately produces death in 30-50% of ipsilateral neurons (Born and Rubel, 1985, Edmonds et al., 1999, Karnes et al., 2009). NM neurons destined to die show early signs of cell compromise, including ribosomal disassembly and degradation of rough endoplasmic reticulum (ER); consequently, Thionin staining of ribosomal Nissl substance has been used to distinguish dying from surviving neurons in deafferented NM (Born et al., 1991, Rubel et al., 1991). Neurons that stain poorly with Thionin, so-called "ghost" neurons, represent the subpopulation of deafferented neurons that will die following cochlea removal (Karnes et al., 2009). Figure 1 reveals the characteristic Thionin staining pattern in NM from an animal sacrificed 24 hours after cochlea removal (Figure 1A, B). Note the marked presence of Nissl substance throughout the cytoplasm of unperturbed, contralateral NM neurons: nucleoli and cytoplasm stain intensely for Thionin, while the intact nucleus is devoid of stain (Figure 1A). In ipsilateral NM, Thionin-positive neurons are present as are an abundant number of Thionin-negative "ghost" neurons (Figure 1B, inset). To assess differences in mitochondrial function between deafferented, surviving NM neurons and deafferented, dying NM neurons, we stained adjacent sections for succinate dehydrogenase (SDH) (Figure 1C, D), cytochrome

oxidase (CO) (Figure 1E, F), and ATP synthase (ATPase) (Figure 1G, H) and compared staining intensities of enzyme reaction products throughout the nucleus. Previous reports in NM have shown global oxidative upregulation early following cochlea removal (Durham and Rubel, 1985, Hyde and Durham, 1990). The profile of "ghost" neurons corresponds well with the subset of deafferented neurons that preferentially elevates SDH (Figure 1D) and ATPase (Figure 1H) reaction products. Interestingly, all NM neurons ipsilateral to cochlea removal exhibit unimodally elevated levels of CO (Figure 1F) compared to contralateral, unperturbed neurons (Figure 1E). The widespread upregulation of CO across the deafferented nucleus accompanies the marked expansion of mitochondria (Hyde and Durham, 1994). The differential staining intensities for SDH and ATPase across the deafferented nucleus suggest that mitochondrial functional differences exist between dying, "ghost" neurons and surviving, Thionin-positive neurons.

SDH histochemistry

SDH is the catalytic enzyme comprising complex II of the mitochondrial electron transport chain (ETC) (Saraste, 1999). SDH is a multi-subunit protein, entirely derived from nuclear-encoded DNA, which is responsible for transferring electrons from $FADH_2$, a tricarboxylic acid (TCA) cycle intermediate, to ubiquinone for entry into the ETC (Stryer, 1995, Saraste, 1999). Interestingly, this activity directly links SDH to the TCA cycle, as well as the ETC (Scheffler, 2001, Foster et al., 2006).

Intensity of SDH reaction product has been used as a qualitative histochemical indicator to assess mitochondrial integrity in auditory neurons (Durham and Rubel, 1985) and other systems (Rivner et al., 1989, Reichmann and Wildenauer, 1991, Taylor et al., 1996, Vladutiu and Heffner, 2000). SDH activity is known to rapidly increase in deafferented NM neurons and gradually decline after cochlea removal (Durham and Rubel, 1985). Comparison of median OD values ipsilateral and contralateral to cochlea removal using the Kruskal-Wallis one-way ANOVA on ranks across all time points suggests significant deafferentation-induced differences in SDH activity ($H= 1052.793$, 11 degrees of freedom, p-value $\leq 0.001$). Interestingly, however, prior reports of SDH activity in NM, using less precise methods of OD measurement, showed relatively uniform enzymatic levels across all deafferented neurons (Durham and Rubel, 1985). Our results, using a more sensitive method for OD measurement, suggest otherwise. Figure 2 illustrates a bimodal distribution of SDH reaction product intensity in NM neurons ipsilateral to cochlea removal. Twelve to 24 hours after deafferentation, ipsilateral NM neurons (blue bars) separate into two distinct categories based on their staining intensity for SDH: (1) those with median SDH OD values comparable (12 hours=0.313; 24 hours=0.463) to that of contralateral neurons (12 hours= 0.00677; 24 hours=0.00916) and (2) those with significantly (p-value<0.05) elevated median SDH OD values (12 hours=2.89; 24 hours=2.779) compared to contralateral neurons (Figure 1D

and Figure 2A and 2B). By 48 hours, when 30-50% of deafferented NM neurons begin to degrade, SDH staining intensity declines in ipsilateral NM and shifts towards a unimodal distribution of enzyme activity (Figure 2C). By seven days, SDH levels in ipsilateral neurons have declined, although a bimodal distribution of SDH staining intensity persists (Figure 2D). Previous reports, using less precise measurements of SDH reaction product, demonstrated a reduction in SDH activity 3-35 days following cochlea removal (Durham and Rubel, 1985). Our results suggest that the population of ipsilateral neurons that survives deafferentation is transitioning to a reduced metabolic state, although at the last time point examined, deafferented neurons exhibit a wide range of OD values compared to contralateral neurons (Figure 2D). Examination at lengthier survival times should reveal an overall reduction in SDH staining intensity as has been previously described (Durham and Rubel, 1985).

To assess percent neuronal loss, the number of neurons reacting positively for SDH was compared in ipsilateral and contralateral NM at 7 days. On average, 31.0±12.9% of deafferented neurons underwent cell death. To determine whether NM neurons with increased SDH staining at 12 and 24 hours represented the population eventually targeted to die, we calculated the average number of ipsilateral neurons with OD Z-scores ≥ 2 at 12- and 24-hour survival times to be 29.3% and 29.4%, respectively. Our results suggest that neurons destined to die experience early upregulation of SDH levels

compared to adjacent ipsilateral NM neurons that survive deafferentation. This preferential increase in SDH activity within deafferented, dying neurons may occur due to increased utilization of the TCA cycle (see Discussion).

CO histochemistry

CO is a large, multi-subunit protein that comprises complex IV of the mitochondrial ETC (Saraste, 1999). CO histochemistry has been used extensively to examine mitochondrial integrity in a variety of systems (Wong-Riley et al., 1981, Kennedy et al., 1985, Wong-Riley et al., 1989, Hevner et al., 1995) including NM (Hyde and Durham, 1990). Here, we examined CO reaction product in NM neurons ipsilateral and contralateral to cochlea removal over a time course of 12 hours to seven days. As has been described previously, CO reaction product in deafferented NM (blue bars) increases significantly compared to contralateral neurons (orange bars) (*t*-test, p-value=0.009) as early as 12 hours following cochlea removal (Figure 3A). By 48 hours, the average OD of CO reaction product is not significantly different than in contralateral neurons (*t*-test, p-value=0.222) (Figure 3C). By seven days, there is a reduction in the number of neurons ipsilateral to cochlea removal (42.0%±3.9), consistent with the cell death that is known to occur by this time, but no appreciable difference in CO activity exists between ipsilateral and contralateral brainstem nuclei. This finding contradicts a previous report describing reductions in CO activity within deafferented

versus contralateral NM neurons three to 14 days after cochlea removal (Hyde and Durham, 1990). Interestingly, however, both ipsilateral and contralateral neurons exhibit relatively normal, unimodal OD distributions of CO reaction product accumulation (Figure 3), indicating that all deafferented neurons within NM exhibit similar demands for CO, albeit at higher levels than in contralateral neurons.

ATPase histochemistry

ATPase is an $F_0$-$F_1$ protein complex embedded within the inner mitochondrial membrane, which comprises complex V of the ETC, and which utilizes the electrochemical gradient of $H^+$ generated by complexes I-IV to synthesize ATP (Abrahams et al., 1994, Stryer, 1995, Junge et al., 1997, Saraste, 1999). The final step in oxidative phosphorylation, ATPase directly couples the electrochemical gradient to energy generation (Mitchell, 1961). As a consequence, ATPase is the central enzyme in mitochondrial energy conversion (Abrahams et al., 1994), and its integrity is crucial to aerobically-respiring cells, particularly those, like neurons, that rely almost exclusively on oxidative metabolism (Almeida et al., 2004, Knott et al., 2008, Pope et al., 2008). Disruption of the electrochemical gradient, and subsequent uncoupling of ATP synthesis, is known to trigger cell death in several systems (Schinder et al., 1996, White and Reynolds, 1996, Wadia et al., 1998).

The histochemical staining solution used to detect the coupling state of mitochondrial ATPase includes the known uncoupler dinitrophenol. Figure 1 illustrates the characteristic staining pattern for ATPase in contralateral NM (Figure 1G) and ipsilateral NM (Figure 1H) 24 hours following cochlea removal. Note that ATPase reaction product is located cytoplasmically, as expected for a mitochondrial enzyme, but neuronal nuclei are unstained. OD measurements of ATPase reaction product in contralateral NM show a relatively normal, unimodal distribution of staining intensities (Figure 4, orange bars). In deafferented NM neurons ipsilateral to cochlea removal, average ATPase levels are increased compared to contralateral neurons (Kruskal-Wallis ANOVA on ranks: $H=661.241$, 11 degrees of freedom, p-value$\leq 0.001$) (Figure 1H, Figure 4, blue bars), indicative of mitochondrial distress throughout the nucleus. As early as 24 hours, two neuronal populations with different levels of ATPase staining emerge in deafferented NM: one with a median OD value (0.224) similar to that of contralateral neurons (0.0405), and one with a significantly ($p<0.05$) greater median OD value (2.722) compared to contralateral neurons (Figure 1H, Figure 4B). By 48 hours, as the number of ipsilateral neurons undergoing mitochondrial uncoupling increases, pronounced differences in staining intensity are evident in the deafferented nucleus: ipsilateral NM neurons with less intense ATPase reaction product (median OD value=0.649) is significantly ($p<0.05$) different from ipsilateral, “uncoupled” NM neurons (median OD value=3.134) (Figure

4C). The number of ipsilateral neurons with Z-scores ≥ 2 at 48 hours (38.6%) approximate the number of neurons that die by seven days (39.8±14.0%); thereby, suggesting that deafferented neurons which undergo ATPase uncoupling represent the subset that dies following deafferentation.

Mitotracker Red

Mitotracker Red is a fluorescent, cationic, lipophilic dye that measures qualitative fluctuations in mitochondrial membrane potential ($\Delta\Psi_m$) in fixed tissues (Macho et al., 1996). $\Delta\Psi_m$ relies on the existence of a proton gradient across the inner mitochondrial membrane, which contributes to a mitochondrial matrix that is negative relative to the cell cytoplasm (Gunter et al., 1994, Lemasters et al., 1995, Macho et al., 1996, Mostafapour et al., 1997). Like other indicators of $\Delta\Psi_m$ (e.g. rhodamine 123, cationic cyanine dyes, and safranine 0), Mitotracker Red passively diffuses across the plasma membrane and subsequently accumulates within the negatively-charged inner membrane of intact mitochondria, where it is partially quenched (Johnson et al., 1980, Mostafapour et al., 1997, Nicholls and Budd, 2000, Buckman et al., 2001). Following mitochondrial depolarization, or loss of $\Delta\Psi_m$, the dye redistributes from the mitochondrial matrix to the cytoplasm, where it is dequenched, and visualized by an increase in fluorescence intensity (Johnson et al., 1980, Johnson et al., 1981, Mostafapour et al., 1997, Nicholls and Budd, 2000).

Although our methods do not allow visualization of $\Delta\Psi_m$ reversal *in situ*, our results demonstrate that Mitotracker Red staining intensity corresponds well with cell death. Intact mitochondria, with negatively-maintained membrane potentials, accumulate Mitotracker Red from the cytoplasm and do not fluoresce; accordingly, intact NM neurons in contralateral (Figure 5A) and in the lateral region of ipsilateral NM (Figure 5B) exhibit no evidence of Mitotracker Red illumination. In contrast, deafferented NM neurons destined to die contain dysfunctional mitochondria, which have already undergone $\Delta\Psi_m$ reversal. These depolarized mitochondria cannot accumulate Mitotracker Red and consequently, exhibit intense cytoplasmic fluorescence as early as 24 hours after cochlea removal (Figure 5B). The intense Mitotracker Red fluorescence is observed in the subset of deafferented neurons also undergoing mitochondrial DNA fragmentation, as evidenced by TUNEL labeling (Figure 5B and 5D). This correlative pattern persists 48 hours following deafferentation (data not shown), but is gone at seven days when cell death is complete (Figure 5F and 5H). These results demonstrate that $\Delta\Psi_m$ reversal precedes cell death.

In summary, we have shown that mitochondrial function is impaired in the subset of deafferented NM neurons destined to die. SDH, CO, and ATPase activities are globally elevated in ipsilateral NM neurons compared to contralateral control neurons (Figures 1, 2, 3, and 4). Furthermore, differences in SDH and ATPase activities emerge within deafferented NM as

early as 12 hours and 24 hours, respectively, following cochlea removal (Figure 2 and Figure 3). This demonstrates that early alterations in mitochondrial function may selectively identify neurons susceptible to deafferentation-induced cell death. In addition, we have shown that NM neurons destined to die undergo mitochondrial uncoupling and loss of $\Delta\Psi_m$ (Figure 1H, Figure 4, Figure 5B).

## Summary and Discussion

Mitochondria are required by all respiring cells for maintenance of cellular integrity (Stryer, 1995, Saraste, 1999, Scheffler, 2001, Brookes et al., 2004). In the nervous system, in particular, mitochondrial oxidative phosphorylation is critical for neuronal energy production, as the latter cannot occur via glycolytic pathways (Almeida et al., 2004, Knott et al., 2008, Pope et al., 2008). In addition to ATP generation, neuronal mitochondria play direct roles in chaperone protein folding (Szabadkai and Rizzuto, 2007), axonal transport (Morris and Hollenbeck, 1993, Overly et al., 1996, Baloh, 2008), reactive oxygen species (ROS) production (Stewart and Heales, 2003, Pope et al., 2008), maintenance of plasma membrane potential (Knott et al., 2008), and perhaps most importantly, calcium regulation (Nishikawa et al., 2000, Green et al., 2004), including control of synaptic neurotransmission (Ly and Verstreken, 2006, Mattson, 2007). Mitochondria are also direct activators of intrinsic apoptosis in response to specific cellular stressors (Liu et al., 1996, Susin et al., 1999, Yuan and Yankner, 2000, Danial and Korsmeyer, 2004).

In nucleus magnocellularis (NM) brainstem auditory neurons, mitochondria are clearly involved in the cellular response to deafferentation. Previous studies revealed significant morphological changes in neuronal mitochondria, including rapid proliferation across the entire deafferented nucleus (Hyde and Durham, 1994); ultrastructural vacuolization within the neuronal subset also undergoing ribosomal degradation and endoplasmic

reticulum fragmentation (Born and Rubel, 1985, Rubel et al., 1991, Hyde and Durham, 1994, Hartlage-Rubsamen and Rubel, 1996); and loss of mitochondrial DNA integrity in NM neurons destined to die (Karnes et al., 2009). Here, we demonstrate disturbances in mitochondrial functional status in deafferented neurons, a direct corollary to the previously described alterations of mitochondrial structure.

Succinate dehydrogenase (SDH) and cytochrome oxidase (CO) upregulation have been noted previously in deafferented NM neurons (Durham and Rubel, 1985, Hyde and Durham, 1990); however, this is the first report of ATP synthase (ATPase) upregulation, observed as early as 24 hours, and peaking 48 hours, following cochlea removal (Figure 4). In addition, we describe a novel distribution of staining intensities for SDH and ATPase reaction products across NM, a finding that implies differential enzyme activity in dying versus surviving neurons (Figures 2 and 4). Finally, we demonstrate that mitochondrial membrane potential status ($\Delta\Psi_m$) can be assessed in fixed NM tissue sections, and that a loss of $\Delta\Psi_m$ occurs in neurons undergoing mitochondrial DNA degradation prior to dying (Figure 5). In the paragraphs that follow, we (1) describe the significance of our results in the context of our model system and (2) propose a mechanism underlying cell fate determination in deafferented NM neurons.

Deafferentation of chick NM by cochlea removal triggers a cascade of cellular events producing death in 30-50% of ipsilateral neurons (Born and

Rubel, 1985, Edmonds et al., 1999). Cochlea removal permanently disrupts delivery of glutamate to NM (Nemeth et al., 1983, Jackson et al., 1985, Martin, 1985, Zhou and Parks, 1992a, Zhou and Parks, 1992b), which in turn, abruptly reduces the activity of metabotropic glutamate receptors (Lachica et al., 1995, Zirpel and Rubel, 1996, Hyson, 1998, Nicholas and Hyson, 2004). Glutamate receptor activity is in delicate balance with calcium regulation; thus, perturbations in glutamate signaling create calcium fluxes in NM neurons and lead to a sizable increase in intracellular calcium (Lachica et al., 1995, Zirpel and Rubel, 1996, Zirpel et al., 1998, Kato and Rubel, 1999). The source of this calcium influx remains undetermined, but has been speculated to derive from AMPA receptor activation by residual glutamate (Zirpel et al., 2000b), N-type voltage-gated calcium channels at the plasma membrane (Lu and Rubel, 2005), or release from internal stores (Lachica et al., 1995).

Intracellular calcium accumulation, beyond a certain threshold, is detrimental to neurons (Choi, 1988, Zirpel et al., 2000b, Pfeiffer et al., 2001, Nicholls, 2008). A rise in intracellular calcium triggers an abundant mitochondrial expansion (Gunter et al., 1994, Hyde and Durham, 1994, Zirpel et al., 1998, Pinton et al., 2008) as well as a global upregulation in oxidative enzyme activity within neurons (Duchen, 2004, Gunter et al., 2004, Nicholls, 2008). In NM, this is evidenced by the elevated SDH, CO, and ATPase staining intensities observed throughout the ipsilateral nucleus as early as 12 hours following cochlea removal (see Results section). Mitochondria

scavenge calcium as part of a protective buffering mechanism (Gunter and Gunter, 1994, Hansford, 1994, Budd and Nicholls, 1996, Scheffler, 2001, Nicholls, 2008). In deafferented NM, however, a subset of neurons contains morphologically impaired mitochondria (Hyde and Durham, 1994), which presumably compromises organelle function as well as calcium uptake mechanisms. These same neurons undergo ER fragmentation (Born and Rubel, 1985, Rubel et al., 1991), loss of protein synthetic capacity (Steward and Rubel, 1985, Kelley et al., 1997, Lu et al., 2004), and cell death. We speculate that loss of ER and mitochondrial integrities, together, perpetuate the death that occurs in some deafferented NM neurons, and that the mechanism of death involves a calcium-mediated attack on mitochondrial function.

Mitochondria and ER are intimately linked both in structure and in function (Hajnoczky et al., 1995, Rizzuto et al., 1998, Pinton et al., 2008). It is estimated that, in a given cell, as much as 20% of the mitochondrial surface area directly contacts the ER (Rizzuto et al., 1998, Pinton et al., 2008). This physical apposition facilitates a unique communication between the organelles that allows direct transfer (rather than vesicular trafficking) across ER-mitochondrial junctions (Vance, 1990, Pinton et al., 2008). These ER-mitochondrial junctions are enriched sites of lipid transfer (Piccini et al., 1998, Stone and Vance, 2000) and calcium exchange (Berridge, 2002, Pinton et al., 2008, Rimessi et al., 2008), and their disruption has been increasingly linked

to apoptotic death in many systems (Demaurex and Distelhorst, 2003, Orrenius et al., 2003, Rizzuto et al., 2003, Scorrano et al., 2003).

It is likely that the ER degradation that occurs within a subset of deafferented NM neurons perpetuates intracellular calcium flux via activation of inositol triphosphate receptors (IP3Rs), the latter being enriched at ER-mitochondrial junctions (Pinton et al., 2008) and also regulated by glutamate in NM (Zirpel et al., 1994). The calcium released from perturbed ER-mitochondrial junctions activates several parallel pathways, all of which target the mitochondria for destruction. First, calcium triggers nitric oxide synthase (NOS) generation (Alderton et al., 2001) and nitric oxide (NO) (Knott et al., 2008, Nicholls, 2008) production. NO, along with calcium directly, attacks constituents of the mitochondrial inner membrane, disrupting ATPase activity (see below) (Cleeter et al., 1994) and perpetuating production of reactive oxygen species (ROS), namely $O_2^-$ and $H_2O_2$ (Inoue et al., 1999, Stewart and Heales, 2003, Turrens, 2003, Balaban et al., 2005, Pope et al., 2008). Lipid peroxidation as a consequence of ROS generation (Ohinata et al., 2000, Cheng et al., 2001, Kelada et al., 2003) has been described in deafferented NM neurons six hours after cochlea removal (Nicholas and Hyson, 2006), and probably contributes to our observed increases in SDH activity within some neurons. As a tricarboxylic acid (TCA) cycle enzyme, SDH utilizes a number of substrates, including oxidized fatty acids for energy production (Stryer, 1995, Duchen, 2004). A switch in metabolic substrate may account for the

increased SDH activity observed in a subset of deafferented NM neurons (Figure 1D, Figure 2).

Second, as mentioned briefly above, intracellular calcium directly attacks the ATPase proton pump (complex V) embedded within the mitochondrial inner membrane (Shiva and Darley-Usmar, 2003), a phenomenon that disrupts electron transport chain efficiency, inhibits mitochondrial capacity to maintain the energy needs of the cell, and produces cell death from ATP uncoupling (Pfeiffer et al., 2001, Nicholls, 2008). The differential staining intensities for ATPase across deafferented NM (Figure 4) suggests that mitochondrial uncoupling occurs in the subset of NM neurons targeted to die.

Third, calcium overload, beyond the buffering capacity of mitochondria, also triggers the formation of a permeability transition pore in the mitochondrial outer membrane (Nicholls, 2008, Pinton et al., 2008), which results in loss of $\Delta\Psi_m$ as well as collapse of the cellular energetic apparatus (Gunter et al., 2004). Membrane potential reversal correlates strongly with cytochrome *c* release and initiation of intrinsic mitochondrial-mediated apoptosis (Foster et al., 2006). Mitotracker Red fluoresces intensely in the cytoplasm of deafferented NM neurons known to undergo cell death. This suggests that deafferentation-induced death in NM neurons is accompanied by loss of $\Delta\Psi_m$.

Although abundant evidence supports the use of fluorescent, cationic, lipophilic dyes to accurately detect $\Delta\Psi_m$ (Johnson et al., 1980, Johnson et al., 1981, Macho et al., 1996, Mostafapour et al., 1997), some controversy surrounds this premise (Poot et al., 1996, Nicholls and Budd, 2000, Buckman et al., 2001, Foster et al., 2006). Mitotracker Green, in particular, is not equipped with chloromethyl moieties, and consequently is insensitive to fluctuations in $\Delta\Psi_m$. This dye has been used as a general index of mitochondrial mass (Poot et al., 1996, de la Monte et al., 2000, Buckman et al., 2001). Mitotrackers Red and Orange, on the other hand, are equipped with chloromethyl-X-rosamine groups, uptake of which has been shown to be $\Delta\Psi_m$ dependent (Macho et al., 1996). Interestingly, however, Mitotracker Red fluorescence is also influenced by ROS generation (Buckman et al., 2001, Kim et al., 2002). ROS generation is known to occur in deafferented NM (Nicholas and Hyson, 2006); whether Mitotracker Red measures ROS accumulation or $\Delta\Psi_m$ reversal must be determined in future experiments.

## Conclusions

In summary, the results presented here demonstrate differential upregulation of SDH and ATPase across deafferented NM neurons. This suggests that mitochondrial functional deficits differ across the deafferented nucleus, most likely differentiating neurons that will die from neurons that will survive deafferentation. It is certainly counterintuitive that oxidative enzyme upregulation accompanies a reduction in glucose utilization; however, previous studies in NM neurons, as well as other neurodegenerative states, have demonstrated marked increases in TCA cycle enzymes despite glucose depletion (Durham and Rubel, 1985, Durham et al., 1993, Gibson et al., 2008). Additionally, the marked expansion in mitochondrial number in deafferented NM promotes the global upregulation of oxidative metabolism (Hyde and Durham, 1994), including increased activity of CO unimodally across all deafferented NM neurons. We attribute a preferential increase in SDH within some deafferented neurons to a shift in metabolic status: the release of calcium and lipids from compromised ER-mitochondrial junctions stimulates TCA cycle dehydrogenases (Brookes et al., 2004, Pinton et al., 2008) and makes available fatty acid byproducts for use as substrates by TCA cycle enzymes (Pope et al., 2008). We also describe a robust correlation between Mitotracker Red staining intensity and mitochondrial DNA fragmentation, a known indicator of cell death. Our findings provide valuable insight towards understanding the cellular events underlying deafferentation-

induced cell death in NM, for which we propose the following mechanism (Figure 6).

Cochlea removal permanently disrupts glutamate delivery to NM neurons. This, in turn, abruptly terminates activation of neuronal metabotropic glutamate receptors, which are the primary regulators of intracellular calcium in NM (Zirpel and Rubel, 1996, Zirpel et al., 1998, Kato and Rubel, 1999, Zirpel et al., 2000a). Calcium dysregulation leads to calcium influx most probably via activation of AMPA receptors by residual glutamate (Zirpel et al., 2000b), entry through N-type calcium channels (Lu and Rubel, 2005), and/or the potential release from internal stores (Missiaen et al., 1991). Calcium influx triggers rapid proliferation of mitochondria within NM neurons (Hyde and Durham, 1994). Mitochondria unable to buffer the rise in calcium undergo vacuolization (Hyde and Durham, 1994), whether in response to persistent elevated calcium levels (Brookes et al., 2004) or from the loss of ER-mitochondrial junctional integrity (Pinton et al., 2008). ER-mitochondrial junctional impairment releases lipids and calcium into the cellular cytoplasm, which perpetuates ROS generation (Nicholas and Hyson, 2006, Nicholls, 2008) and shifts metabolism towards the TCA cycle (Duchen, 2004, Gunter et al., 2004), ramping up SDH levels. Calcium directly impairs ATPase activity (Cleeter et al., 1994), leading to metabolic uncoupling; activates anti-apoptotic bcl2 gene expression (Wilkinson et al., 2002, Scorrano et al., 2003), which, in ribosomal-deficient, dying neurons, cannot

be translated to protein; activates mitochondrial permeability transition, which elaborates intrinsic apoptosis (Gunter et al., 2004); and directly activates endonucleases, which degrade mitochondrial DNA. Future investigations of the molecular genetic contributions to cell-specific death in deafferented NM should further elucidate this mechanism.

**Figure 1:** Photomicrographs of ipsilateral (B, D, F, H) and contralateral (A, C, E, G) sections through NM from an animal sacrificed 24 hours following cochlea removal. Adjacent sections are stained for Thionin (A, B), SDH (C, D), CO (E, F), or ATPase (G, H). Intact contralateral neurons exhibit robust Thionin staining of ribosomal Nissl substance throughout neuronal cytoplasm (A). Ipsilateral neurons that will die undergo ribosomal disassembly, which is observed as a loss of cytoplasmic Thionin staining (B, inset). The entire population of ipsilateral neurons undergoes oxidative upregulation, which is evidenced by global increases in SDH (D vs. C), CO (F vs. E), and ATPase (H vs. G) relative to the contralateral nucleus. All ipsilateral neurons upregulate CO activity unimodally (F); however, some ipsilateral neurons exhibit preferentially elevated SDH (D) and ATPase (H) levels. Scale bar=100μm

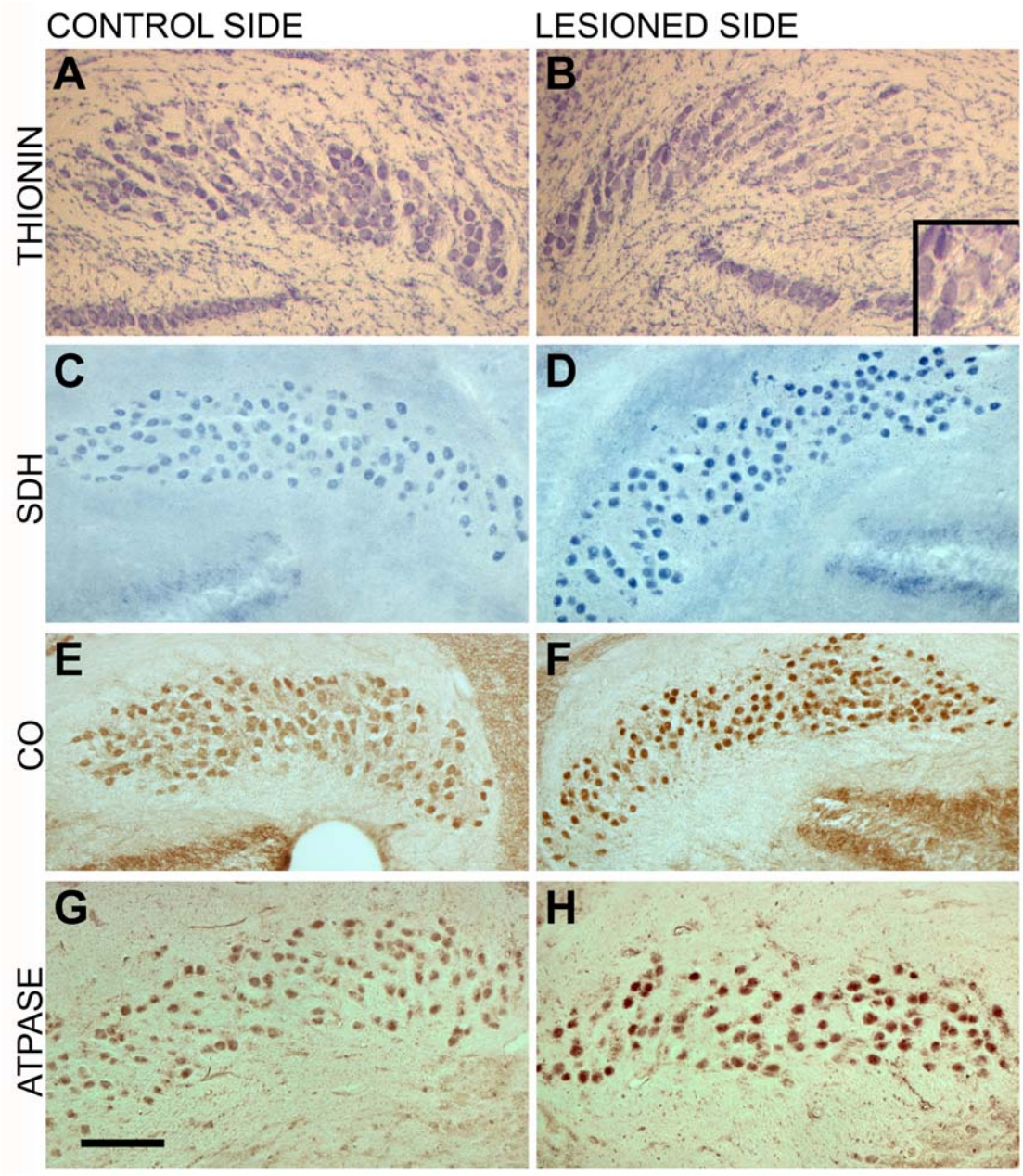
CONTROL SIDE
LESIONED SIDE
THIONIN
SDH
CO
ATPASE
A
B
C
D
E
F
G
H

**Figure 2:** Histograms showing succinate dehydrogenase (SDH) histochemical reaction product measured as optical density (OD) and plotted as Z-scores from animals sacrificed 12 hours (A), 24 hours (B), 48 hours (C), or 7 days (D) following cochlea removal. At all time points examined, NM neurons contralateral to cochlea removal exhibit unimodal distributions of SDH activity (orange bars). Comparatively, SDH reaction product in NM neurons ipsilateral to cochlea removal (blue bars) exhibits bimodal distributions at 12- and 24-hour survival times (A and B). Ipsilateral NM neurons with the most intense SDH reaction product (Z-score ≥ 2) at 12- and 24-hour survival times coincide numerically with those neurons that eventually undergo cell death (A, B). By 48 hours, the bimodal distribution of SDH staining intensity is no longer evident in ipsilateral neurons (C). By seven days, when cell death is complete, ipsilateral neurons transition towards an overall reduction in SDH activity, suggesting that metabolic demand in deafferented NM neurons that survive drastically declines (D). This reduction in metabolic demand accompanies the loss of 31.0±12.9% of the neuronal population in NM.

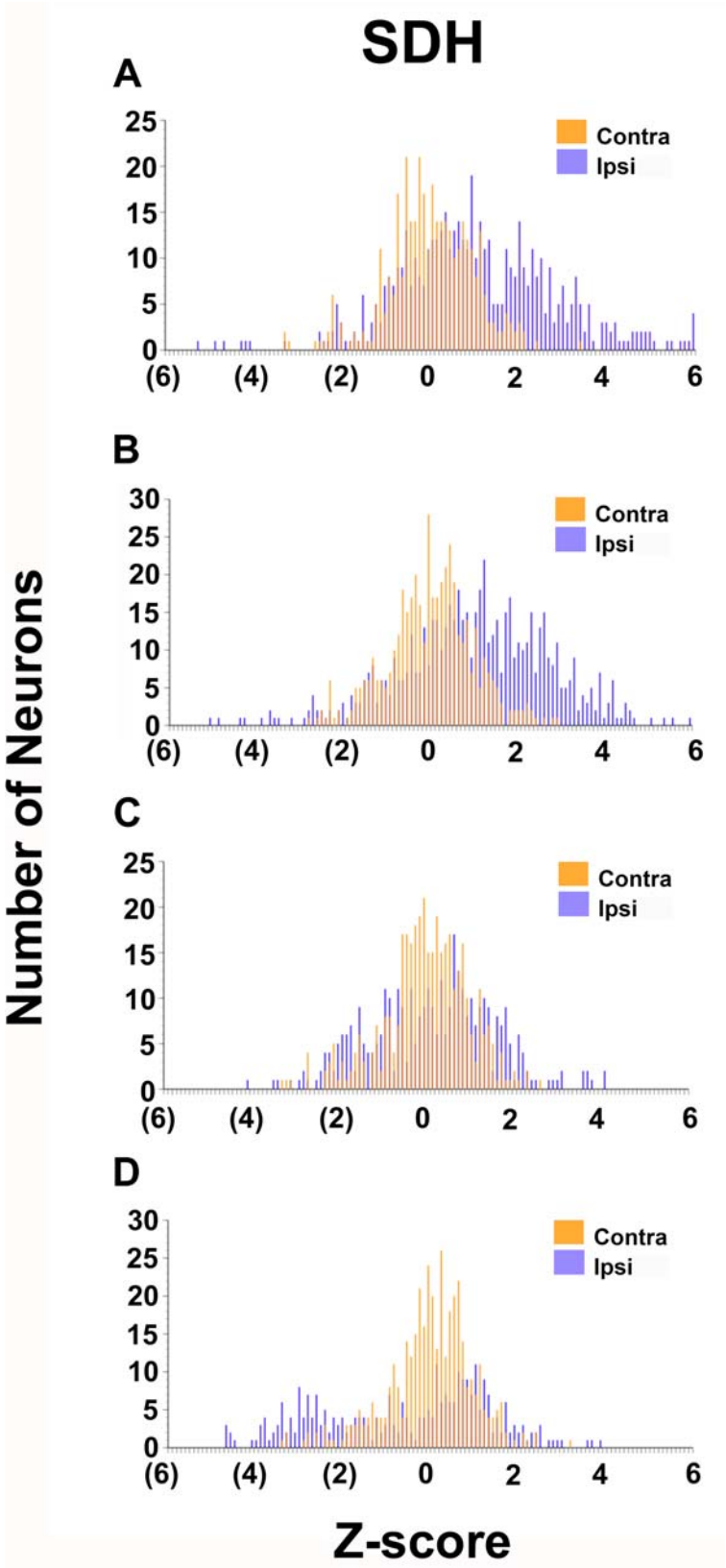
SDH
A
B
C
D
Contra
Ipsi
Number of Neurons
Z-score
(6)
(4)
(2)
0
2
4
6

**Figure 3:** Histograms showing cytochrome oxidase (CO) histochemical reaction product measured as optical density (OD) and plotted as Z-scores from animals sacrificed 12 hours (A), 24 hours (B), 48 hours (C), or 7 days (D) following cochlea removal. Across all time points examined, NM neurons contralateral (orange bars) and ipsilateral (blue bars) to cochlea removal exhibit unimodal distributions of CO activity. At 12 hours, CO reaction product in ipsilateral neurons is significantly higher (*t*-test, p-value=0.009) than in contralateral neurons (A). Thereafter, no significant differences between sides exist. By seven days, approximately 42.0±3.9% of ipsilateral neurons have died (D).

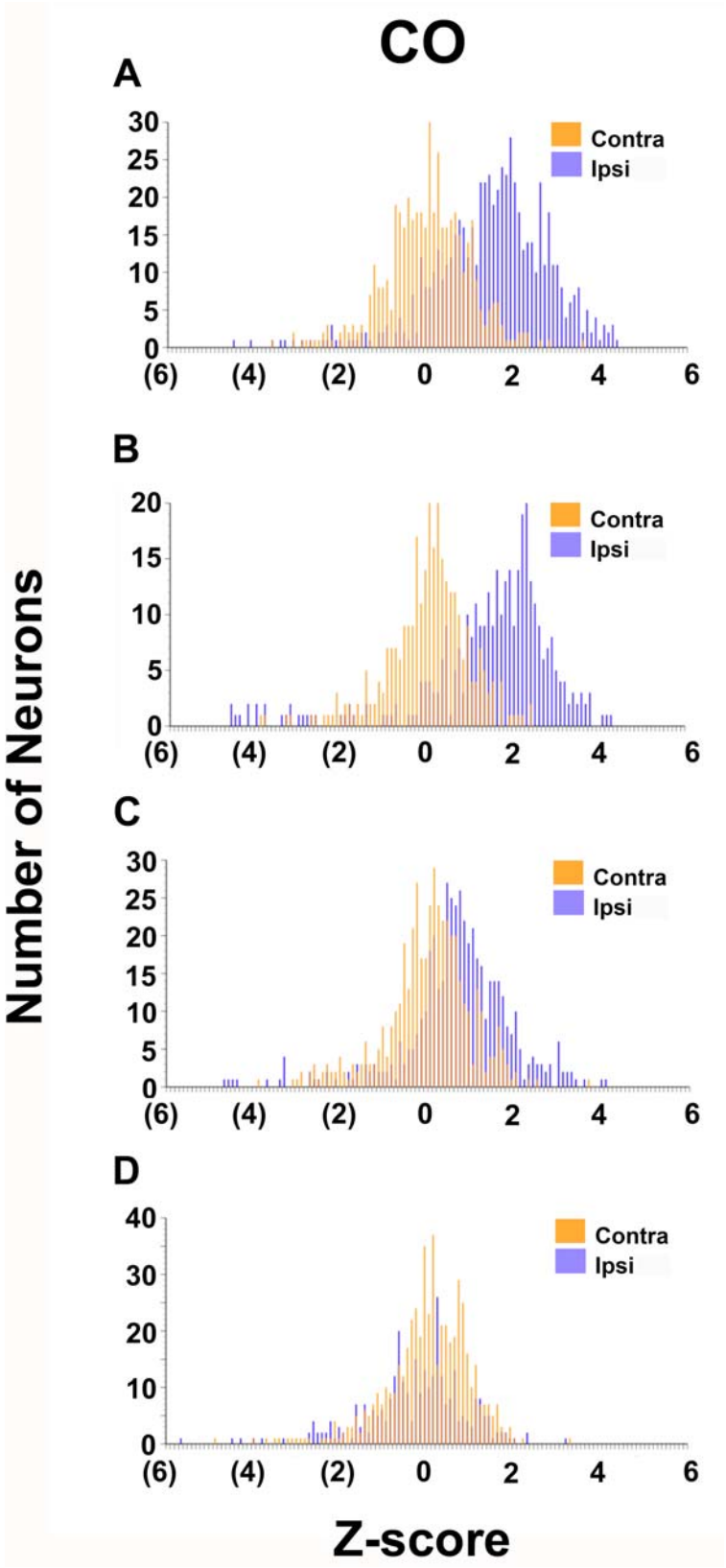
CO
A
B
C
D
Contra
Ipsi
Number of Neurons
Z-score
(6)
(4)
(2)
0
2
4
6

**Figure 4:** Histograms showing ATP synthase (ATPase) histochemical reaction product measured as optical density (OD) and plotted as Z-scores from animals sacrificed 12 hours (A), 24 hours (B), 48 hours (C), or 7 days (D) following cochlea removal. At all time points examined, NM neurons contralateral to cochlea removal exhibit unimodal distributions of ATPase staining intensity (orange bars). As early as 24 hours, ATPase reaction product accumulates differentially across the population of ipsilateral (blue bars) neurons (B). By 48 hours, a bimodal distribution across ipsilateral NM is clearly evident (C). Ipsilateral NM neurons with the most intense ATPase reaction product at 48-hour survival times coincide numerically with those neurons that eventually undergo cell death (C, D). By 7 days, approximately 39.8±14.0% of ipsilateral neurons have died (D).

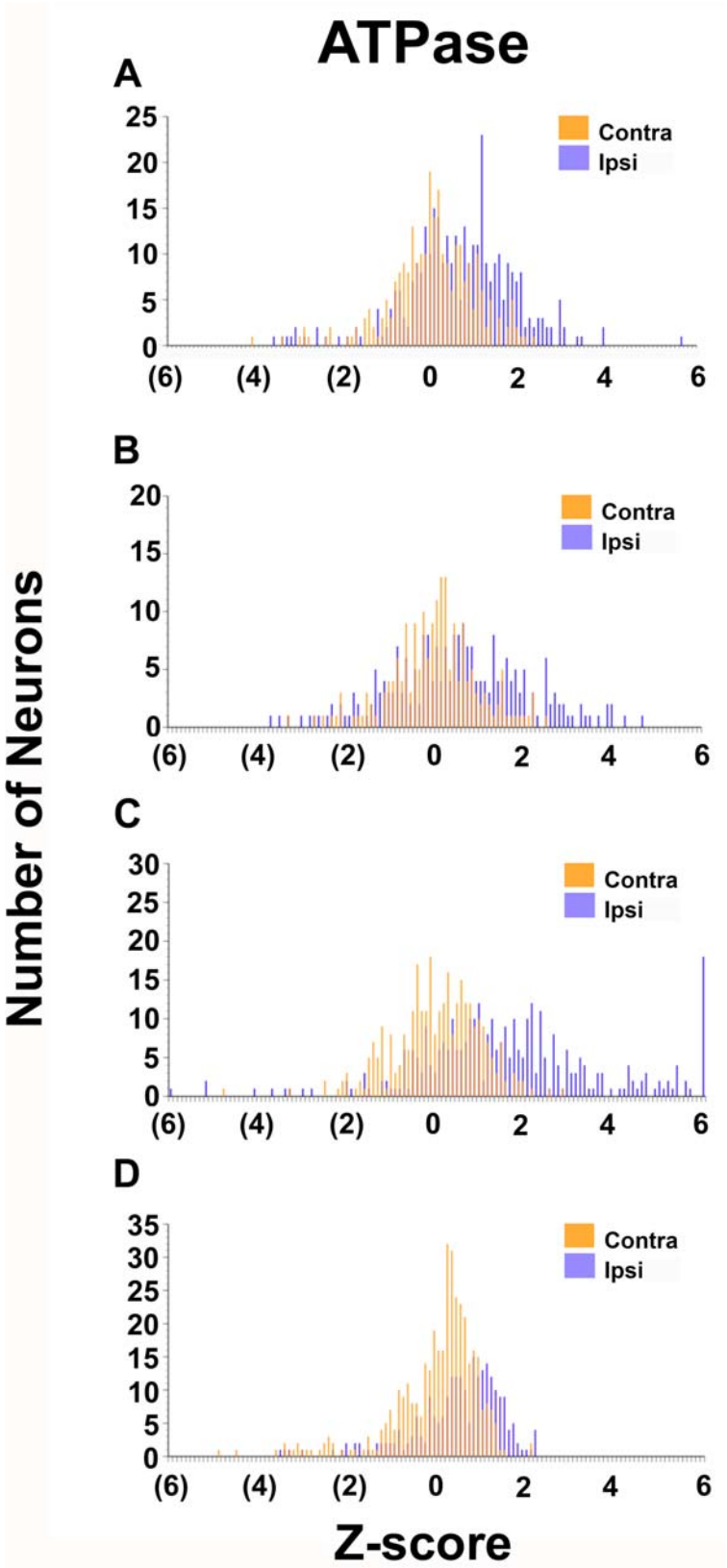
ATPase
A
B
C
D
Contra
Ipsi
Number of Neurons
Z-score
(6)
(4)
(2)
0
2
4
6

**Figure 5:** Photomicrographs of ipsilateral (B, D, F, H) and contralateral (A, C, E, G) sections through NM from an animal subjected to intrathecal injection of Mitotracker Red 24 hours (A, B) or seven days (E, F) following cochlea removal. Following sacrifice, NM sections were reacted for TUNEL (C, D, G, H). A subset of ipsilateral neurons at 24 hours exhibits diffuse cytoplasmic TUNEL labeling, indicative of mitochondrial DNA fragmentation (D). Mitotracker Red accumulates with greater staining intensity within the same subset of neurons (B). By seven days, when cell death is complete, no evidence of TUNEL labeling (H) or Mitotracker Red accumulation (F) exists in deafferented NM neurons. Scale bar=50μm

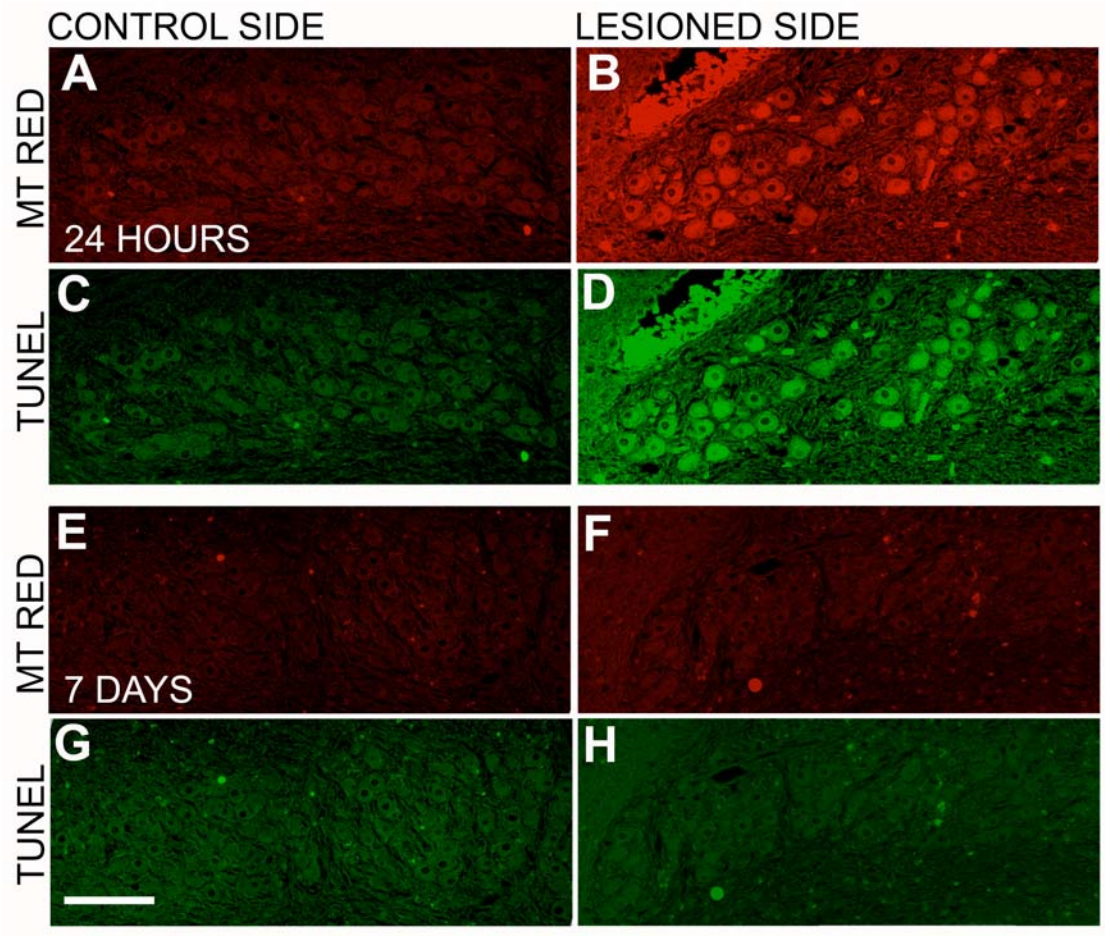
CONTROL SIDE
LESIONED SIDE
MT RED
TUNEL
MT RED
TUNEL
A
B
C
D
E
F
G
H
24 HOURS
7 DAYS

**Figure 6:** A schematic illustrating the proposed mechanism of deafferentation-induced cell death in NM neurons. In deafferented NM neurons destined to die, calcium accumulates beyond sustainable levels. Calcium most likely enters deafferented NM neurons via three routes: 1) plasma membrane AMPA receptors, 2) N-type voltage sensitive calcium channels (NCC), and/or 3) release from internal organelle stores. Compromised mitochondria and degenerating endoplasmic reticulum (ER) perpetuate the release of lipids and calcium into the neuronal cytoplasm. Calcium-mediated lipid peroxidation makes available fatty acid substrates for tricarboxylic acid (TCA) cycle energy production, preferentially upregulating succinate dehydrogenase (SDH) and other TCA cycle dehydrogenases. Calcium, as well as reactive oxygen species from lipid peroxidation, attack ATP synthase (ATPase) and facilitate formation of the mitochondrial transition pore, which metabolically uncouples energy production, perpetuates the intrinsic, mitochondrially-mediated apoptosis cascade, and activates endonucleases that degrade mitochondrial DNA.

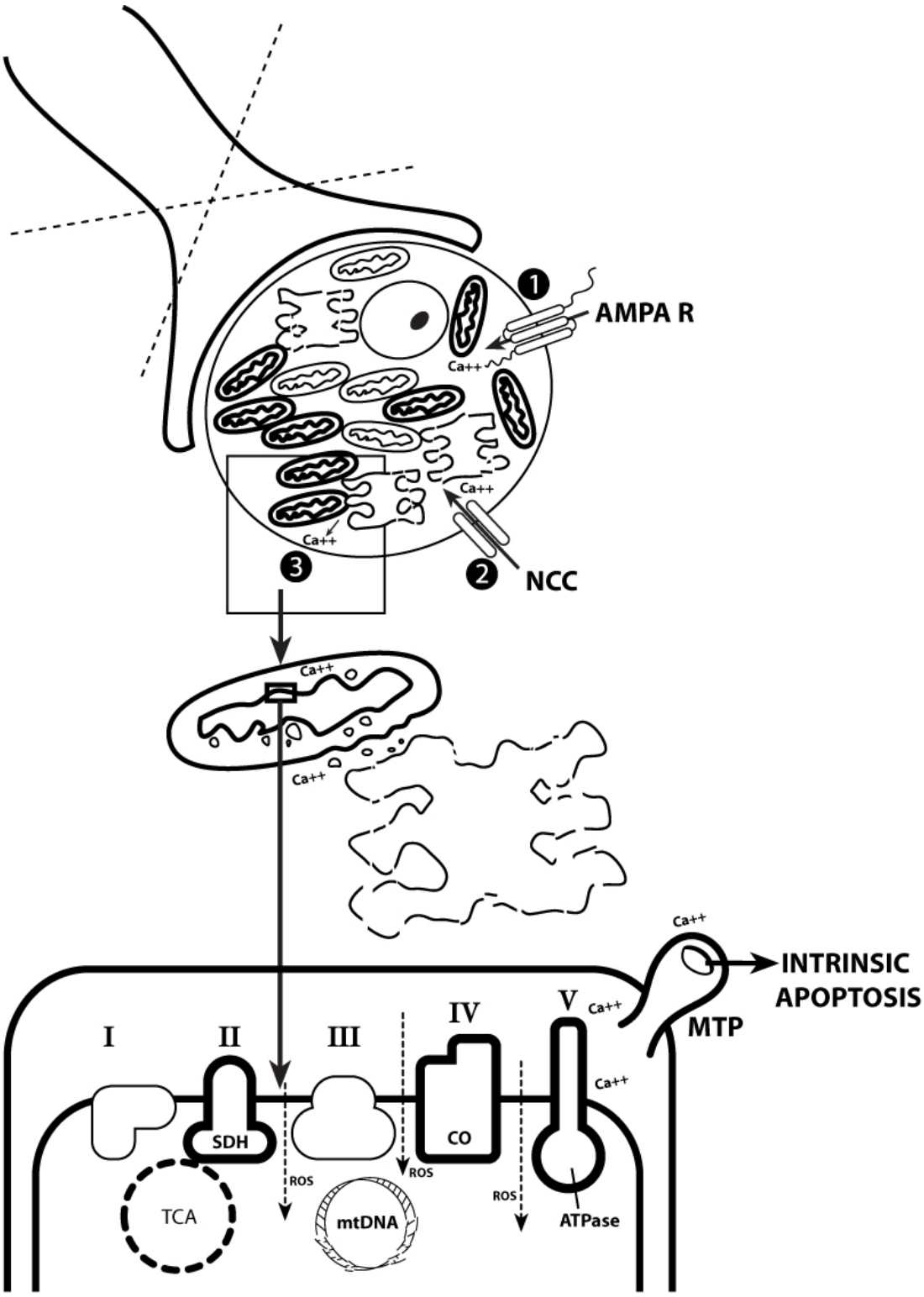
1
AMPA R
Ca++
Ca++
Ca++
3
2
NCC
Ca++
Ca++
Ca++
INTRINSIC
APOPTOSIS
MTP
I
II
III
IV
V
Ca++
Ca++
SDH
CO
ROS
ROS
ROS
TCA
mtDNA
ATPase

# CHAPTER IV

# DIFFERENTIAL GENE EXPRESSION PROFILES IN DEAFFERENTED CHICK AUDITORY NEURONS IDENTIFIED USING LASER CAPTURE MICRODISSECTION

## Introduction

Chick auditory neurons within brainstem nucleus, nucleus magnocellularis (n. magnocellularis, NM), receive excitatory innervation exclusively from ipsilateral cochlear ganglion neurons that send afferent projections with the eighth nerve (Parks and Rubel, 1978). Permanent disruption of afferent support, by cochlea removal, triggers a series of cellular perturbations that culminate in cell death (Born and Rubel, 1985, Edmonds et al., 1999, Karnes et al., 2009). Interestingly, cell death is restricted to a subset (30-50%) of deafferented NM neurons, which exhibit specific signs of cell compromise prior to dying. Ribosomal disassembly (Rubel et al., 1991, Karnes et al., 2009), deficient protein synthesis (Steward and Rubel, 1985, Garden et al., 1994, Kelley et al., 1997), and mitochondrial structural (Hyde and Durham, 1994) and functional impairments (Durham and Rubel, 1985, Hyde and Durham, 1990, Durham et al., 1993) are observed in deafferented NM neurons destined to die as early as 1-6 hours after cochlea removal. Thionin, an acidic stain for ribosomal Nissl substance, has been used to distinguish neurons destined to die from neurons destined to survive deafferentation: Thionin-negative NM neurons, so-called “ghost” neurons due to their hollowed appearances under light microscopy (Born and Rubel,

1985), effectively approximate the 30-50% of neurons that will die (Karnes et al., 2009). "Ghost" neurons are observable within hours of deafferentation, well before neuronal death occurs. Consequently, Thionin staining can be used to effectively predict cell fate in deafferented NM.

Here, populations of neurons with different cellular fates were identified based on their Thionin staining characteristics and were microdissected from NM tissue sections using laser capture microdissection (LCM). RNA extracted from 1) Thionin-negative "ghost" neurons fated to die, 2) Thionin-positive neurons fated to survive deafferentation, and 3) healthy NM neurons contralateral to cochlea removal remained viable for use in downstream genetic analyses. Microarray and quantitative Real-Time polymerase chain reaction (RT-PCR) results demonstrated that genes involved in calcium signaling, glutamate receptor signaling, GABA receptor signaling, and phospholipid degradation were differentially expressed across microdissected populations of NM neurons. These results suggest that changes in the expression of specific genes influence deafferentation-induced neuronal fate determination in NM. In addition, we demonstrate that deafferentation affects expression levels of several "traditional" housekeeping genes.

**Materials and Methods:**

Animal preparation and surgery

Cornish Rock broiler chickens (Ross 308 x Ross 308) were obtained as day-old hatchlings from a commercial supplier (Welp Hatchery, Bancroft, IA) and were housed in communal brooders at the University of Kansas Medical Center Lab Animal Resources center with *ad libitum* access to food and water. Eight- (P8) to 12-day (P12) post-hatch chicks were anesthetized with intramuscular injections of Ketamine (35mg/kg; Phoenix Pharmaceutical, Inc., St. Joseph, MO) and Xylazine (2mg/kg; Lloyd Laboratories, Shenandoah, IA) and subjected to unilateral cochlea (basilar papilla) removal as described previously (Born and Rubel, 1985, Hyde and Durham, 1990). Briefly, the left tympanic membrane was punctured and the columella extracted. The cochlea was removed from the oval window aperture using fine forceps. The entire extent of the cochlea from base to apex was examined under brightfied microscopy to ensure complete removal of the organ. Cochlea removal severs the peripheral processes of cochlear ganglion neurons, but leaves cell bodies intact (Born et al., 1991). The cochlear duct was aspirated following surgery, and animals were allowed to recover. Contralateral cochleae remained intact, and contralateral NM neurons served as within-animal controls. All experimental protocols were approved by the University of Kansas Medical Center Institutional Animal Care and Use Committee (IACUC) and carried out in accordance with the National Institutes

of Health Guide for the Care and Use of Laboratory Animals (NIH Publications No. 80-23). All efforts were made to minimize the number and suffering of all animal subjects.

Tissue Preparation

Animals (n=22) were sacrificed by intraperitoneal injections of Beuthanasia-D (Schering-Plough, Union, NJ) and were decapitated 24 hours following cochlea removal, a time point at which apoptotic indicators appear but precede cell death (Karnes et al., 2009). Brains were extracted, and brainstems were rapidly mounted on corkboard using TBS Tissue Freezing Medium (Triangle Biomedical Sciences, Durham, NC). Mounted brainstems were then frozen in heptane cooled by dry ice and stored at -80° C until use. All dissecting instruments and corkboard were decontaminated from nucleases with 100% ethanol followed by RNase-OFF (Takara Bio Inc., Otsu, Shiga, Japan). Brainstems were sectioned on a cryostat, the latter decontaminated with 100% ethanol, through nucleus magnocelluaris (n. magnocellularis, NM), and 10μm coronal sections were serially thaw-mounted onto oven-baked Superfrost/Plus slides (Fisher Scientific, Pittsburgh, PA). Wrinkled sections were discarded. Slides were stored at -80°C until use.

Laser capture microdissection (LCM)

Sections were immersed in 70% ethanol for one minute, distilled water for one minute, and 6% Thionin working stain (containing per 50ml: 600mg Thionin acetate, 2ml glacial acetic acid, and 2.16ml 1M NaOH) for two minutes. Sections were then rapidly dehydrated in nuclease-free reagents as follows: 70% ethanol for one minute, 95% ethanol for one minute, 100% ethanol for four minutes x 3, and xylenes for five minutes x 2. Sections were dried in a hood for 10-15 minutes until all liquid had completely evaporated, and were quickly transported to the Veritas Microdissection system (Molecular Devices, Sunnyvale, CA) for laser capture microdissection (LCM).

Deafferentation triggers ultrastructural degradation of polyribosomes (Rubel et al., 1991) and termination of protein synthesis in the subset of NM neurons known to die following cochlea removal (Steward and Rubel, 1985, Garden et al., 1994, Kelley et al., 1997). Accordingly, Thionin staining of ribosomal Nissl substance can be used to distinguish cell fate early after deafferentation: neurons accumulating intense cytoplasmic Thionin staining will survive, while those devoid of cytoplasmic Thionin staining, so-called "ghost" neurons (Born and Rubel, 1985), will die (Karnes et al., 2009). Three subpopulations of NM neurons, identified based on their Thionin staining characteristics, were adhered to separate Macro caps (Molecular Devices, Sunnyvale, CA) using (on average) a 24.5μm laser spot size, 70mW of laser power, a 2msec laser pulse, and a 200mV laser intensity: (1) Thionin-

negative “ghost” neurons ipsilateral to cochlea removal, (2) Thionin-positive neurons ipsilateral to cochlea removal, and (3) Thionin-positive control neurons contralateral to cochlea removal. Full caps (each containing approximately 360-1200 cells) of microdissected neuronal subpopulations (and adjacent glia) were removed from the Veritas system and transferred immediately to storage at -80°C.

RNA Extraction

RNA was extracted using the Picopure RNA Isolation kit (Molecular Devices, Sunnyvale, CA) according to the manufacturer’s instructions. Briefly, caps were removed from freezer storage and fitted with microcentrifuge tubes containing 50μl of Extraction Buffer. Samples were incubated at 42°C for 25 minutes, and RNA was extracted into tubes. Samples were centrifuged at 800x *g* for two minutes and immediately processed for RNA isolation.

RNA Isolation

RNA was isolated using the Picopure RNA Isolation kit (Molecular Devices, Sunnyvale, CA) according to the manufacturer’s instructions. Briefly, 50μl of 70% ethanol was added to the cell extract, and the extract/ethanol mixture transferred to a purification column, pre-treated with the kit’s Conditioning Buffer. RNA was adhered to the purification column by

centrifuging the sample at 100x *g* for two minutes, and excess flowthrough eliminated by an additional centrifugation at 16,000x *g* for 30 seconds. 100μl of the kit's Wash Buffer 1 was then added to the purification column, and the sample was centrifuged again at 8,000x *g* for one minute. The sample was treated on-column with DNAse I (Qiagen, Valencia, CA) to reduce genomic DNA contamination and was briefly rinsed with Wash Buffer 1. The sample was then washed with Wash Buffer 2 and centrifuged at 16,000x *g* until the purification column was free of residual buffer. RNA was eluted from the purification column into a clean microcentrifuge tube for a final volume of 11μl, and the sample was either immediately analyzed for integrity or stored at -80°C.

RNA integrity analyses

All RNA samples were assessed for quality and quantity using an Agilent 2100 Bioanalyzer (Agilent Technologies, Santa Clara, CA) and an RNA 6000 Pico LabChip kit (Agilent Technologies, Santa Clara, CA). This platform generates an electropherogram and digitized gel electrophoretic profile to assess RNA quality. Sharp peaks at 40 seconds and 45 seconds on the electropherogram indicate intact 18s and 28s ribosomal RNA subunits, respectively, and suggest minimal RNA degradation. Likewise, visibly delineated bands on the digitized gel electrophoretic profile suggest maintenance of RNA integrity. The platform also generates an RNA Integrity

Number (RIN) for each sample. RIN values are derived using several indices of RNA integrity and range from 10 (intact RNA) to 1 (totally degraded RNA) (Schroeder et al., 2006). RNA samples with sharp peaks, distinct electrophoretic bands, and RIN ≥ 7 were utilized in our experiments.

Microarray Analyses

Intact RNA from NM subpopulations was pooled in equal amounts (21.1±0.53ng) to form three microarray profiles: deafferented NM "ghost" neurons that stained poorly with Thionin; deafferented, surviving NM neurons that stained intensely with Thionin; and healthy control neurons from contralateral NM. In all cases, adjacent glial cells were present as well. Triplicates of each microarray profile were prepared for microarray hybridization.

All microarray analyses were conducted by the University of Kansas Medical Center Microarray Facility. cRNA targets were generated using the Affymetrix Small Sample Labeling Protocol vII (Affymetrix, Santa Clara, CA) according to the manufacturer's instructions. Briefly, RNA underwent two rounds of amplification, each of which included a reverse transcription step mediated by a T7 oligo(dT) promoter primer and an *in vitro* transcription (IVT) reaction step. The second IVT reaction step included biotin labeling of cRNA nucleotides. Biotinylated cRNA targets were then purified using the RNeasy Mini Protocol for RNA cleanup (Qiagen, Valencia, CA) and fragmented and

hybridized to Affymetrix GeneChip chicken genome microarrays in triplicate, according to the manufacturer's instructions. Nine arrays were used in total. The Affymetrix GeneChip chicken genome array provides comprehensive coverage of 32,773 transcripts corresponding to more than 28,000 genes. Microarrays were scanned using an Affymetrix GeneChip Scanner 3000 7G with autoloader, and detection signals were analyzed using Partek Genomic Suite software, revision 6.3, Copyright 2008 (Partek Inc., St. Louis, MO).

Microarray signal analysis was conducted by the University of Kansas Medical Center Bioinformatics Core facility. In brief, Partek Genomic Suite was used to adjust probe signal intensities for properties such as fragment length, GC content, sequence allele position, and background. The signal intensities between probe sets for a given gene were analyzed using Robust Multi-array Analysis (RMA) in Partek. Partek designated a gene present if its probe pairs were a perfect match (PM) and absent if its probe pairs were a mismatch (MM). RMA transforms probe signal intensity data into meaningful expression level data by (1) correcting for background levels from perfect match (PM) signal differences between gene probe sets, (2) normalizing signal intensities across all GeneChips used in the experiment, (3) applying a $\log_2$ transformation of signal differences, and (4) summarizing data as expression values (average differences in signal intensity) (Irizarry et al., 2003). Fold change (FC) differences in expression values between groups (Thionin-positive ipsilateral neurons, Thionin-negative ipsilateral "ghost"

neurons, and contralateral control neurons) were computed via a two-way analysis of variance (ANOVA) using the Least Squares Means method. Genes with statistically significant (p-value ≤ 0.05 and FC ≥ $|2|$) differences in RMA-normalized expression values between groups were analyzed using GeneSpring GX software, v. 7.3.1 (Agilent Technologies, Wilmington, DE) and GeneChip Operating Software (GCOS; Affymetrix, Santa Clara, CA).

Pathway Analysis

RMA-normalized data were analyzed further using Ingenuity Pathways Analysis (IPA) software (Ingenuity Systems, Redwood City, CA). Expression values with p-value ≤ 0.05 and FC ≥ $|2|$ were included in the analysis. 723/38,536 probe sets met these inclusion criteria. A comparison analysis was performed using all three microarray profiles, and genes were grouped by canonical pathway. Six canonical pathways were selected for quantitative Real-Time PCR verification based on biologic significance: GABA receptor signaling, glutamate receptor signaling, calcium signaling, oxidative phosphorylation, phospholipid degradation, and PTEN signaling. In total, twelve genes were selected for verification by quantitative Real-Time PCR.

Quantitative Real-Time PCR

*Primer design*

Genome sequences for genes of interest were obtained using the UCSC Chicken (*Gallus gallus)* Genome Browser Gateway (http://genome.ucsc.edu/). Sequences containing both exons and introns were examined, and the locations of introns were identified. Exon-only sequences were imported into Primer Express version 3.0 (Applied Biosystems, Foster City, CA), and the locations of all introns were annotated. Intron-spanning primers (forward and reverse) were selected from those generated by the software. For genes of interest not found in the UCSC database, cDNA nucleotide sequences were obtained from the NCBI nucleotide database (http://www.ncbi.nlm.nih.gov/). For these genes, exon-intron junctions were indeterminable, so the entire sequence was imported into Primer Express version 3.0 (applied Biosystems, Foster City, CA). Primers (forward and reverse) near the 3' coding region were selected from those generated by the software. Primers were purchased from Integrated DNA Technologies, Inc. (IDT; Coralville, IA). The probe used to detect the 18s rRNA subunit was purchased from Applied Biosystems (Applied Biosystems, Foster City, CA). Table 1 lists all primer sequences used in our analyses.

*Reverse transcription*

Pooled cRNA targets (previously used in microarray hybridization) were reverse transcribed to cDNA using the miScript Reverse Transcription (RT) kit (Qiagen, Valencia, CA) according to the manufacturer's instructions. Each 20μl RT reaction (containing 100ng cRNA, in 10μl RNAse-free water; 4μl miScript RT 5x Buffer; 1μl miScript RT master mix; and 5μl RNAse-free water) was incubated at 25°C for one hour, at 95°C for 5 minutes, and then transferred on ice for immediate use in RT-PCR or stored at -20°C.

*RT-PCR*

Quantitative Real-Time PCR was performed on an ABI Prism 7900HT Sequence Detection System (Applied Bioscience, Foster City, CA), using Power SYBR Green PCR Master Mix (Applied Biosystems, Foster City, CA). Each PCR reaction contained 5μl Power SYBR Green Master Mix, 1μl cDNA (diluted 1:10 in RNAse-free water), 0.34μl primer mix (300nM forward and 300nM reverse in RNAse-free water), and 3.66μl RNAse-free water. PCR reactions for each RNA profile (from ipsilateral, Thionin-positive NM neurons, ipsilateral, Thionin-negative "ghost" neurons, or contralateral control neurons) were run in triplicate for all primer pairs tested. Negative controls, using water in lieu of cDNA were also run in triplicate. Thermocycler program parameters were set as follows: 50°C for two minutes, 95°C for ten minutes, followed by 45 cycles of 95°C for 15 seconds, followed by 60°C for one minute.

Dissociation curves were generated for each reaction (95°C for 15 seconds, 60°C for 15 seconds, 95°C for 15 seconds), and were assessed to ensure absence of primer dimerization and detection of a single gene product.

*Standard curve analysis*

The standard curve method of analysis was used to quantify gene expression levels. Accordingly, each PCR reaction was run with a series of serial cDNA dilutions (1:5, 1:10, 1:50, 1:100, 1:500, and 1:1,000). For each gene of interest, an equation was fitted to the corresponding standard curve and used to derive arbitrary expression values for each sample (tested in triplicate). Expression values for triplicates ($\Delta Ct \leq 0.3$) were averaged and normalized, using Microsoft Excel (Microsoft Corp., Seattle, WA), against the average expression values for triplicates ($\Delta Ct \leq 0.3$) of the ribosomal protein S6 kinase-like1 (RPS6KL1), whose mRNA levels were consistent across the three NM subpopulations of interest (as observed via microarray results, see Table 3).

*Statistical analyses*

To identify differences in gene expression across NM subpopulations, normalized ratios (average expression of gene of interest / average expression of RPS6KL1) were compared across all NM groups (ipsilateral, Thionin-positive NM neurons destined to survive deafferentation; ipsilateral, Thionin-negative “ghost” neurons destined to die; and contralateral control

NM neurons) via one-way analyses of variance (ANOVA), followed by pair-wise comparisons via the Holm-Sidak Test, using SigmaStat 3.5 (SYSTAT Software, Inc., San Jose, CA). For ATP2B1, CAMK4, and CASQ2, where either the normality test or equal variance test failed, a one-way ANOVA on ranks using the Kruskal-Wallis test and post-hoc comparisons using Dunn's Method were performed using SigmaStat 3.5.

## Results

NM neuronal subpopulations can be microdissected from tissue sections using LCM

Thionin staining of ribosomal Nissl substance has been used in NM to differentiate dying versus surviving neurons following cochlea removal: deafferented NM neurons that stain poorly with Thionin (so called “ghost” neurons due to their hollowed appearances under light microscopy (Born and Rubel, 1985)) accurately identify the 30-50% subset of NM neurons that will die following cochlea removal (Karnes et al., 2009). Figure 1 shows representative tissue sections through ipsilateral and contralateral NM from an animal sacrificed 24 hours following cochlea removal. Contralateral, unperturbed NM neurons, visualized under brightfield microscopy, exhibit intense Thionin staining throughout the cytoplasm (Figure 1A). Similarly, a subset of NM neurons ipsilateral to cochlea removal (Figure 1B) exhibits robust cytoplasmic Thionin staining, suggesting that these neurons maintain intact ribosomal integrity and will survive deafferentation (Karnes et al., 2009). Also abundant within deafferented NM are “ghost” neurons devoid of functional ribosomes. “Ghost” neurons have visibly intact nuclei and nucleoli; do not accumulate Thionin in their cytoplasm; and represent the population of NM neurons that undergo apoptotic cell death following cochlea removal (Karnes et al., 2009).

Based on their Thionin staining characteristics, three homogeneous subpopulations of NM neurons (and glia) were microdissected from tissue sections using laser capture microdissection (LCM): Thionin-positive NM neurons contralateral to cochlea removal, Thionin-positive NM neurons ipsilateral to cochlea removal, and Thionin-negative "ghost" neurons ipsilateral to cochlea removal. Figure 1C-E shows representative sections through ipsilateral NM visualized through the LCM. Figure 1C shows ipsilateral NM prior to microdissection. Note that ipsilateral neurons with different Thionin staining characteristics are easily identifiable. Figure 1D shows ipsilateral NM just prior to capture. Here, "ghost" neurons were targeted for microdissection. Figure 1E shows ipsilateral NM after successful capture of "ghost" neurons from the tissue section. Figure 1F is a photomicrograph taken of the cap. Note individual "ghost" neurons are adhered to the cap, indicating effective microdissection from slide-mounted tissue sections. Each full cap contained cells microdissected from 45-54 tissue sections. From each tissue section, approximately 30-100 cells (corresponding to 399-11,839 laser pulses) were microdissected.

RNA extracted from LCM-dissected neurons is viable for downstream genetic analyses

From each LCM-captured neuronal subpopulation (Thionin-positive NM neurons ipsilateral to cochlea removal, Thionin-negative "ghost" neurons

ipsilateral to cochlea removal, and Thionin-positive, contralateral NM neurons), RNA was extracted and purified, and was assessed for quality and quantity using an Agilent Bioanalyzer 2100. Figure 2 shows a representative digitized gel electrophoretic profile (Figure 2A) and electropherogram (Figure 2B) generated by the Bioanalyzer. The digitized gel shows ten lanes (1-11) of individual RNA samples (1N-11N) alongside a known standard (lane L, Ladder). Delineated bands on the digitized gel indicate intact 18s and 28s rRNA ribosomal subunits, respectively, and imply overall preservation of RNA integrity. All ten RNA samples exhibit two distinct bands on the digitized gel. Band intensity corresponds to RNA concentration. Sample 8N (Figure 2A, arrow) shows two dark, crisp bands on the digitized gel profile and two distinct sharp peaks on the electropherogram (Figure 2B), consistent with the 18s and 28s rRNA ribosomal subunits. Sample 8N represents RNA extracted from LCM-captured NM "ghost" neurons ipsilateral to cochlea removal, and has an RNA Integrity Number (RIN) of 8.9 and an RNA concentration of 415pg/μl. RNA extracted from microdissected NM neuronal populations remains intact and of sufficient quantity for use in downstream genetic analyses.

Microarray analyses

Signal intensities from GeneChip microarray hybridizations were analyzed and normalized using Robust Multi-array Analysis (RMA) using

Partek software. Additional stringency parameters were assigned to results from all pair-wise comparisons across groups (ipsilateral, Thionin-positive neurons; Ipsilateral, Thionin-negative “ghost” neurons; and contralateral control neurons): genes exhibiting differences in expression levels between groups (p-value≤ 0.05, via one-way ANOVA using the Least Squares method) and a fold change (FC) ≥ $\left|2\right|$ were considered significant. Using these criteria, 310 genes were up-regulated (Figure 3A) and 170 genes were down-regulated (Figure 3B) in ipsilateral, Thionin-positive NM neurons destined to survive deafferentation (Ipsi) compared to contralateral controls (Contra). Similarly, 1,029 genes were up-regulated (Figure 4A), and 553 genes were down-regulated (Figure 4B) in ipsilateral, Thionin-negative “ghost” NM neurons destined to die (ghost) versus contralateral control neurons (contra). Five hundred and thirty-five genes were up-regulated (Figure 5A), and 147 down-regulated (Figure 5B) in ipsilateral, “ghost” neurons (ghost) versus ipsilateral, surviving NM neurons (Ipsi). Figures 3-5 profile the molecular classifications of annotated genes showing differential expression between groups.

Real-Time PCR analyses

In applying Integrated Pathways Analysis (IPA) software to the microarray results, thirty-nine genes from six canonical pathways (GABA receptor signaling, glutamate receptor signaling, calcium signaling, oxidative

phosphorylation, phospholipid degradation, and PTEN signaling) were examined for differential gene expression across microdissected subpopulations of NM using quantitative RT-PCR. Thirty-nine primer pairs were designed and tested for primer dimerization and product detection. Of those primers tested, 12/39 successfully detected products in our system. Table 1 shows the primer sequences used to detect 12 genes of interest and four "housekeeping" genes. The sequences for 18s rRNA were proprietary. Only four genes (CASQ2, GRIN1, NSF, and PLA2G10) exhibited statistically significant differential expression across NM subpopulations (see Table 2, asterisks); however, results from all 12 genes will be presented (see Table 2).

Figures 6-9 display average expression levels (in arbitrary values) of genes of interest, normalized to the average expression of RPS6KL1 and grouped by canonical pathway, across subpopulations of NM neurons. Figure 6 shows differentially expressed genes involved in calcium signaling. ATP2B1 (Figure 6A) is one of four genes encoding subunits of a plasma membrane calcium ATPase (PMCA) pump, responsible for actively pumping calcium from the cytoplasm to the extracellular space (Tempel and Shilling, 2007, Di Leva et al., 2008). Activity of PMCA is influenced by intracellular calcium levels and plasma membrane lipid composition: elevated calcium levels increase pump activity (Di Leva et al., 2008), as do increased levels of acidic phospholipids and polyunsaturated free fatty acids (Adamo and King, 1967, Brodin et al., 1992). Interestingly, a targeted null mutation of ATP2B1

is embryonic lethal to developing mice; however, spontaneous, acquired mutations in a related gene family member, ATP2B2, is known to produce deafness (Tempel and Shilling, 2007). Results from microarray analyses showed significantly elevated levels of ATP2B1 mRNA in “ghost” neurons, as compared to ipsilateral, Thionin-positive NM neurons (Ipsi) destined to survive (p-value=0.00319) and in “ghost” versus contralateral (Contra) control NM neurons (p-value=0.00774). Quantitative RT-PCR revealed similar trends in ATP2B1 mRNA expression across NM, but statistical significance was not established (Kruskal-Wallis one-way ANOVA on ranks p-value=0.446). Interestingly, each of the ATP2B genes (1-4) undergoes extensive alternative splicing in response to calcium demands (Di Leva et al., 2008); thus, it is possible that the microarray probes detected an alternative isoform of ATP2B1 than was detected by the primers used in quantitative RT-PCR.

Calcium/calmodulin-dependent protein kinases (CaMKs) represent a family of enzymes activated by elevations in intracellular calcium (Takemoto-Kimura et al., 2007). CAMK1G (Figure 6B) was observed by microarray to be up-regulated in ipsilateral “ghost” neurons destined to die, compared to ipsilateral, surviving neurons (Ipsi) (p-value= 0.0272), as well as in “ghost” neurons versus contralateral (Contra) NM neurons (p-value=0.0181). CAMK4 (Figure 6C) was also shown by microarray to be significantly up regulated in “ghost” versus contra NM (p-value=0.0358). However, neither CAMK1G (one-way ANOVA p-value=0.184) nor CAMK4 (Kruskal-Wallis one-way

ANOVA on ranks p-value=0.219) was observed to be significantly differentially expressed using RT-PCR.

Calsequestrin2 (CASQ2), a gene activated in cardiac myocytes in response to calcium released from internal stores (Gyorke et al., 2007) was verified by RT-PCR to be differentially expressed across NM subpopulations (Kruskal-Wallis one-way ANOVA on ranks p-value=0.025) (Figure 6D). Microarray results showed significantly elevated (p-value=0.0198) mRNA levels in ghost versus ipsilateral, Thionin-positive NM neurons, while pair-wise post-hoc comparisons, using Dunn's Method, on RT-PCR results were insignificant. CASQ2, whose expression has been described in mammalian myocardium (Knollmann et al., 2006) is localized to the junctional sarcoplasmic reticulum and is thought to be the major calcium storage protein in the heart (Jones and Cala, 1981). CASQ2 overexpression in cardiomyocytes produces defects in calcium-mediated excitation-contraction coupling (Knollmann et al., 2006). CASQ2 may influence calcium dynamics similarly in neurons.

Figure 7 shows differentially expressed genes involved in glutamate receptor signaling. Glutamate receptors are directly linked to calcium signaling within neurons, and are fundamental to synaptic plasticity and excitatory neurotransmission (Lipsky and Goldman, 2003). Due to their plastic nature, glutamate receptors (as well as GABA receptors) are expressed at neuronal surfaces in response to genetically inherited

instructions *or* as an adaptive response to the environment. Fluctuations in expression, therefore, confound the study of these receptors, making it difficult to determine whether expression is a cause of or a response to a cellular perturbation. The glutamate receptor delta 1 (GRID1) gene, which encodes a glutamate receptor subunit, structurally classified as an ionotropic receptor (Guo et al., 2007), was found to be up-regulated in deafferented "ghost" neurons by microarray results (p-value=0.0356) but not by RT-PCR (one-way ANOVA p-value=0.102; Figure 7A). Interestingly, GRID1 is abundantly expressed in auditory and vestibular hair cells and spiral ganglion neurons (Safieddine and Wenthold, 1997), but its function in the nervous system is not well defined.

The gene encoding the glutamate receptor 5 kainate receptor (GRIK1) is also an ionotropic glutamate receptor, which is activated by kainate (Lipsky and Goldman, 2003). GRIK1 was observed by microarray analysis to be up-regulated in ipsilateral "ghost" neurons versus contralateral control neurons (p-value=0.00852) and in ipsilateral, Thionin-positive neurons versus contralateral controls (p-value= 0.0104). By RT-PCR, however, differences were statistically insignificant (one-way ANOVA p-value=0.268; Figure 7B). Activity of glutamate receptors is critical to neuronal transmission. Polymorphisms in GRIK1 mRNA have been associated with a number of neuropathologies, including schizophrenia (Shibata et al., 2001) and epilepsy (Sander et al., 1997).

Like GRID1 and GRIK1, G protein-regulated inducer of neurite outgrowth1 (GRIN1) is an ionotropic glutamate receptor. GRIN1 encodes the ionotropic glutamate receptor subunit, NR1, and is activated by *N*-methyl-D-aspartate (NMDA) (Lipsky and Goldman, 2003). The NR1 subunit forms a calcium channel and is required for receptor activity (Moreno-Gonzalez et al., 2008). GRIN1 was observed via microarray analysis to be differentially up-regulated in "ghost" versus contralateral (p-value=0.0102) and in "ghost" versus ipsilateral, Thionin-positive NM neurons (p-value=0.0422), as well as in ipsilateral, Thionin-positive NM neurons compared to contralateral controls (p-value=0.0247). Quantitative RT-PCR verified significant differences in GRIN1 expression across NM (one-way ANOVA p-value=0.016; Figure 7C). Specifically, post-hoc, pair-wise comparisons using the Holm-Sidak method confirmed GRIN1 transcripts were expressed in significantly greater abundance in "ghost" neurons versus contralateral control neurons (Figure 7C).

Figure 8 shows genes involved in $\gamma$-aminobutyric acid (GABA) receptor signaling that exhibited differential mRNA levels across NM subpopulations based on microarray analyses. Neurons within chick NM receive descending GABAergic input from the ipsilateral superior olivary nucleus (Lachica et al., 1994, Lu et al., 2005). The gene encoding subunit $\alpha$3 of the GABA, type A receptor (GABRA3) is involved in inhibitory neurotransmission in neurons (Mu and Burt, 1999) and is observed to be significantly down-regulated in

deafferented “ghost” neurons destined to die versus contralateral control neurons (p-value=0.0429) via microarray, but not via RT-PCR (one-way ANOVA p-value=0.096; Figure 8A). Interestingly, RT-PCR results suggest a trend opposite to that observed using microarray.

Inhibitory neuroplasticity is regulated by trafficking of $GABA_A$ receptors between the Golgi and the plasma membrane (Leil et al., 2004). *N*-ethylmaleimide-sensitive factor (NSF), is an ‘ATPase Associated to various cellular Activities (AAA)’ (Whiteheart and Matveeva, 2004), which has been shown to mediate a number of intracellular vesicular transport and fusion phenomena (May et al., 2001). In deafferented NM “ghost” neurons, NSF mRNA was significantly increased compared to contralateral control neurons (microarray p-value=0.0356). RT-PCR analyses confirmed this finding (one-way ANOVA p-value<0.001; Figure 8B). In addition, RT-PCR results showed that NSF mRNA levels were significantly elevated in ipsilateral, Thionin-positive NM neurons compared to contralateral NM neurons (Figure 8B). Perhaps NSF expression increases in deafferented NM neurons in an attempt to modulate GABRA3 levels and elicit (albeit ineffectively) descending support from superior olivary neurons.

Figure 9 shows differentially expressed genes involved in oxidative phosphorylation (ATP5J2), phosphatase and tensin homologue (PTEN) signaling (CASP3), and phospholipid degradation (PLA2G10). Results from quantitative RT-PCR results for ATP5J2 expression are shown in Figure 9A.

Microarray results showed a significant increase in ATP5J2 transcript levels in "ghost" NM neurons versus ipsilateral, Thionin-positive NM neurons (p-value=0.0234). RT-PCR results, however, did not confirm this finding (one-way ANOVA p-value=0.052). ATP5J2 encodes a portion of the $F_0$ subunit of the mitochondrial inner membrane $F_0$-$F_1$ ATPase pump that is required for ATP synthesis during oxidative phosphorylation; consequently, ATP5J2 expression is directly linked to the metabolic energy state of the cell (Chu and Peters, 2008, Saiki et al., 2008). Evidence to suggest loss of $F_0$-$F_1$ ATPase (also called ATP synthase or plainly, ATPase) function in deafferented NM neurons that die was presented in Chapter III. ATPase activity, based on histological evaluation of enzymatic reaction product accumulation, is compromised in a subset of deafferented NM neurons as early as 24 hours after cochlea removal. Results from molecular genetic analyses, however, were unable to confirm differential expression of ATP5J2 in NM neurons.

Also observed via microarray analyses to be differentially downregulated in "ghost" versus contralateral NM neurons (p-value=0.035), caspase 3 (CASP3), is an effector caspase activated late during apoptosis, which is responsible for cleavage of cellular components in preparation for death. CASP3 is involved in PTEN signaling, the latter regulating cell cycle progression, apoptosis, and phosphatidylinositol-3,4,5 triphosphate regulation (Castellino and Durden, 2007). Active caspase-3 protein is detected immunocytochemically in deafferented NM neurons as early as 12 hours after

cochlea removal (Karnes et al., 2009). Interestingly, by 24 hours, no appreciable differences in active caspase-3 immunoreactivity are observed between deafferented NM neurons targeted to die and those targeted to survive (Karnes et al., 2009). In this study, CASP3 mRNA message was not significantly changed across NM subpopulations (one-way ANOVA p-value=0.131; Figure 9B). Similar disassociations in mRNA and protein levels have been previously described in NM: 24% of deafferented NM neurons exhibit an up-regulation of Bcl-2 mRNA, but not protein, 6-12 hours after cochlea removal (Wilkinson et al., 2002). In addition, levels of β–Tubulin and β–Actin mRNA were found to be unaffected by cochlea removal (by *in situ* hybridization), although, corresponding protein levels were down-regulated 3 hours to 4 days afterwards (Kelley et al., 1997).

PLA2G10 was observed to be differentially upregulated in ipsilateral "ghost" neurons versus contralateral controls via microarray (p-value=0.0114), and was confirmed using RT-PCR (one-way ANOVA p-value=0.004). PLA2G10 is one of the most potent members of the group X secreted phopholipase $A_2$ family (Henderson et al., 2007). PLA2G10 hydrolyzes glycerophospholipids, present within cell membranes, and liberates free fatty acids (Henderson et al., 2007). PLA2G10 is activated by rising levels of intracellular calcium and is indicative of tissue injury (Fujioka et al., 2008). Consequently, it may be involved in mediating a neuron's response to deafferentation-induced death in chick NM.

The variability in results obtained from microarray and quantitative RT-PCR platforms will be explored in detail in the subsequent section; however, it is interesting to note that only 4 genes (compared to the 39 originally identified as significant from microarray results) were verified to be differentially expressed using RT-PCR. Also interesting was the observation that mRNA levels of several "traditional" housekeeping genes across NM subpopulations were affected by cochlea removal. Table 3 shows average $C_t$ values across NM for three "traditional" housekeeping genes (β-Actin, GAPDH, and 18s rRNA) and for the gene encoding ribosomal protein S6 kinase-like 1 (RPS6KL1). Previous studies of the genomic (using *in situ* hybridization) and proteomic changes in cytoskeletal elements in NM following deafferentation showed that levels of β-Actin mRNA remained unchanged (Kelley et al., 1997). As a consequence, β-Actin was initially evaluated for use as a standard against which all RT-PCR data could be normalized. Table 3 shows, however, that β-Actin mRNA levels are, indeed, influenced by deafferentation. In fact, β-Actin as well as 18s rRNA, had most abundant transcripts in deafferented "ghost" neurons destined to die. GAPDH showed the opposite trend, having a higher average $C_t$ value (i.e. a lower mRNA abundance) in "ghost" neurons. To date, a true standard has not been identified in NM whose gene expression is unaffected by deafferentation; however, we identified a gene RPS6KL1, which encodes a ribosomal protein that is largely consistent in mRNA expression across the NM subpopulations

evaluated. These findings affirm that cochlea removal has widespread effects on NM neuronal physiology. In addition, the novel identification of a gene, whose expression in NM is unaltered by cochlea removal, provides a valuable tool for additional molecular analyses within the chick auditory brainstem

**Summary and Discussion**

The results presented here demonstrate successful separation of homogeneous cell (neuronal and glial) populations from nucleus magnocellularis (NM) tissue sections using laser capture microdissection (LCM). RNA extracted from microdissected cells remains intact and viable for downstream genetic analyses. Microarray analysis and subsequent data mining of differentially expressed genes across NM subpopulations (deafferented NM neurons known to survive deafferentation; deafferented NM neurons known to die following deafferentation; and healthy NM neurons from the contralateral nucleus) revealed six canonical pathways involved in cell fate determination: glutamate receptor signaling, GABA receptor signaling, calcium signaling, oxidative phosphorylation, phospholipid degradation, and PTEN signaling. Validation of microarray results confirmed the differential expression of genes involved in calcium signaling (CASQ2), glutamate receptor signaling (GRIN1), GABA receptor signaling (NSF), and phospholipid degradation (PLA2G10). Interestingly, traditional housekeeping genes were also observed to change in response to NM deafferentation. The identification of a gene encoding the ribosomal protein S6 kinase-like 1 (RPS6KL1), with consistent mRNA expression across NM subpopulations, allowed the use of quantitative Real-Time Polymerase Chain Reaction (RT-PCR) technology to begin the elucidation of a molecular mechanism underlying deafferentation-induced neuronal death in NM. In the discussion

that follows, we examine potential factors underlying differences between microarray and RT-PCR results. We then discuss the significance of our findings within the context of our system.

Differences in our results could derive from either platform: microarray or PCR. Historically, molecular genetic evaluation of the auditory system has proven difficult due to the relatively low abundance of sensory tissue *and* the low levels of key molecular transducers within that tissue (Steel and Kros, 2001). Consequently, auditory neurons within chick NM were pooled across animals to achieve working concentrations of RNA compatible with downstream applications. Pooling, although beneficial when (as here) nucleic acid levels from individual animals are too small for data analysis, potentially accentuates within-group variability and may obscure the true effects of the manipulation (Macdonald et al., 2008). As the same pooled samples were used in both microarray and RT-PCR reactions, pooling, alone, is an unlikely source of discordance, although it may affect the overall quality of our results. The high intra-group variance observed in some of our RT-PCR results (Figures 6-9) demonstrates the need for greater sample sizes and repeated measures. In a number of cases, statistical significance was not established due to the high degree of variance. Polymorphisms within individual animal subjects may have influenced the overall expression level of the pooled sample, and subsequently, affected the interpretation of the data.

In the context of the neuronal system under investigation, however, the four genes observed to be significantly differentially expressed by both platforms, merit further examination based on their biologic significance. CASQ2 is a gene that mediates calcium release from the sarcoplasmic reticulum in cardiac myocytes (Gyorke et al., 2007) and is thought to be a major calcium storage protein in the heart (Jones and Cala, 1981). Calcium dysregulation is known to occur in deafferented NM (Zirpel et al., 1995, Zirpel and Rubel, 1996) and is increasingly thought to influence NM neuronal death following cochlea removal. Calcium dysregulation occurs within one hour of cochlea removal (Lachica et al., 1995, Zirpel et al., 1995), and has been hypothesized to underlie many of the neuropathic changes observed in deafferented NM neurons that eventually die (see Chapter III). Calcium is known to be released from compromised endoplasmic reticulum (ER)-mitochondrial junctions (Pinton et al., 2008). Fragmentation of ribosomes is a well-documented event in deafferented NM neurons, occurring as early as 6 hours following cochlea removal (Rubel et al., 1991), and effectively identifying NM neurons destined to die (Karnes et al., 2009). In addition, mitochondrial structural (Hyde and Durham, 1994) and functional changes (see Chapter III) accompany deafferentation-induced neuronal death in NM. Additionally, calcium is known to perpetuate oxygen free radical production, which has been described in deafferented NM (Nicholas and Hyson, 2006), as well as to directly attack membranes and mitochondrial proteins involved in

energy generation (see Chapter III). This combination of events strongly implicates calcium in the mechanism of NM neuronal fate determination. CASQ2, which was found to be differentially expressed at the transcriptional level across NM, may be influential in calcium signaling events in deafferented “ghost” neurons destined to die.

Integrally linked to calcium signaling in neurons, glutamate receptors are fundamental for neuronal excitation and plasticity (Lipsky and Goldman, 2003). GRIN1 encodes the NR1 subunit of a glutamate-gated cation channel of the NMDA receptor subtype (Hollmann and Heinemann, 1994). NMDA receptor activity has been shown to be tightly linked to energy metabolism (Dhar and Wong-Riley, 2009), especially to the activity of cytochrome oxidase (CO) (Wong-Riley, 1989). CO activity is known to increase in deafferented NM neurons as early as 6 hours after cochlea removal (Hyde and Durham, 1990), and to be significantly elevated in ipsilateral versus contralateral NM neurons by 24 hours (see Chapter III), probably as a result of the expansive proliferation of mitochondria across deafferented NM at this time point (Hyde and Durham, 1994). It is not surprising that metabolically active neurons require greater excitatory support: GRIN1 activity may be involved in the active but futile attempt to increase glutamatergic input to these metabolically active neurons in NM.

NMDA receptor activity is also observed to change in NM in response to developmental remodeling and synaptic plasticity (Lu and Trussell, 2007).

NMDA subunits NR1 and NR2 are expressed in developing chick NM neurons as early as E10 (Tang and Carr, 2007), when eighth nerve afferent activity can be recorded from NM (Jackson et al., 1982). NR1 mRNA (using *in situ* hybridization) and protein levels fluctuate transiently during NM neuronal development, and show little change in mature adult neurons (Tang and Carr, 2004, Tang and Carr, 2007). NMDA functional activity in NM neurons, measured via electrophysiologic methods, declines over development and does not appear crucial to neurotransmission (Lu and Trussell, 2007) in NM neurons. GRIN1 up-regulation in deafferented NM "ghost" neurons destined to die may serve as a "last ditch" mechanism to increase glutamatergic support to neurons.

In addition to glutamatergic support from eighth nerve afferents, NM neurons receive GABAergic inputs from the superior olivary nucleus (Lachica et al., 1994). This GABAergic input, mediated by $GABA_A$ receptors on NM neurons, can produce depolarizing, asynchronous spikes in NM under high stimulation as a means to modulate and preserve timing of excitatory inputs (Lu and Trussell, 2000). In response to deafferentation, NM neurons experience an abrupt loss of glutamatergic input from eighth nerve afferents. Deafferented NM "ghost" neurons destined to die might increase levels of $GABA_A$ receptors as a means to recruit depolarizing, GABAergic support from the superior olivary nucleus. *N*-ethylmaleimide-sensitive factor (NSF) is known to mediate the intracellular transport of $GABA_A$ receptors to the cell

surface (May et al., 2001) and may be involved in mediating the response to deafferentation-induced neuronal death in NM after cochlea removal.

PLA2G10, a potent phospholipase $A_2$ (Henderson et al., 2007), is also observed to be up-regulated in deafferented NM “ghost” neurons. PLA2G10 activation occurs in response to elevated intracellular calcium and is an effective indicator of cellular compromise (Fujioka et al., 2008). We speculate that elevated calcium triggers a series of cellular events that ultimately result in death of 30-50% of deafferented NM neurons. Calcium, released from damaged endoplasmic reticulum (ER)-mitochondrial junctions, perhaps involving up-regulation of CASQ2, may perpetuate the rise in intracellular calcium observed in deafferented NM “ghost” neurons destined to die. Calcium influx may also occur via differential activation of NMDA receptors, perhaps mediated by GRIN1 up-regulation. Alternatively, NMDA up-regulation may occur in response to elevations in metabolism, which have been previously described in deafferented NM (see Chapter III). Calcium perpetuates reactive oxygen species generation and membrane peroxidation, the latter possibly being modulated by increased levels of PLA2G10 in deafferented NM “ghost” neurons. In an effort to recover from the abrupt loss of excitatory support, “ghost” neurons may upregulate NSF as a means to promote depolarizing, GABAergic input from higher-order auditory nuclei.

It is obvious that deafferentation by cochlea removal perturbs multiple facets of NM cellular physiology, including affecting the expression of

traditional housekeeping genes often used as “standards,” against which to normalize gene expression data. Likely to influence the differences we observed across microarray and RT-PCR analyses are the different standards utilized in each platform. Microarray GeneChips are equipped with several internal controls. Poly-adenylated genes from *B. subtilis* are often “spiked” into sample RNA and used to monitor the target labeling process from start to finish. Similarly *E. coli* genes may be introduced to the sample, at a later stage, to assess GeneChip hybridization efficiency. In addition, two housekeeping genes (β-Actin and GAPDH) are present within most GeneChips to serve as internal gene expression controls (Affymetrix, 2002). Unfortunately, *B. subtilis* “spike” controls were omitted from our sample preparation; *E. coli* probe sequences are proprietary; and at least 1 internal housekeeping control gene was “outside the range” of detection on each microarray GeneChip.

Unexpected changes in expression of traditional housekeeping genes were also observed in our RT-PCR results (see Table 3). Although mRNA levels of cytoskeletal elements (β-Actin and β-Tubulin) in NM neurons have been previously reported to be unaffected by cochlea removal using *in situ* hybridization techniques (Kelley et al., 1997), our examination of β-Actin, as well as of GAPDH and 18s rRNA across NM, revealed transcriptional differences. As microarrays utilized housekeeping standards, which do not

appear to function as such in our system, it is not surprising that our results differed from the RT-PCR results.

Although mRNA levels change directly in response to gene promoter activation, epigenetic effects (i.e. DNA methylation and histone deacetylation) may also influence expression levels across neuronal subpopulations. These effects should be considered as potential contributions to the deafferentation-induced mechanism of NM neuronal death. Further experimentation is necessary to elucidate these influences.

## Conclusions

In summary, we have shown that despite the low abundance of auditory sensory material, individual cells may be selectively removed from complex tissue sections using laser capture microdissection (LCM) and used in downstream molecular analyses. RNA remains intact and viable for genetic evaluation. Examination of genetic contributions to neuronal death in chick auditory brainstem revealed the differential expression of genes related to calcium signaling (CASQ2), glutamate receptor signaling (GRIN1), GABA receptor signaling (NSF), and phospholipid degradation (PLA2G10). Interestingly, typical housekeeping genes (β-Actin, GAPDH, and 18s rRNA) within NM neurons were also influenced by deafferentation, a finding that contradicts the literature. Additional investigations into genes that do not change with deafferentation would provide valuable insight to further elucidate the molecular mechanism underlying deafferentation-induced cell death in NM.

**Table 1**

**Primer sequences used to detect gene products in quantitative RT-PCR**

| Gene | Forward primer (5'-3') | Reverse primer (5'-3') |
|---|---|---|
| Genes of interest | | |
| ATP2B1 | CACGCTGAGCGAGAATTACGT | CCACTCGTATCTGAGTTTGTATTCTGT |
| ATP5J2 | ATGACCGCCGCAGGAA | CCACAAGCTGCACCTTCACTT |
| CAMK1G | GGATACGTCGCCCCTGAA | GCAGTCCACGGCTTTGCT |
| CAMK4 | TGGCCCTGAAGTGGACATG | TGGTTCAAAGCCACATAGTAGAATG |
| CASP3 | CCAGATGAAACAGTGTGTCAAAAAA | GGAGTAGTAGCCTGGAGCAGTAGAATA |
| CASQ2 | CCCAGTGCAGGAGGAAAGC | AAAATACAAACTGGCTCCCTGTGT |
| GABRA3 | CAGCGCAAGAAACTCGTTACC | AGACGGCTATGAACCAGTCCAT |
| GRID1 | ATGAAGACATAGCCCACAAGCA | ACCGATCTCCAAGGCTGAGA |
| GRIK1 | GGAGTGGGAACCCCTATTGG | GCTGGAGGATGGCAATGGT |
| GRIN1 | AGGAGTGTGATTCCCGTAGCA | AAACACACCTGCCATATTTTCAAA |
| NSF | GCGTTTTTTCAGGCCCAAA | GAAACACTCTGATTGCCCTAAGTATG |
| PLA2G10 | TGCGGACTGGGAGGACAA | CCTGTGGCAGCACCAGTCT |
| Housekeeping genes | | |
| β-Actin | TCCACCTTCCAGCAGATGTG | AATGGAGGGTCCGGATTCAT |
| GAPDH | AGATGCAGGTGCTGAGTATGTTG | GATGAGCCCCAGCCTTCTC |
| 18s rRNA | probe purchased from Applied Biosystems (Part #4310893E) | |
| RPS6KL1 | GAGGGCACACGTGAGGTTTC | GCTAGTAAGCGTAGGCAGCAACA |

**Figure 1**

Photomicrographs through NM from an animal sacrificed 24 hours following cochlea removal, visualized under brightfield microscopy (A, B) and through the laser capture microdissection (LCM) system (C-F). Sections were stained with Thionin to visualize cytoplasmic ribosomal Nissl substance. Note the abundance of Nissl substance in healthy contralateral NM neurons (A) indicative of intact ribosomes. Two populations of neurons within ipsilateral NM are observable at this time point (B, C): Thionin-positive neurons, which represent those neurons destined to survive deafferentation, and Thionin-negative “ghost” neurons, which represent the population that will die following deafferentation. LCM was used to visualize populations of NM neurons based on their Thionin-staining characteristics (C), and selectively target subpopulations (in this case, “ghost” neurons) for microdissection from the tissue section (D). Targeted neurons are effectively removed from the tissue (E) and adhered to LCM caps for subsequent extraction of RNA (F).

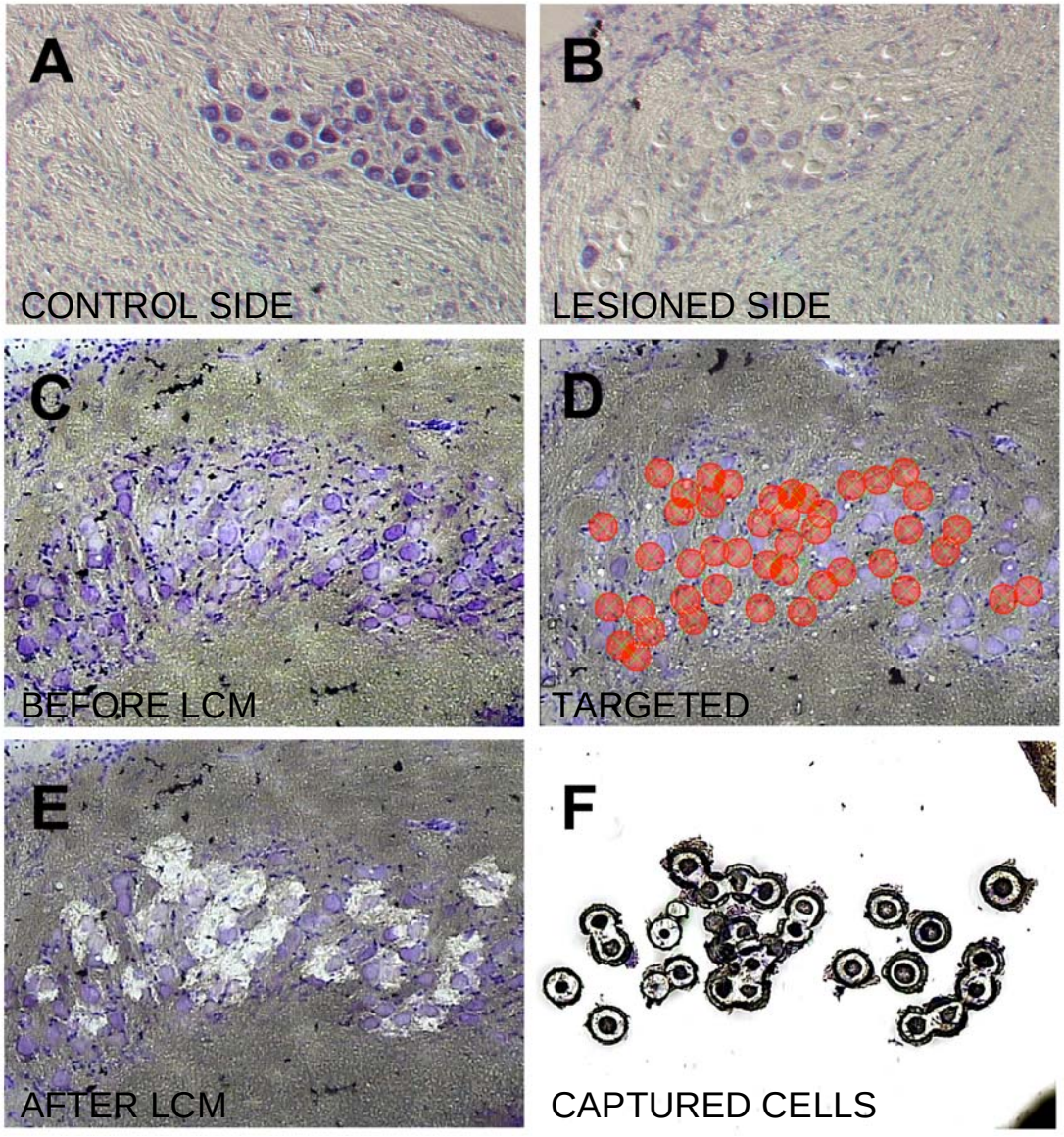
A
CONTROL SIDE
B
LESIONED SIDE
C
BEFORE LCM
D
TARGETED
E
AFTER LCM
F
CAPTURED CELLS

**Figure 2**

Representative profiles from Agilent Bioanalyzer assessment of RNA quality. RNA samples showing clearly delineated bands on the digitized gel electrophoretic profile (A) and sharp peaks at 40s and 45s on the electropherogram (B) indicate intact 18s and 28s rRNA subunits, respectively. Here sample 18N (A, arrow, B), representing RNA extracted from microdissected NM “ghost” neurons exhibits minimal signs of RNA degradation and is viable for use in downstream genetic analyses.

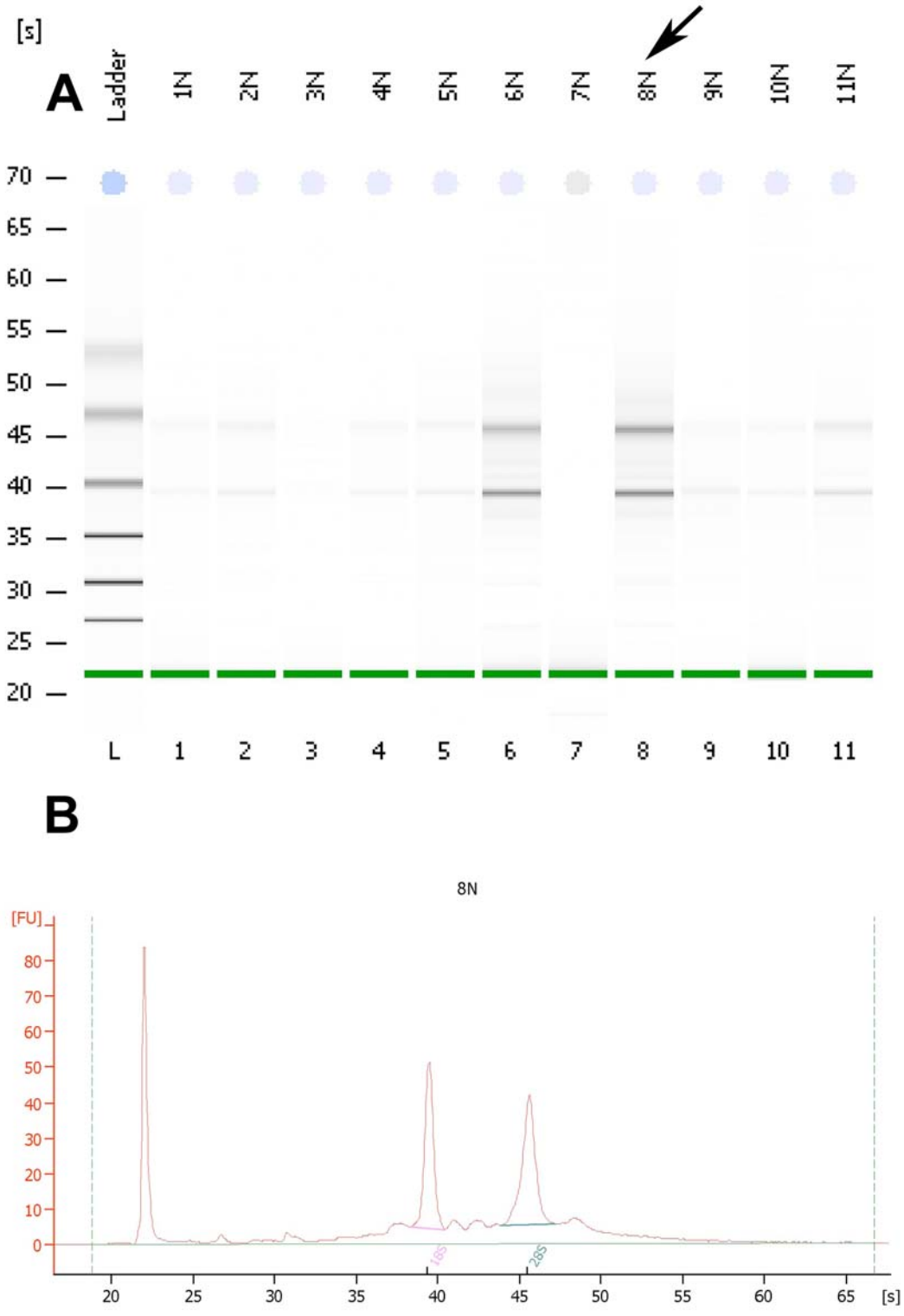
A
[s]
Ladder
1N
2N
3N
4N
5N
6N
7N
8N
9N
10N
11N
70
65
60
55
50
45
40
35
30
25
20
L
1
2
3
4
5
6
7
8
9
10
11
B
8N
[FU]
80
70
60
50
40
30
20
10
0
165
265
20
25
30
35
40
45
50
55
60
65
[s]

**Figure 3**

Ontology pie charts illustrating the molecular profiles of gene products observed to be significantly (p-value ≤ 0.05 and FC ≥ $\left|2\right|$) up-regulated (A) and down-regulated (B) between ipsilateral, Thionin-positive NM neurons destined to survive deafferentation (ipsi) and contralateral control neurons (contra) based on microarray analyses.

Upregulated Ipsi versus Contra

**A**

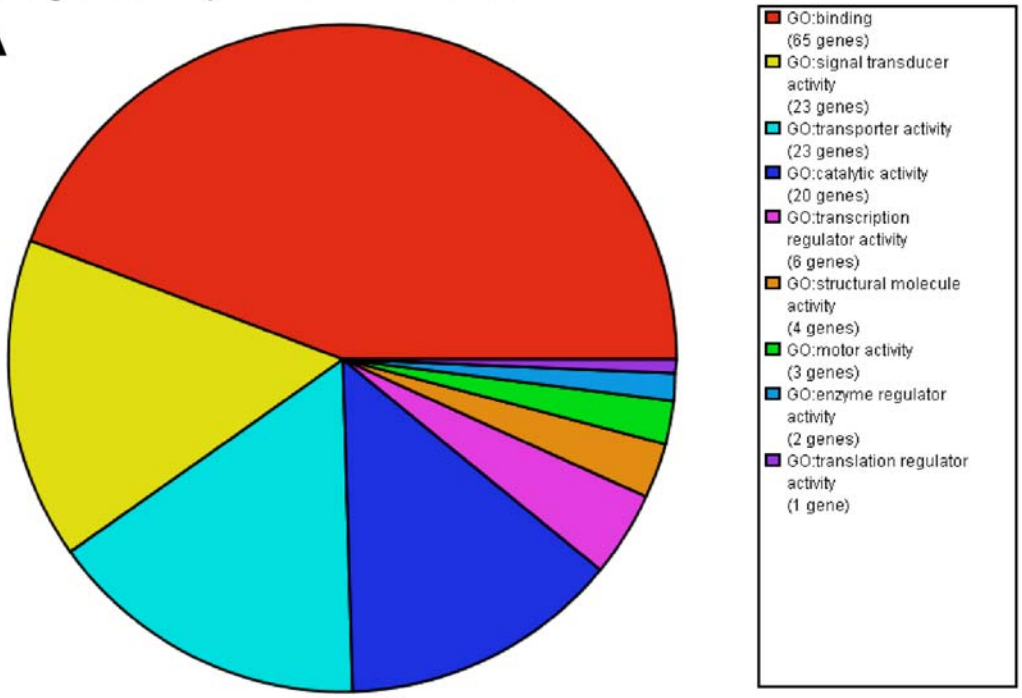


Downregulated Ipsi versus Contra

**B**

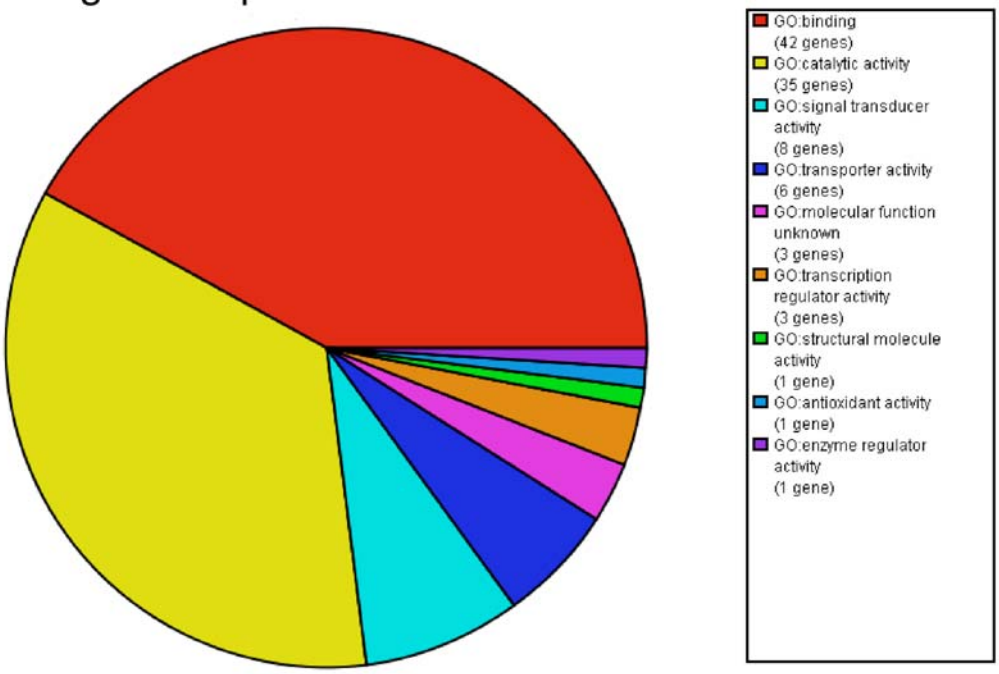

**Figure 4**

Ontology pie charts illustrating the molecular profiles of gene products observed to be significantly (p-value ≤ 0.05 and FC ≥ $\left|2\right|$) up-regulated (A) and down-regulated (B) between ipsilateral, Thionin-negative “ghost” neurons destined to die (ghost) and contralateral control neurons (contra) based on microarray analyses.

Upregulated “Ghost” versus Contra

**A**

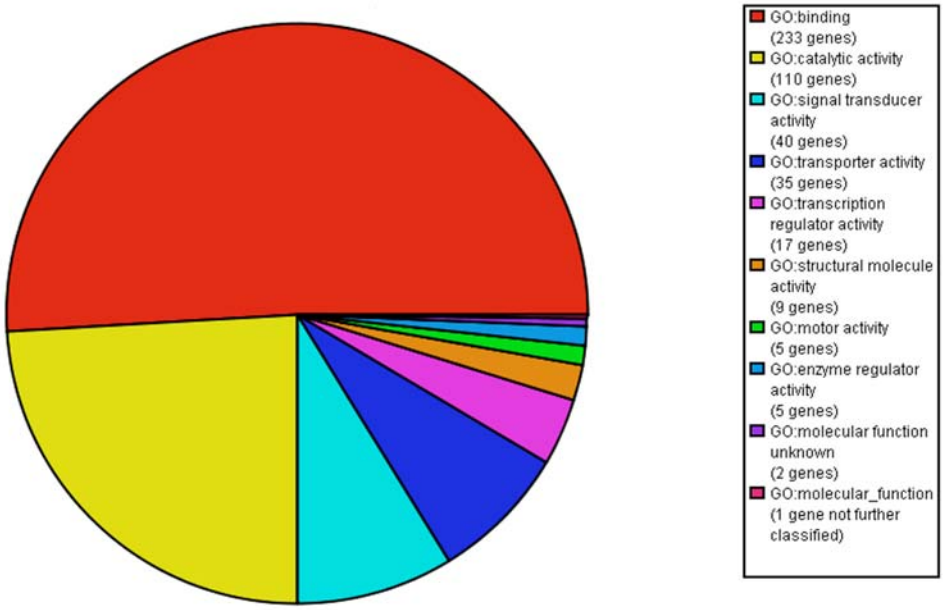


Downregulated “Ghost” versus Contra

**B**

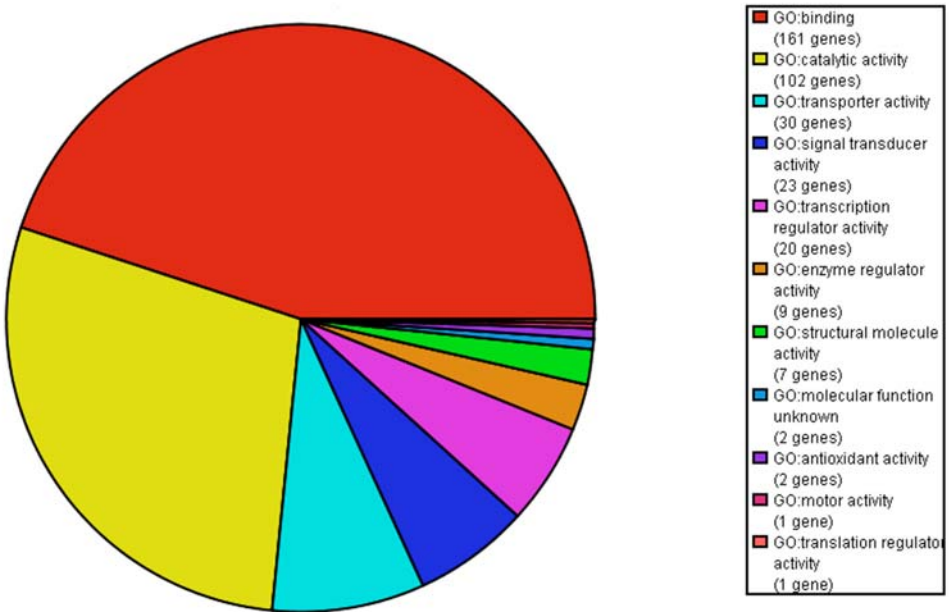

**Figure 5**

Ontology pie charts illustrating the molecular profiles of gene products observed to be significantly (p-value ≤ 0.05 and FC ≥ $\left|2\right|$) up-regulated (A) and down-regulated (B) between ipsilateral, Thionin-negative “ghost” neurons destined to die (ghost) and ipsilateral, Thionin-positive NM neurons destined to survive deafferentation (ipsi) based on microarray analyses.

Upregulated “Ghost” versus Ipsi

**A**

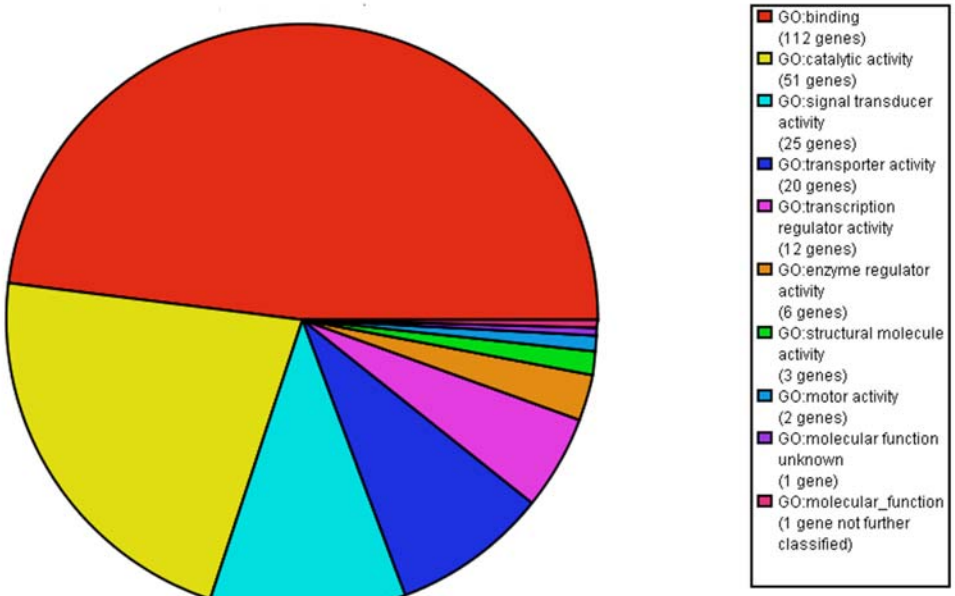


Downregulated “Ghost” versus Ipsi

**B**

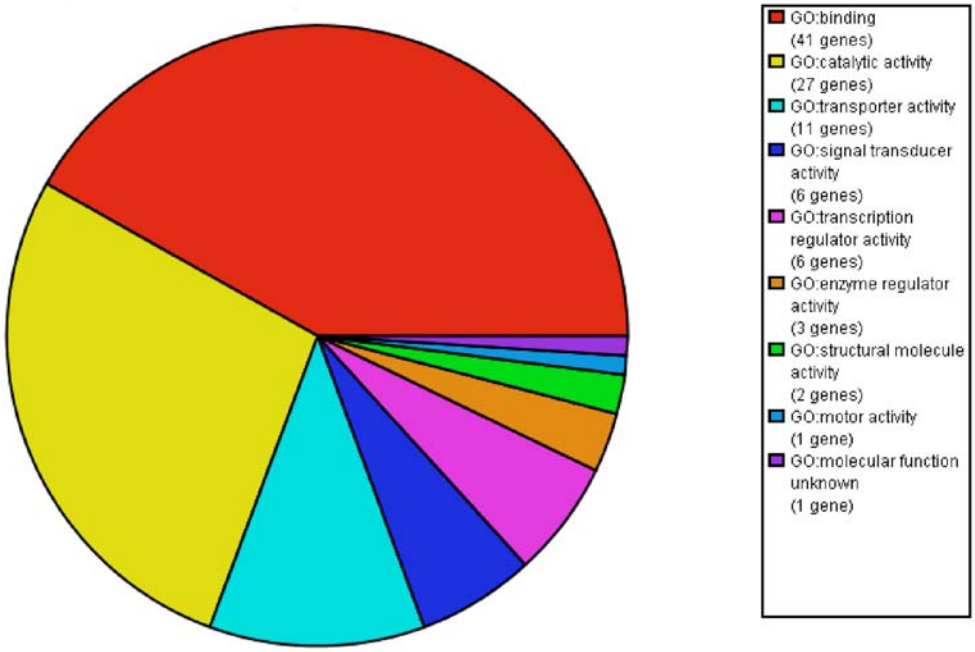

**Table 2**

**Statistical analyses of quantitative RT-PCR results**

| Gene | RT-PCR p-value |
|---|---|
| ATP2B1 | 0.446 |
| ATP5J2 | 0.052 |
| CAMK1G | 0.184 |
| CAMK4 | 0.219 |
| CASP3 | 0.131 |
| CASQ2 | 0.025*# |
| GABRA3 | 0.096 |
| GRID1 | 0.102 |
| GRIK1 | 0.268 |
| GRIN1 | 0.016* |
| NSF | <0.001* |
| PLA2G10 | 0.004* |

* Denotes statistical significance via one-way ANOVA

# Denotes insignificant pair-wise post-hoc comparisons

(ATP2B1, CAMK4, and CASQ2 were analyzed using Kruskal-Wallis one-way ANOVA on ranks followed by post-hoc comparisons using Dunn's Method).

**Figure 6**

Bar graphs showing differences in gene expression (arbitrary values, normalized to expression of RPS6KL1) across groups (Contra, Ipsi, and Ghost) for genes involved in calcium signaling, identified using IPA analyses of biological canonical pathways. Gene expression values were obtained by RT-PCR using the standard curve data analysis technique. ATP2B1 (A) and CAMK1G (B) showed the same trend as microarray results, seemingly expressed in higher levels in “ghost” versus contralateral NM neurons and in “ghost” versus ipsilateral, Thionin-positive NM neurons, although, differences in expression were not statistically significant across groups. CAMK4 expression was not seen to differ statistically across NM subpopulations(C). CASQ2 expression was statistically different across NM (Kruskal-Wallis one-way ANOVA on ranks p-value=0.025); however post-hoc pair-wise comparisons using Dunn’s Method failed to show statistically significant differences (D).

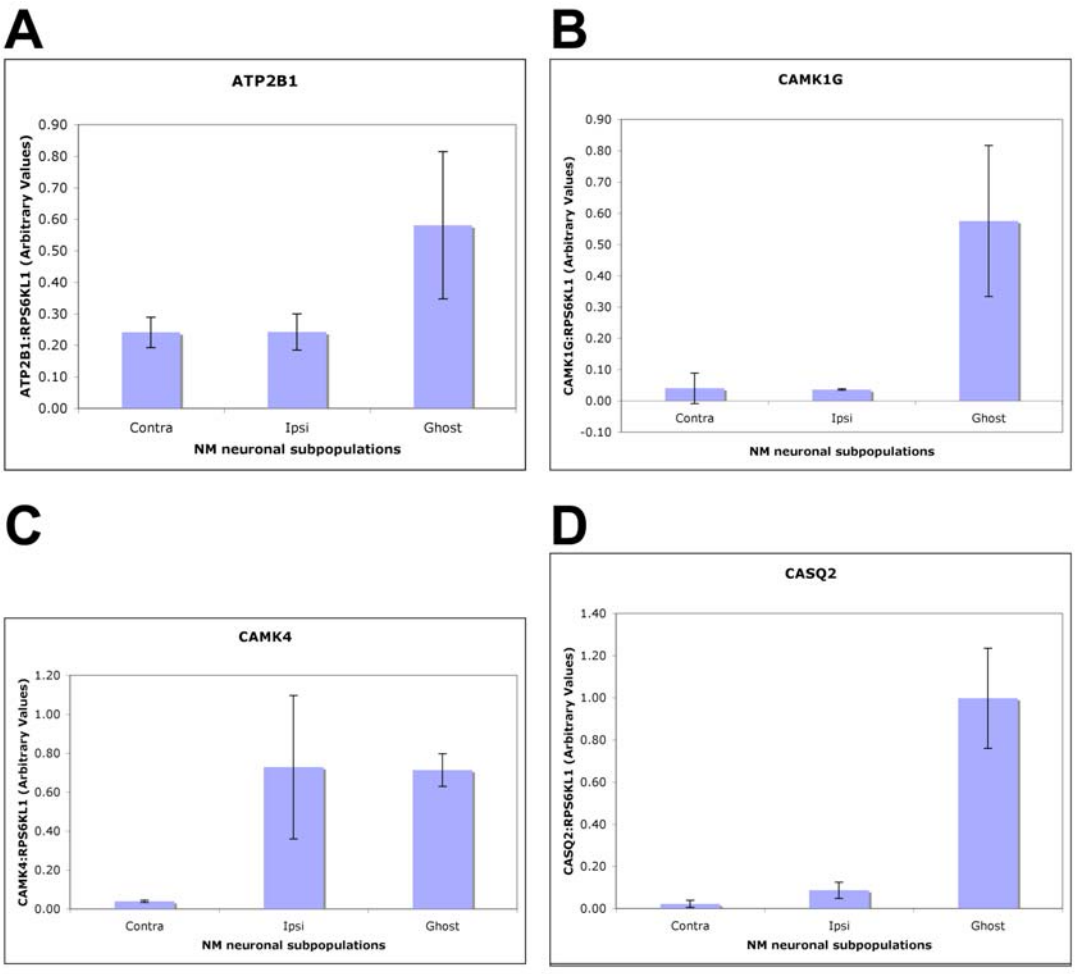
A
ATP2B1
ATP2B1:RPS6KL1 (Arbitrary Values)
0.90
0.80
0.70
0.60
0.50
0.40
0.30
0.20
0.10
0.00
Contra
Ipsi
Ghost
NM neuronal subpopulations
B
CAMK1G
CAMK1G:RPS6KL1 (Arbitrary Values)
0.90
0.80
0.70
0.60
0.50
0.40
0.30
0.20
0.10
0.00
-0.10
Contra
Ipsi
Ghost
NM neuronal subpopulations
C
CAMK4
CAMK4:RPS6KL1 (Arbitrary Values)
1.20
1.00
0.80
0.60
0.40
0.20
0.00
Contra
Ipsi
Ghost
NM neuronal subpopulations
D
CASQ2
CASQ2:RPS6KL1 (Arbitrary Values)
1.40
1.20
1.00
0.80
0.60
0.40
0.20
0.00
Contra
Ipsi
Ghost
NM neuronal subpopulations

**Figure 7**

Bar graphs showing differences in gene expression (arbitrary values, normalized to expression of RPS6KL1) across groups (Contra, Ipsi, and Ghost) for genes involved in glutamate receptor signaling, identified using IPA analyses of biological canonical pathways. Gene expression values were obtained by RT-PCR using the standard curve data analysis technique. GRID1 (A) and GRIK1 (B) were not expressed at significantly different levels across NM subpopulations, although show the same trends in expression as were described using microarray analyses. GRIN1 expression, however, was statistically different across NM subpopulations (one-way ANOVA p-value=0.016), showing significantly more abundant mRNA levels in “ghost” versus contralateral NM neurons (Holm-Sidak post-hoc comparison) (C).

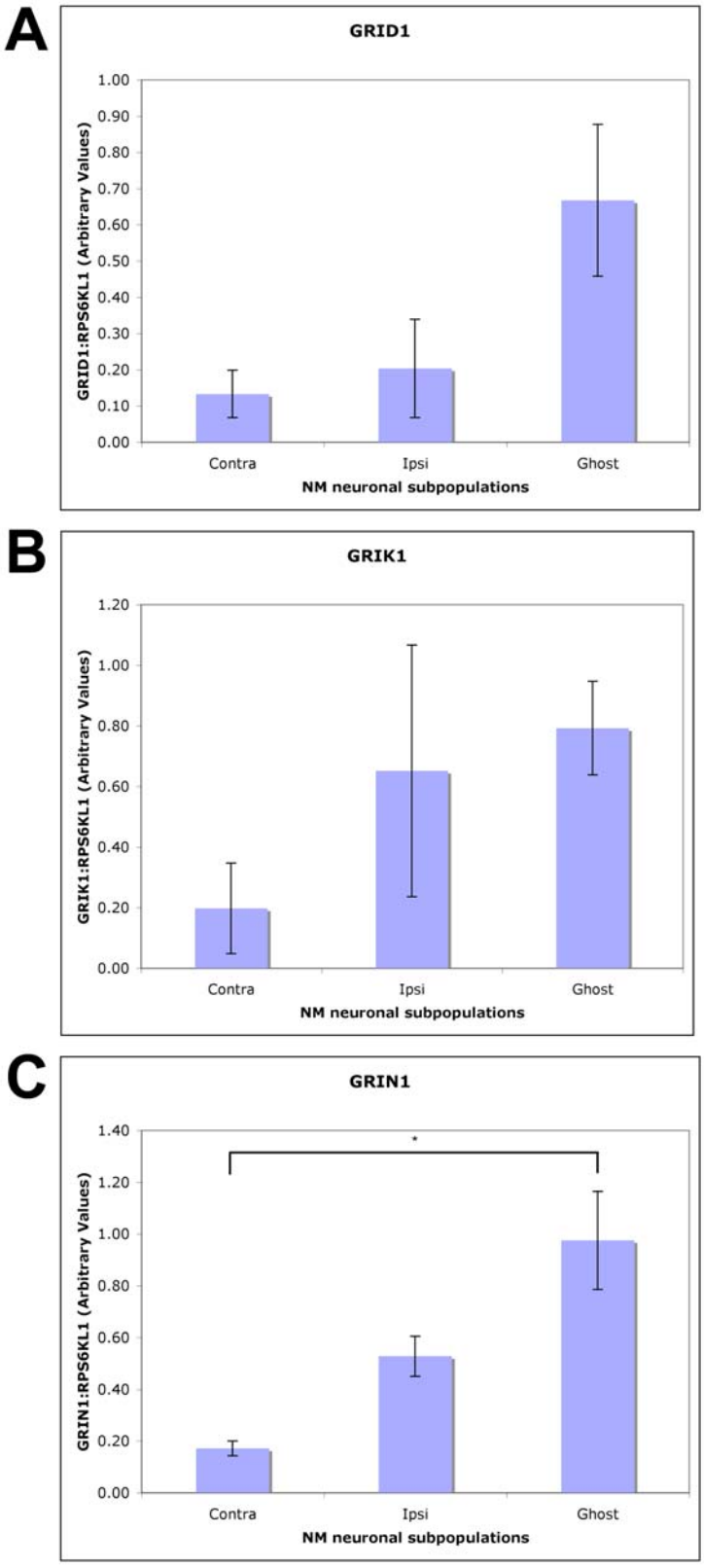
A
GRID1
GRID1:RPS6KL1 (Arbitrary Values)
1.00
0.90
0.80
0.70
0.60
0.50
0.40
0.30
0.20
0.10
0.00
Contra
Ipsi
Ghost
NM neuronal subpopulations
B
GRIK1
GRIK1:RPS6KL1 (Arbitrary Values)
1.20
1.00
0.80
0.60
0.40
0.20
0.00
Contra
Ipsi
Ghost
NM neuronal subpopulations
C
GRIN1
GRIN1:RPS6KL1 (Arbitrary Values)
*
1.40
1.20
1.00
0.80
0.60
0.40
0.20
0.00
Contra
Ipsi
Ghost
NM neuronal subpopulations

**Figure 8**

Bar graphs showing differences in gene expression (arbitrary values, normalized to expression of RPS6KL1) across groups (Contra, Ipsi, and Ghost) for genes involved in GABA receptor signaling, identified using IPA analyses of biological canonical pathways. Gene expression values were obtained by RT-PCR using the standard curve data analysis technique. GABRA3 was not expressed at significantly different levels across NM subpopulations and showed a trend opposite to that described by microarray analyses (A). NSF was observed to be significantly differentially expressed across all NM subpopulations (one-way ANOVA p-value <0.001), and pairwise post-hoc comparisons using the Solm-Hidak method confirmed these differences (B).

A

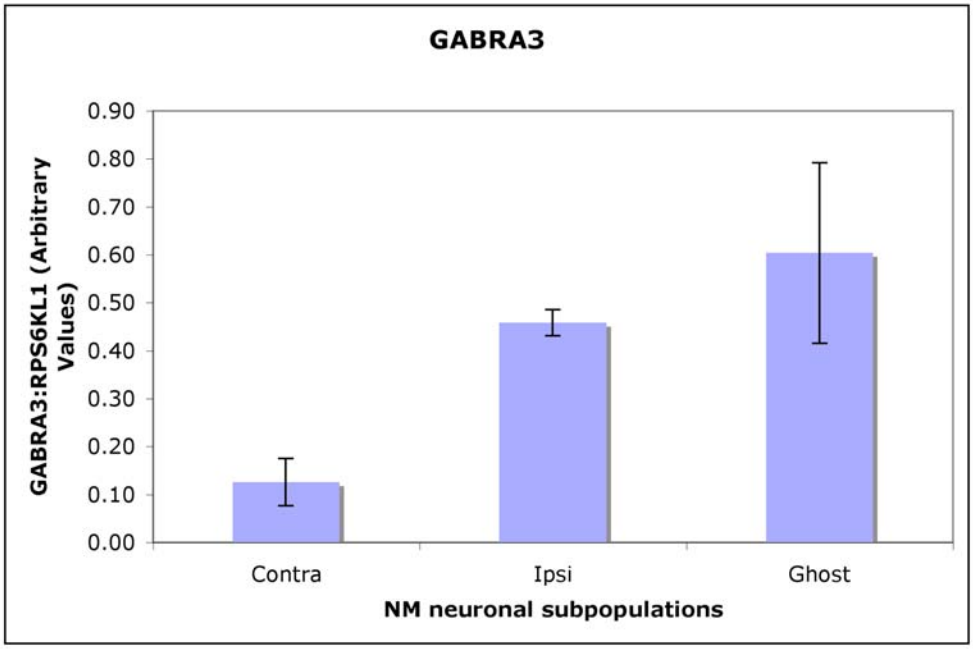
GABRA3
GABRA3:RPS6KL1 (Arbitrary Values)
0.90
0.80
0.70
0.60
0.50
0.40
0.30
0.20
0.10
0.00
Contra
Ipsi
Ghost
NM neuronal subpopulations

B

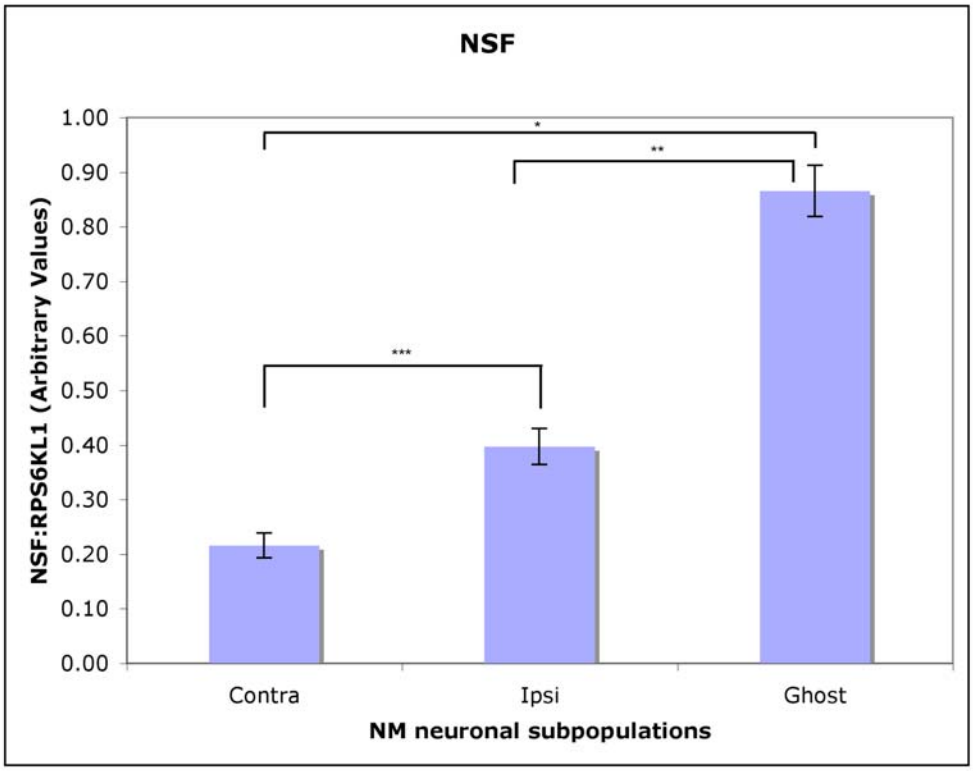
NSF
NSF:RPS6KL1 (Arbitrary Values)
1.00
0.90
0.80
0.70
0.60
0.50
0.40
0.30
0.20
0.10
0.00
*
**
***
Contra
Ipsi
Ghost
NM neuronal subpopulations

**Figure 9**

Bar graphs showing differences in gene expression (arbitrary values, normalized to expression of RPS6KL1) across groups (Contra, Ipsi, and Ghost) for genes involved in oxidative phosphorylation (A), PTEN signaling (B), and phospholipid degradation (C), identified using IPA analyses of biological canonical pathways. Gene expression values were obtained by RT-PCR using the standard curve data analysis technique. ATP5J2 (A) and CASP3 (B) were not expressed at significantly different levels across NM. PLA2G10, however, was found to be differentially expressed across NM (one-way ANOVA p-value=0.004). Holm-Sidak post-hoc comparisons showed significantly greater PLA2G10 expression in “ghost” versus contralateral NM neurons, and in “ghost” versus ipsilateral NM neurons (D).

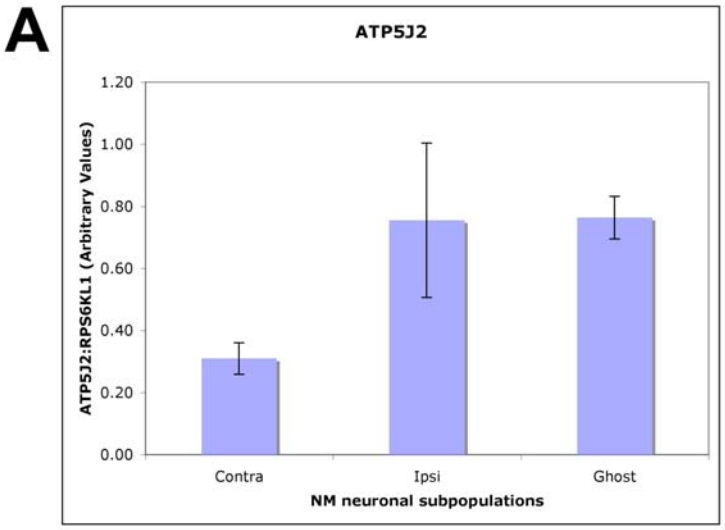
A
ATP5J2
ATP5J2:RPS6KL1 (Arbitrary Values)
1.20
1.00
0.80
0.60
0.40
0.20
0.00
Contra
Ipsi
Ghost
NM neuronal subpopulations

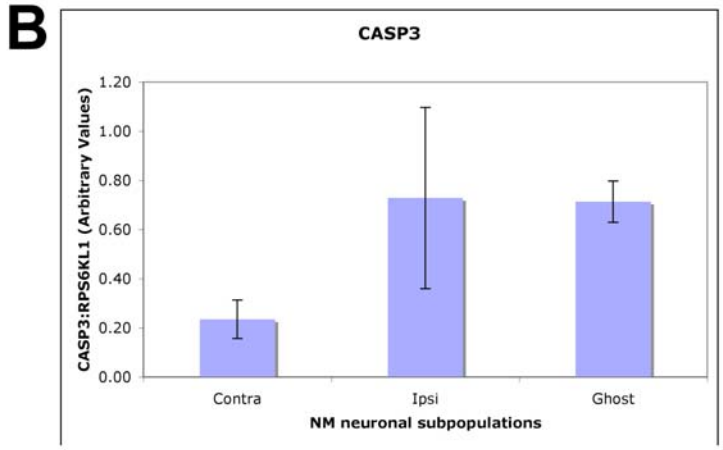
B
CASP3
CASP3:RPS6KL1 (Arbitrary Values)
1.20
1.00
0.80
0.60
0.40
0.20
0.00
Contra
Ipsi
Ghost
NM neuronal subpopulations

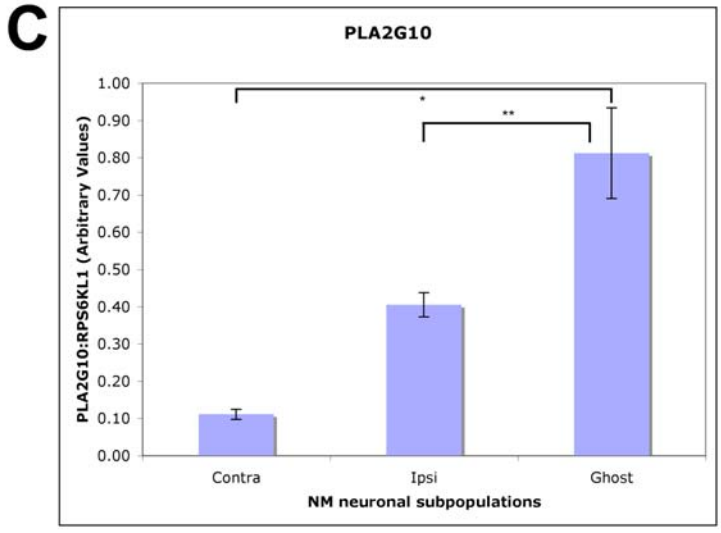
C
PLA2G10
PLA2G10:RPS6KL1 (Arbitrary Values)
1.00
0.90
0.80
0.70
0.60
0.50
0.40
0.30
0.20
0.10
0.00
*
**
Contra
Ipsi
Ghost
NM neuronal subpopulations

**Table 3: Average $C_t$ values of housekeeping genes across NM Subpopulations**

| Gene | Contralateral NM | Ipsilateral, Thionin+ NM | Ipsilateral, Thionin- NM |
|---|---|---|---|
| β-Actin | 25.04 ±0.26 | 22.85 ±0.32 | 20.83 ±0.41 |
| GAPDH | 19.39 ±0.28 | 21.02 ±1.27 | 25.78 ±1.81 |
| 18s rRNA | 22.44 ±0.19 | 21.24 ±0.06 | 18.76 ±0.38 |
| RPS6KL1 | 26.22 ±0.24 | 25.97 ±0.47 | 24.65 ±0.08 |

Mean $C_t$ value ±SEM

# CHAPTER V

# SUMMARY AND DISCUSSION

## Summary of Results

The objectives of these experiments were two-fold: (1) to characterize the mechanism of auditory neuronal death in chick brainstem nucleus magnocellularis (n. magnocellularis, NM) following afferent disruption, and (2) to identify molecular factors differentially involved in mediating CNS neuronal fate. In other words, to determine what makes one neuron in a homogeneous system susceptible to death and another seemingly impervious to death. We found that cochlea removal triggers signs of cellular compromise that precede and effectively identify NM neurons susceptible to death following deafferentation. TdT-mediated dUTP Nick-End Labeling (TUNEL) is observed within nuclei of a subset of deafferented NM neurons as early as 12 hours following cochlea removal. Twenty-four to 48 hours following deafferentation, TUNEL labeling of neuronal cytoplasm emerges and more effectively approximates the subset of deafferented NM neurons destined to eventually die. The cytoplasmic TUNEL labeling pattern coincides with a loss of propidium iodide (PI) in the cytoplasm, suggesting that degradation of nucleic acid, presumably mitochondrial DNA, predisposes NM neurons to deafferentation-induced death (see Chapter II).

In addition, we described a histologic method to quickly and definitively

distinguish “dying” from “surviving” NM neurons following cochlea removal. Ribosomal disassembly (Born and Rubel, 1985, Rubel et al., 1991) and loss of protein synthetic capacity (Steward and Rubel, 1985, Kelley et al., 1997, Lu et al., 2004) are well-described phenomena known to occur within hours of deafferentation in the subset of NM neurons destined to die. Quantitative analyses demonstrated that Thionin staining of ribosomal Nissl substance, observable in NM neurons 12-48 hours after cochlea removal, accurately predicts cell survival at seven days. In other words, Thionin-negative “ghost” neurons, present 12-48 hours following cochlea removal, reproducibly represent the 30-50% of deafferented NM neurons that will ultimately die. Interestingly, cell death in NM, as assessed by “ghost” neuronal counts, exhibited a tonotopic predilection for the rostromedial, high frequency region of NM (see Chapter II). The tonotopic pattern of cell death warrants further investigation, but may occur due to greater glial support, and consequent neuronal survival, within caudolateral NM. Alternatively, differences in synaptic vesicle density across the extent of the nucleus may predispose rostro-medial NM neurons to excitotoxic death. Further experimentation is necessary to determine the cause of tonotopic differences in neuronal degeneration.

Mitochondria rapidly proliferate across deafferented NM, and exhibit morphologic compromise within the subpopulation that ultimately dies (Hyde and Durham, 1994). It is not surprising that we observed mitochondrial

functional differences between deafferented NM neurons that die from those that survive (see Chapter III). Three electron transport chain (ETC) enzymes: succinate dehydrogenase (SDH), cytochrome oxidase (CO), and ATP synthase (ATPase) exhibited globally elevated levels of cytoplasmic reaction product 12-48 hours after deafferentation compared to contralateral control neurons. CO activity was unimodally elevated across the deafferented nucleus at these time points, suggesting that CO levels accompany the general rise in mitochondrial number within all ipsilateral neurons. Interestingly, however, two populations of neurons with different SDH and ATPase activities emerged in deafferented NM as early as 12 and 24 hours, respectively, following cochlea removal. The population of deafferented neurons exhibiting the greatest elevations in SDH and ATPase activities (Z-score ≥ 2) accurately approximate the percentage of neurons that die by seven days. This implies that oxidative enzymatic stress and mitochondrial uncoupling occur within deafferented NM neurons destined to die.

We speculate that calcium, which accumulates within all deafferented NM neurons, is ineffectively buffered in those neurons with structurally impaired mitochondria. In addition, we suspect that degraded endoplasmic reticulum (ER) in Thionin-negative “ghost” neurons destined to die contributes to rising intraneuronal calcium levels, as ER-mitochondrial junctions are known to release calcium and lipid vesicles into cellular cytoplasm when compromised (Pinton et al., 2008). Beyond a certain threshold, calcium

attacks lipid membranes, perpetuating lipid peroxidation. The increased availability of free fatty acids from lipid peroxidation of membranes, as well as from release from ER- mitochondrial junctions, ramps up SDH activity via the Tricarboxylic Acid (TCA) cycle. Calcium also directly attacks the ATP-generating ATPase pump, effectively uncoupling ATPase activity from energy generation. This phenomenon is observable in deafferented neurons destined to die by the increased accumulation of ATPase histochemical reaction product.

We also demonstrated a marked correlation in staining patterns between cytoplasmic TUNEL labeling and Mitotracker Red accumulation. Mitotracker Red is a cationic, lipophilic dye used to assess mitochondrial membrane potential ($\Delta\Psi_m$) integrity. In intact cells, Mitotracker Red passively diffuses across membranes maintaining negative potentials, where its intensity is quenched. If that cell should become compromised, membrane depolarization would release Mitotracker Red into the cytoplasm, where its staining intensity would increase.

In our system, impaired mitochondria within the subset of deafferented neurons destined to die undergo energetic uncoupling as early as 24 hours following cochlea removal (as evidenced by elevated ATPase histochemical reaction product). In those neurons, $\Delta\Psi_m$ has already reversed, so Mitotracker Red never enters mitochondria. As a consequence, the dye remains cytoplasmically localized where it fluoresces intensely. In contrast,

NM neurons with intact mitochondria take up the cationic dye and do not exhibit cytoplasmic fluorescence. Mitotracker Red labeling is observable within a subset of neuronal cytoplasm as early as 24 hours following cochlea removal, a time point at which we also observed cytoplasmic accumulation of TUNEL. By seven days, both markers are absent from deafferented NM, as cell death is complete, and labeling patterns resemble the contralateral, unperturbed nucleus (see Chapter III).

Since Thionin staining of ribosomal Nissl substance reliably predicts whether an NM neuron will survive or die following cochlea removal (Karnes et al., 2009), we stained brainstem sections through NM with Thionin and microdissected subpopulations from tissue sections using laser capture microdissection (LCM): (1) Thionin-positive, ipsilateral neurons known to survive deafferentation, (2) Thionin-negative, ipsilateral “ghost” neurons known to die, and (3) Thionin-positive control neurons from contralateral NM. RNA extracted from pooled samples of microdissected cell (neuron and glia) populations remained intact with minimal signs of degradation, and was viable for downstream genetic analyses (see Chapter IV).

Microarray chicken genome GeneChips were hybridized in triplicate with cDNA derived from RNA pools from the three NM cell populations of interest. Signal intensities were normalized and converted to expression values using the Robust Multi-Array Analysis (RMA) algorithm in Partek Genomic Suite software (Partek, Inc., St. Louis, MO). Differences in

expression values between groups with p-values≤ 0.05 and fold change (FC) values ≥ $|2|$ were considered significant and analyzed using Ingenuity Pathways Analysis software (IPA). Six biologically significant canonical pathways were selected for further evaluation: glutamate receptor signaling, GABA receptor signaling, calcium signaling, oxidative phosphorylation, phospholipid degradation, and PTEN signaling. Thirty-nine genes were evaluated using quantitative Real-Time PCR (RT-PCR), and 12 genes were observed to be expressed differently across NM subpopulations. Of those twelve genes, four (CASQ2, GRIN1, NSF, and PLA2G10) showed statistically significant differential expression across NM. CASQ2 encodes part of a calcium pump at the sarcoplasmic reticulum in cardiac myocytes, which is critically involved in calcium release from internal stores. GRIN1 encodes the NR1 subunit of the NMDA receptor and is involved in excitatory glutamatergic neurotransmission. NSF is involved in $GABA_A$ receptor trafficking to the plasma membrane and mediates inhibitory neurotransmission. And, PLA2G10 is a potent phospholipase $A_2$ involved in lipid peroxidation of cellular membranes following stress (see Chapter IV).

In summary, we have demonstrated that specific indicators of cellular compromise, including ribosomal disassembly and mitochondrial functional impairment, serve as effective predictors of cell death in deafferented NM neurons. We showed that death of NM neurons following cochlea removal occurs in a tonotopic pattern across the nucleus. We also proposed a

mechanism of cell death based on histochemical and fluorescent measures of mitochondrial integrity, which is supported by the literature. Finally, we initiated the molecular elucidation of a method underlying NM neuronal fate determination following loss of peripheral afferent support. We successfully demonstrated that NM neurons could be microdissected from tissue section and used in downstream genetic analyses, which significantly expands the breadth of experiments open to our system. Table 4 summarizes our novel findings in NM.

Genetic versus proteomic analyses

Hearing impairment may result from endogenous genetic factors passed from parents to offspring or from exogenous sources in the environment (i.e. noise exposure, ototoxic drugs, or inflammation) (Bess and Humes, 2003). Advances in molecular genetics have broadened our knowledge of the genome and greatly expanded interest in identifying and treating heritable diseases. Heritable deafness is estimated to underlie approximately 50% of cases (Steel and Kros, 2001), and efforts are underway to evaluate genetic characteristics of hearing loss in animal and human subjects alike. The unique regenerative capacity of the chick auditory system to spontaneously recover following acoustic trauma makes it an exceptional model in which to pursue these studies. Furthermore, the elucidation of the chick genome and the rapid development of advanced molecular techniques

make genetic analyses feasible. It is important to keep in mind, however, that genetic contributions to disease pathologies are multi-faceted. Single polymorphisms do not represent a significant proportion of most diseases. And, basic laboratory techniques assessing mRNA expression levels are usually one-dimensional, capable of assessing specific, single mutations. Epigenetic contributions to gene expression, not assessable by standard PCR techniques, are now widely known to influence transcriptional activity. Untranslated microRNAs are becoming more important in gene regulation. Corresponding levels of protein translation are equally as important, if not more so, in elucidating mechanisms of disease pathology. And, the influence of one's environment on his/her genome is fascinatingly complex.

In the chick auditory brainstem nucleus, nucleus magnocellularis (NM), ribosomal disassembly occurs within an hour of deafferentation (Born and Rubel, 1985, Rubel et al., 1991), and protein synthesis remains deficient in the population of deafferented neurons that will die. Several groups have documented discordant changes in mRNA and protein levels in NM (Kelley et al., 1997, Wilkinson et al., 2002). To exhaustively define a mechanism, thorough examinations of epigenetic, genetic, proteomic, and environmental factors are required.

Enzymatic reaction product intensity as an indicator of activity

The small number of auditory neurons within the context of the brain at large complicates the direct measurement of enzyme activity within auditory neurons. Consequently, we must rely on techniques that at best estimate or model the parameter under investigation. Because mitochondria represent the primary ATP generators within neurons, activities of enzymes directly involved in energy generation should reliably estimate cellular metabolic status (Stryer, 1995). Investigators elsewhere have developed and correlated histologic staining of enzyme reaction products with metabolic status (Wong-Riley, 1979, Meijer and Vloedman, 1980, Vladutiu and Heffner, 2000), thus, allowing us to derive meaningful assessments of respiratory state from staining intensity.

Unfortunately, this estimation technique limits our analyses. We cannot draw true quantitative conclusions from these data. Instead, all interpretations are qualitative and largely descriptive. Staining intensity may be sensitive to (1) the amount of substrate made available to neurons, (2) the amount of each enzyme per mitochondrion, (3) the number of mitochondria present within neurons, and/or (4) the true activity of the mitochondrial enzyme. These parameters must be carefully controlled so as to limit fluctuations introduced by the technique itself.

**Future direction**

To better characterize the process of NM neuronal cell loss following deafferentation, an *in vivo* model using cultures of brainstem slice preparations could be developed. From them, electrophysiological measurements of calcium flux and loss of membrane potential could be more accurately assessed. True mitochondrial enzyme activities could be recorded using microelectrodes, and parameters of enzyme kinetics ($V_{max}$) could be measured.

To further elucidate molecular contributions to neuroplasticity in deafferented NM, *in situ* hybridization of NM tissue sections could be employed. This method would provide information regarding timing and location (i.e. neuronal versus glial) of gene expression, and could be used in combination with immunocytochemical techniques to monitor mRNA and protein levels simultaneously.

It would also be interesting to apply the aforementioned techniques to studies of the developing cochlear nucleus. A number of studies have described neuronal properties that exhibit graded patterns of activity along the anterior to posterior tonotopic axis of NM (see Chapter II). These coordinated specializations presumably exist to deliver specific aspects of sound timing to particular frequency regions of NM. These specializations may also influence the genes and/or proteins expressed at high versus low frequency regions of the nucleus. Understanding the influence of tonotopy in NM neuronal

physiology is crucial towards elucidating a mechanism underlying the neuroplastic response to deafferentation.

**Relevance**

Hearing loss is a significant public health concern, affecting 250 million people worldwide. Hearing loss is associated with social withdrawal, communication delays, and reduced comprehension. It is a frustrating disorder, which is expensive and difficult to treat, and it is growing in magnitude as the population ages. Current therapies to treat the symptoms of hearing impairment, like hearing aids and cochlear implants are limited to manipulating peripheral auditory structures. The central nervous system (CNS) component is equally as important as the inner ear component in preserving auditory function, but little is known about the process of auditory neuronal damage and recovery. With its relative simplicity, spontaneous recovery after damage, and clearly examinable patterns of cell compromise, the chick auditory system is an excellent model in which to study the process of auditory neuronal damage and recovery.

**Table 4: Summary of novel findings in NM and corresponding times (post-cochlea removal) of onset**

| HOURS POST-COCHLEA REMOVAL | NOVEL FINDINGS |
|---|---|
| 12 hours | • Nuclear TUNEL labeling in a subset of NM neurons<br>• Loss of cytoplasmic propidium iodide in a subset of NM neurons<br>• Tonotopic pattern of cell loss favoring rostromedial NM<br>• Bimodal distribution of SDH activity in deafferented NM |
| 24 hours | • Caspase-3 activation throughout NM<br>• Cytoplasmic TUNEL labeling in a subset of NM neurons<br>• Bimodal distribution of ATPase activity in deafferented NM<br>• Loss of mitochondrial membrane integrity ($\Delta\Psi m$) in a subset of NM neurons<br>• Differential expression of CASQ2, GRIN1, NSF, and PLA2G10 across NM<br>• Differential expression of traditional housekeeping genes across NM |
| 7 days | • Tonotopic pattern of cell loss favoring rostromedial NM |

## REFERENCES


Abercrombie, M., 1946. Estimation of nuclear population from microtome sections. AnatRec. 94, 239-247.

Abrahams, J. P., Leslie, A. G., Lutter, R. and Walker, J. E., 1994. Structure at 2.8 A resolution of F1-ATPase from bovine heart mitochondria. Nature. 370, 621-628.

Adamo, N. J. and King, R. L., 1967. Evoked responses in the chicken telencephalon to auditory, visual, and tactile stimulation. ExpNeurol. 17, 498-504.

Alam, S. A., Robinson, B. K., Huang, J. and Green, S. H., 2007. Prosurvival and proapoptotic intracellular signaling in rat spiral ganglion neurons in vivo after the loss of hair cells. J Comp Neurol. 503, 832-852.

Alderton, W. K., Cooper, C. E. and Knowles, R. G., 2001. Nitric oxide synthases: structure, function and inhibition. Biochem J. 357, 593-615.

Almeida, A., Moncada, S. and Bolanos, J. P., 2004. Nitric oxide switches on glycolysis through the AMP protein kinase and 6-phosphofructo-2-kinase pathway. Nat Cell Biol. 6, 45-51.

Affymetrix, I., 2002. GeneChip Expression Analysis: Data Analysis Fundamentals. GeneChip Expression Analysis, 36-39.

Attardi, G. and Schatz, G., 1988. Biogenesis of mitochondria. AnnuRevCell Biol. 4, 289-333.

Bae, J. S., Jang, M. K., Hong, S., An, W. G., Choi, Y. H., Kim, H. D. and Cheong, J., 2003. Phosphorylation of NF-kappa B by calmodulin-dependent kinase IV activates anti-apoptotic gene expression. Biochem Biophys Res Commun. 305, 1094-1098.

Balaban, R. S., Nemoto, S. and Finkel, T., 2005. Mitochondria, oxidants, and aging. Cell. 120, 483-495.

Baloh, R. H., 2008. Mitochondrial dynamics and peripheral neuropathy. Neuroscientist. 14, 12-18.

Berridge, M. J., 2002. The endoplasmic reticulum: a multifunctional signaling organelle. Cell Calcium. 32, 235-249.

Bess, F. H. and Humes, L., 2003. Audiology: The Fundamentals. 145-184.

Bevensee, M. O., Schwiening, C. J. and Boron, W. F., 1995. Use of BCECF and propidium iodide to assess membrane integrity of acutely isolated CA1 neurons from rat hippocampus. J Neurosci Methods. 58, 61-75.

Boise, L. H. and Thompson, C. B., 1997. Bcl-xL can inhibit apoptosis in cells that have undergone Fas-induced protease activation. ProcNatlAcadSciUSA. 94, 3759-3764.

Bok, J., Wang, Q., Huang, J. and Green, S. H., 2007. CaMKII and CaMKIV mediate distinct prosurvival signaling pathways in response to depolarization in neurons. Mol Cell Neurosci. 36, 13-26.

Bonner, R. F., Emmert-Buck, M., Cole, K., Pohida, T., Chuaqui, R., Goldstein, S. and Liotta, L. A., 1997. Laser capture microdissection: molecular analysis of tissue. Science. 278, 1481,1483.

Born, D. E., Durham, D. and Rubel, E. W., 1991. Afferent influences on brainstem auditory nuclei of the chick: nucleus magnocellularis neuronal activity following cochlea removal. Brain Res. 557, 37-47.

Born, D. E. and Rubel, E. W., 1985. Afferent influences on brain stem auditory nuclei of the chicken: neuron number and size following cochlea removal. J Comp Neurol. 231, 435-445.

Born, D. E. and Rubel, E. W., 1988. Afferent influences on brain stem auditory nuclei of the chicken: Presynaptic action potentials regulate protein synthesis in nucleus magnocellularis neurons. JNeurosci. 8, 901-919.

Boyle, C. A., Decoufle, P. and Yeargin-Allsopp, M., 1994. Prevalence and health impact of developmental disabilities in US children. Pediatrics. 93, 399-403.

Bratton, S. B., MacFarlane, M., Cain, K. and Cohen, G. M., 2000. Protein complexes activate distinct caspase cascades in death receptor and stress-induced apoptosis. Exp Cell Res. 256, 27-33.

Bratton, S. B., Walker, G., Srinivasula, S. M., Sun, X. M., Butterworth, M., Alnemri, E. S. and Cohen, G. M., 2001. Recruitment, activation and retention of caspases-9 and -3 by Apaf-1 apoptosome and associated

XIAP complexes. Embo J. 20, 998-1009.

Brodin, P., Falchetto, R., Vorherr, T. and Carafoli, E., 1992. Identification of two domains which mediate the binding of activating phospholipids to the plasma-membrane Ca2+ pump. Eur J Biochem. 204, 939-946.

Brookes, P. S., Yoon, Y., Robotham, J. L., Anders, M. W. and Sheu, S. S., 2004. Calcium, ATP, and ROS: a mitochondrial love-hate triangle. Am J Physiol Cell Physiol. 287, C817-833.

Buckman, J. F., Hernandez, H., Kress, G. J., Votyakova, T. V., Pal, S. and Reynolds, I. J., 2001. MitoTracker labeling in primary neuronal and astrocytic cultures: influence of mitochondrial membrane potential and oxidants. J Neurosci Methods. 104, 165-176.

Budd, S. L. and Nicholls, D. G., 1996. Mitochondrial calcium regulation and acute glutamate excitotoxicity in cultured cerebellar granule cells. JNeurochem. 67, 2282-2291.

Bush, A. L. and Hyson, R. L., 2008. Effects of lithium and deafferentation on expression of glycogen synthase kinase-3beta, NFkappaB, beta-catenin and pCreb in the chick cochlear nucleus. Brain Res. 1203, 18-25.

Canady, K. S., Hyson, R. L. and Rubel, E. W., 1994. The astrocytic response to afferent activity blockade in chick nucelus magnocellularis is independent of synaptic activation, age, and neuronal survival. JNeurosci. 14, 5973-5985.

Castellino, R. C. and Durden, D. L., 2007. Mechanisms of disease: the PI3K-Akt-PTEN signaling node--an intercept point for the control of angiogenesis in brain tumors. Nat Clin Pract Neurol. 3, 682-693.

Cheng, J. Z., Yang, Y., Singh, S. P., Singhal, S. S., Awasthi, S., Pan, S. S., Singh, S. V., Zimniak, P. and Awasthi, Y. C., 2001. Two distinct 4-hydroxynonenal metabolizing glutathione S-transferase isozymes are differentially expressed in human tissues. Biochem Biophys Res Commun. 282, 1268-1274.

Choi, D. W., 1988. Calcium-mediated neurotoxicity: Relationship to specific channel types and role in ischemic damage. TINS. 11, 465-469.

Chu, T. J. and Peters, D. G., 2008. Serial analysis of the vascular endothelial transcriptome under static and shear stress conditions. Physiol Genomics. 34, 185-192.

Clarke, P. G. H. and Oppenheim, R. W., 1995. Neuron death in vertebrate development: In vivo methods. MethCell Biol. 46, 277-321.

Cleeter, M. W., Cooper, J. M., Darley-Usmar, V. M., Moncada, S. and Schapira, A. H., 1994. Reversible inhibition of cytochrome c oxidase, the terminal enzyme of the mitochondrial respiratory chain, by nitric oxide. Implications for neurodegenerative diseases. FEBS Lett. 345, 50-54.

Corwin, J. T. and Cotanche, D. A., 1988. Regeneration of sensory hair cells after acoustic trauma. Science. 240, 1772-1774.

Cotanche, D. A., 1987. Regeneration of hair cell stereociliary bundles in the chick cochlea following severe acoustic trauma. Hearing Res. 30, 181-196.

Crews, J. E. and Campbell, V. A., 2004. Vision impairment and hearing loss among community-dwelling older Americans: implications for health and functioning. Am J Public Health. 94, 823-829.

Crumling, M. A. and Saunders, J. C., 2007. Tonotopic distribution of short-term adaptation properties in the cochlear nerve of normal and acoustically overexposed chicks. J Assoc Res Otolaryngol. 8, 54-68.

Cruz, R. M., Lambert, P. R. and Rubel, E. W., 1987. Light microscopic evidence of hair cell regeneration after gentamicin toxicity in chick cochlea. ArchOtolaryngolHead Neck Surg. 113, 1058-1062.

Danial, N. N. and Korsmeyer, S. J., 2004. Cell death: critical control points. Cell. 116, 205-219.

de la Monte, S. M., Luong, T., Neely, T. R., Robinson, D. and Wands, J. R., 2000. Mitochondrial DNA damage as a mechanism of cell loss in Alzheimer's disease. Lab Invest. 80, 1323-1335.

Demaurex, N. and Distelhorst, C., 2003. Cell biology. Apoptosis--the calcium connection. Science. 300, 65-67.

Denecker, G., Vercammen, D., Steemans, M., Vanden Berghe, T., Brouckaert, G., Van Loo, G., Zhivotovsky, B., Fiers, W., Grooten, J., Declercq, W. and Vandenabeele, P., 2001. Death receptor-induced

apoptotic and necrotic cell death: differential role of caspases and mitochondria. Cell Death Differ. 8, 829-840.

Dengler, W. A., Schulte, J., Berger, D. P., Mertelsmann, R. and Fiebig, H. H., 1995. Development of a propidium iodide fluorescence assay for proliferation and cytotoxicity assays. Anticancer Drugs. 6, 522-532.

Dhar, S. S. and Wong-Riley, M. T., 2009. Coupling of energy metabolism and synaptic transmission at the transcriptional level: role of nuclear respiratory factor 1 in regulating both cytochrome c oxidase and NMDA glutamate receptor subunit genes. J Neurosci. 29, 483-492.

Di Leva, F., Domi, T., Fedrizzi, L., Lim, D. and Carafoli, E., 2008. The plasma membrane Ca2+ ATPase of animal cells: structure, function and regulation. Arch Biochem Biophys. 476, 65-74.

Duchen, M. R., 2004. Section III: Mitochondria, Beta-Cell Function, and Type 2 Diabetes. Diabetes. 53, S96-S102.

Duncan, L. J., Mangiardi, D. A., Matsui, J. I., Anderson, J. K., McLaughlin-Williamson, K. and Cotanche, D. A., 2006. Differential expression of unconventional myosins in apoptotic and regenerating chick hair cells confirms two regeneration mechanisms. J Comp Neurol. 499, 691-701.

Durham, D., Matschinsky, F. M. and Rubel, E. W., 1993. Altered malate dehydrogenase activity in nucleus magnocellularis of the chicken following cochlea removal. Hear Res. 70, 151-159.

Durham, D. and Rubel, E. W., 1985. Afferent influences on brain stem auditory nuclei of the chicken: changes in succinate dehydrogenase activity following cochlea removal. J Comp Neurol. 231, 446-456.

Edmonds, J. E., Hoover, L. A. and Durham, D., 1999. Breed differences in cochlear nucleus neuronal cell death and shrinkage in adult chickens after cochlea removal. Hearing Res. 127, 62-76.

Embley, T. M. and Martin, W., 2006. Eukaryotic evolution, changes and challenges. Nature. 440, 623-630.

Embley, T. M., van der Giezen, M., Horner, D. S., Dyal, P. L., Bell, S. and Foster, P. G., 2003a. Hydrogenosomes, mitochondria and early eukaryotic evolution. IUBMB Life. 55, 387-395.

Embley, T. M., van der Giezen, M., Horner, D. S., Dyal, P. L. and Foster, P., 2003b. Mitochondria and hydrogenosomes are two forms of the same fundamental organelle. Philos Trans R Soc Lond B Biol Sci. 358, 191-201; discussion 201-192.

Emmert-Buck, M. R., Bonner, R. F., Smith, P. D., Chuaqui, R. F., Zhuang, Z., Goldstein, S. R., Weiss, R. A. and Liotta, L. A., 1996. Laser capture microdissection. Science. 274, 998-1001.

Enari, M., Sakahira, H., Yokoyama, H., Okawa, K., Iwamatsu, A. and Nagata, S., 1998. A caspase-activated DNase that degrades DNA during apoptosis, and its inhibitor ICAD. Nature. 391, 43-50.

Epstein, J. E. and Cotanche, D. A., 1995. Secretion of a new basal layer of tectorial membrane following gentamicin-induced hair cell loss. Hearing Res. 90, 31-43.

Espina, V., Wulfkuhle, J. D., Calvert, V. S., VanMeter, A., Zhou, W., Coukos, G., Geho, D. H., Petricoin, E. F., 3rd and Liotta, L. A., 2006. Laser-capture microdissection. Nat Protoc. 1, 586-603.

Fischel-Ghodsian, N., 1999. Mitochondrial deafness mutations reviewed. Hum Mutat. 13, 261-270.

Forman, M. S., Trojanowski, J. Q. and Lee, V. M., 2004. Neurodegenerative diseases: a decade of discoveries paves the way for therapeutic breakthroughs. Nat Med. 10, 1055-1063.

Foster, K. A., Galeffi, F., Gerich, F. J., Turner, D. A. and Muller, M., 2006. Optical and pharmacological tools to investigate the role of mitochondria during oxidative stress and neurodegeneration. Prog Neurobiol. 79, 136-171.

Friedlander, R. M., 2003. Apoptosis and caspases in neurodegenerative diseases. N Engl J Med. 348, 1365-1375.

Fuentes-Prior, P. and Salvesen, G. S., 2004. The protein structures that shape caspase activity, specificity, activation and inhibition. Biochem J. 384, 201-232.

Fujioka, D., Saito, Y., Kobayashi, T., Yano, T., Tezuka, H., Ishimoto, Y., Suzuki, N., Yokota, Y., Nakamura, T., Obata, J. E., Kanazawa, M.,

Kawabata, K., Hanasaki, K. and Kugiyama, K., 2008. Reduction in myocardial ischemia/reperfusion injury in group X secretory phospholipase A2-deficient mice. Circulation. 117, 2977-2985.

Fukui, H. and Moraes, C. T., 2008. The mitochondrial impairment, oxidative stress and neurodegeneration connection: reality or just an attractive hypothesis? Trends Neurosci. 31, 251-256.

Garden, G. A., Canady, K. S., Lurie, D. I., Bothwell, M. and Rubel, E. W., 1994. A biphasic change in ribosomal conformation during transneuronal degeneration is altered by inhibition of mitochondrial, but not cytoplasmic protein synthesis. JNeurosci. 14, 1994-2008.

Gavrieli, Y., Sherman, Y. and Ben-Sasson, S. A., 1992. Identification of programmed cell death in situ via specific labeling of nuclear DNA fragmentation. J Cell Biol. 119, 493-501.

Gibson, G. E., Karuppagounder, S. S. and Shi, Q., 2008. Oxidant-induced changes in mitochondria and calcium dynamics in the pathophysiology of Alzheimer's disease. Ann N Y Acad Sci. 1147, 221-232.

Girod, D. A., Duckert, L. G. and Rubel, E. W., 1989. Possible precursors of regenerated hair cells in the avian cochlea following acoustic trauma. Hearing Res. 42, 175-194.

Girod, D. A., Park, R. H., Park, D. L. and Durham, D., 2000. Changes in the avian cochlea after single high-dose gentamicin. Am J Otolaryngol. 21, 379-388.

Girod, D. A., Tucci, D. L. and Rubel, E. W., 1991. Anatomical correlates of functional recovery in the avian inner ear following aminoglycoside ototoxicity. Laryngoscope. 101, 1139-1149.

Green, K., Brand, M. D. and Murphy, M. P., 2004. Prevention of mitochondrial oxidative damage as a therapeutic strategy in diabetes. Diabetes. 53 Suppl 1, S110-118.

Guerfali, I., Manissolle, C., Durieux, A. C., Bonnefoy, R., Bartegi, A. and Freyssenet, D., 2007. Calcineurin A and CaMKIV transactivate PGC-1alpha promoter, but differentially regulate cytochrome c promoter in rat skeletal muscle. Pflugers Arch. 454, 297-305.

Gunter, K. K. and Gunter, T. E., 1994. Transport of calcium by mitochondria. J Bioenerg Biomembr. 26, 471-485.

Gunter, T. E., Gunter, K. K., Sheu, S. S. and Gavin, C. E., 1994. Mitochondrial calcium transport: Physiological and pathological relevance. AmJPhysiol. 267, C313-C319.

Gunter, T. E., Yule, D. I., Gunter, K. K., Eliseev, R. A. and Salter, J. D., 2004. Calcium and mitochondria. FEBS Lett. 567, 96-102.

Guo, S. Z., Huang, K., Shi, Y. Y., Tang, W., Zhou, J., Feng, G. Y., Zhu, S. M., Liu, H. J., Chen, Y., Sun, X. D. and He, L., 2007. A case-control association study between the GRID1 gene and schizophrenia in the Chinese Northern Han population. Schizophr Res. 93, 385-390.

Gyorke, S., Hagen, B. M., Terentyev, D. and Lederer, W. J., 2007. Chain-reaction Ca(2+) signaling in the heart. J Clin Invest. 117, 1758-1762.

Hajnoczky, G., Robb-Gaspers, L. D., Seitz, M. B. and Thomas, A. P., 1995. Decoding of cytosolic calcium oscillations in the mitochondria. Cell. 82, 415-424.

Hamburger, V. and Levi-Montalcini, R., 1949. Journal of Experimental Zoology. 111, 457-502.

Hansford, R. G., 1994. Physiological role of mitochondrial Ca2+ transport. J Bioenerg Biomembr. 26, 495-508.

Harris, J. A., Hardie, N. A., Bermingham-McDonogh, O. and Rubel, E. W., 2005. Gene expression differences over a critical period of afferent-dependent neuron survival in the mouse auditory brainstem. J Comp Neurol. 493, 460-474.

Harris, J. A. and Rubel, E. W., 2006. Afferent regulation of neuron number in the cochlear nucleus: cellular and molecular analyses of a critical period. Hear Res. 216-217, 127-137.

Hartl, F.-U. and Neupert, W., 1990. Protein sorting to mitochondria: Evolutionary conservations of folding and assembly. Science. 247, 930-938.

Hartlage-Rubsamen, M. and Rubel, E. W., 1996. Influence of mitochondrial protein synthesis inhibition on deafferentation-induced ultrastructural

changes in nucleus magnocellularis of developing chicks. J Comp Neurol. 371, 448-460.

Hashino, E., Tanaka, Y. and Sokabe, M., 1991. Hair cell damage and recovery following chronic application of kanamycin in the chick cochlea. Hearing Res. 52, 356-368.

Heil, P. and Scheich, H., 1986. Effects of unilateral and bilateral cochlea removal on 2-deoxyglucose patterns in the chick auditory system. J Comp Neurol. 252, 279-301.

Henderson, W. R., Jr., Chi, E. Y., Bollinger, J. G., Tien, Y. T., Ye, X., Castelli, L., Rubtsov, Y. P., Singer, A. G., Chiang, G. K., Nevalainen, T., Rudensky, A. Y. and Gelb, M. H., 2007. Importance of group X-secreted phospholipase A2 in allergen-induced airway inflammation and remodeling in a mouse asthma model. J Exp Med. 204, 865-877.

Hevner, R. F., Liu, S. and Wong-Riley, M. T., 1995. A metabolic map of cytochrome oxidase in the rat brain: histochemical, densitometric and biochemical studies. Neuroscience. 65, 313-342.

Hollmann, M. and Heinemann, S., 1994. Cloned glutamate receptors. Annu Rev Neurosci. 17, 31-108.

Honig, L. S. and Rosenberg, R. N., 2000. Apoptosis and neurologic disease. Am J Med. 108, 317-330.

Hoppeler, H., Mathieu, O., Krauer, R., Claassen, H., Armstrong, R. B. and Weibel, E. R., 1981. Design of the mammalian respiratory system. VI.

Distribution of mitochondria and capillaries in various muscles. RespPhysiol. 44, 87-111.

Hu, B. H., Guo, W., Wang, P. Y., Henderson, D. and Jiang, S. C., 2000. Intense noise-induced apoptosis in hair cells of guinea pig cochleae. Acta Otolaryngol. 120, 19-24.

Hu, B. H., Henderson, D. and Nicotera, T. M., 2002. Involvement of apoptosis in progression of cochlear lesion following exposure to intense noise. Hear Res. 166, 62-71.

Hyde, G. E. and Durham, D., 1990. Cytochrome oxidase response to cochlea removal in chicken auditory brainstem neurons. J Comp Neurol. 297, 329-339.

Hyde, G. E. and Durham, D., 1994. Rapid increase in mitochondrial volume in nucleus magnocellularis neurons following cochlea removal. J Comp Neurol. 339, 27-48.

Hyson, R. L., 1998. Activation of metabotropic glutamate receptors is necessary for transneuronal regulation of ribosomes in chick auditory neurons. Brain Res. 809, 214-220.

Inoue, M., Nishikawa, M., Sato, E. F., Ah-Mee, P., Kashiba, M., Takehara, Y. and Utsumi, K., 1999. Cross-talk of NO, superoxide and molecular oxygen, a majesty of aerobic life. Free Radic Res. 31, 251-260.

Irizarry, R. A., Hobbs, B., Collin, F., Beazer-Barclay, Y. D., Antonellis, K. J., Scherf, U. and Speed, T. P., 2003. Exploration, normalization, and

summaries of high density oligonucleotide array probe level data. Biostatistics. 4, 249-264.

Jackson, H., Hackett, J. T. and Rubel, E. W., 1982. Organization and development of brain stem auditory nuclei in the chick: Ontogeny of postsynaptic responses. JCompNeurol. 210, 80-86.

Jackson, H., Nemeth, E. F. and Parks, T. N., 1985. Non-N-methyl-D-aspartate receptors mediating synaptic transmission in the avian cochlear nucleus: Effects of kynurenic acid, dipicolinic acid and streptomycin. Neuroscience. 16, 171-179.

Jacobson, M. D., Weil, M. and Raff, M. C., 1997. Programmed cell death in animal development. Cell. 88, 347-354.

Janas, J. D., Cotanche, D. A. and Rubel, E. W., 1995. Avian cochlear hair cell regeneration: stereological analyses of damage and recovery from a single high dose of gentamicin. Hearing Res. 92, 17-29.

Jiang, X. and Wang, X., 2000. Cytochrome c promotes caspase-9 activation by inducing nucleotide binding to Apaf-1. J Biol Chem. 275, 31199-31203.

Johnson, E. M., Jr., Chang, J. Y., Koike, T. and Martin, D. P., 1989. Why do neurons die when deprived of trophic factor? NeurobiolAging. 10, 549-552.

Johnson, E. M., Jr., Deckwerth, T. L. and Deshmukh, M., 1996. Neuronal death in developmental models: Possible implications in

neuropathology. Brain Pathol. 6, 397-409.

Johnson, L. V., Walsh, M. L., Bockus, B. J. and Chen, L. B., 1981. Monitoring of relative mitochondrial membrane potential in living cells by fluorescence microscopy. J Cell Biol. 88, 526-535.

Johnson, L. V., Walsh, M. L. and Chen, L. B., 1980. Localization of mitochondria in living cells with rhodamine 123. Proc Natl Acad Sci U S A. 77, 990-994.

Jones, L. R. and Cala, S. E., 1981. Biochemical evidence for functional heterogeneity of cardiac sarcoplasmic reticulum vesicles. J Biol Chem. 256, 11809-11818.

Junge, W., Lill, H. and Engelbrecht, S., 1997. ATP synthase: an electrochemical transducer with rotatory mechanics. Trends Biochem Sci. 22, 420-423.

Kaiser, C. L., Chapman, B. J., Guidi, J. L., Terry, C. E., Mangiardi, D. A. and Cotanche, D. A., 2008. Comparison of activated caspase detection methods in the gentamicin-treated chick cochlea. Hear Res. 240, 1-11.

Kandel, E. R., Schwartz, J. H. and Jessell, T. M., 2000. Principles of Neural Science, Fourth Edition. 590-624.

Karnes, H. E., Kaiser, C. L. and Durham, D., 2009. Deafferentation-induced caspase-3 activation and DNA fragmentation in chick cochlear nucleus neurons. Neuroscience. 159, 804-818.

Kato, B. M. and Rubel, E. W., 1999. Glutamate regulates IP3-type and CICR stores in the avian cochlear nucleus. J Neurophysiol. 81, 1587-1596.

Kelada, S. N., Stapleton, P. L., Farin, F. M., Bammler, T. K., Eaton, D. L., Smith-Weller, T., Franklin, G. M., Swanson, P. D., Longstreth, W. T., Jr. and Checkoway, H., 2003. Glutathione S-transferase M1, T1, and P1 polymorphisms and Parkinson's disease. Neurosci Lett. 337, 5-8.

Kelley, M. S., Lurie, D. I. and Rubel, E. W., 1997. Rapid regulation of cytoskeletal proteins and their mRNAs following afferent deprivation in the avian cochlear nucleus. J Comp Neurol. 389, 469-483.

Kennedy, H., Bullier, J. and Dehay, C., 1985. Cytochrome oxidase activity in the striate cortex and lateral geniculate nucleus of the newborn and adult macaque monkey. Exp Brain Res. 61, 204-209.

Kim, D. Y., Won, S. J. and Gwag, B. J., 2002. Analysis of mitochondrial free radical generation in animal models of neuronal disease. Free Radic Biol Med. 33, 715-723.

Kluck, R. M., Bossy-Wetzel, E., Green, D. R. and Newmeyer, D. D., 1997. The release of cytochrome c from mitochondria: A primary site for Bcl-2 regulation of apoptosis. Science. 275, 1132-1136.

Knollmann, B. C., Chopra, N., Hlaing, T., Akin, B., Yang, T., Ettensohn, K., Knollmann, B. E., Horton, K. D., Weissman, N. J., Holinstat, I., Zhang, W., Roden, D. M., Jones, L. R., Franzini-Armstrong, C. and Pfeifer, K., 2006. Casq2 deletion causes sarcoplasmic reticulum volume increase,

premature Ca2+ release, and catecholaminergic polymorphic ventricular tachycardia. J Clin Invest. 116, 2510-2520.

Knott, A. B., Perkins, G., Schwarzenbacher, R. and Bossy-Wetzel, E., 2008. Mitochondrial fragmentation in neurodegeneration. Nat Rev Neurosci. 9, 505-518.

Kokotas, H., Petersen, M. B. and Willems, P. J., 2007. Mitochondrial deafness. Clin Genet. 71, 379-391.

Kolble, K., 2000. The LEICA microdissection system: design and applications. J Mol Med. 78, B24-25.

Kubke, M. F., Gauger, B., Basu, L., Wagner, H. and Carr, C. E., 1999. Development of calretinin immunoreactivity in the brainstem auditory nuclei of the barn owl (Tyto alba). J Comp Neurol. 415, 189-203.

Kuida, K., Zheng, T. S., Na, S., Kuan, C., Yang, D., Karasuyama, H., Rakic, P. and Flavell, R. A., 1996. Decreased apoptosis in the brain and premature lethality in CPP32-deficient mice. Nature. 384, 368-372.

Lachica, E. A., Rubsamen, R. and Rubel, E. W., 1994. GABAergic terminals in nucleus magnocellularis and laminaris originate from the superior olivary nucleus. JCompNeurol. 348, 403-418.

Lachica, E. A., Rubsamen, R., Zirpel, L. and Rubel, E. W., 1995. Glutamatergic inhibition of voltage-operated calcium channels in the avian cochlear nucleus. JNeurosci. 15, 1724-1734. Lee, K. D. and Hollenbeck, P. J., 1995. Phosphorylation of kinesin in vivo correlates

with organelle association and neurite outgrowth. J Biol Chem. 270, 5600-5605.

Leil, T. A., Chen, Z. W., Chang, C. S. and Olsen, R. W., 2004. GABAA receptor-associated protein traffics GABAA receptors to the plasma membrane in neurons. J Neurosci. 24, 11429-11438.

Lemasters, J. J., Chacon, E., Ohata, H., Harper, I. S., Nieminen, A. L., Tesfai, S. A. and Herman, B., 1995. Measurement of electrical potential, pH, and free calcium ion concentration in mitochondria of living cells by laser scanning confocal microscopy. Methods Enzymol. 260, 428-444.

Linden, R., 1994. The survival of developing neurons: a review of afferent control. Neuroscience. 58, 671-682.

Linden, R. and Renteria, A. S., 1988. Afferent control of neuron numbers in the developing brain. DevBrRes. 44, 291-295.

Lippe, W. and Rubel, E. W., 1985. Ontogeny of tonotopic organization of brain stem auditory nuclei in the chicken: Implications for development of the place principle. JCompNeurol. 237, 273-289.

Lipsky, R. H. and Goldman, D., 2003. Genomics and variation of ionotropic glutamate receptors. Ann N Y Acad Sci. 1003, 22-35.

Liu, X., Kim, C. N., Yang, J., Jemmerson, R. and Wang, X., 1996. Induction of apoptotic program in cell-free extracts: Requirement for dATP and cytochrome c. Cell. 86, 147-157.

Liu, X., Zou, H., Slaughter, C. and Wang, X., 1997. DFF, a heterodimeric

protein that functions downstream of caspase-3 to trigger DNA fragmentation during apoptosis. Cell. 89, 175-184.

Liu, X., Zou, H., Widlak, P., Garrard, W. and Wang, X., 1999. Activation of the apoptotic endonuclease DFF40 (caspase-activated DNase or nuclease). Oligomerization and direct interaction with histone H1. J Biol Chem. 274, 13836-13840.

Lu, T. and Trussell, L. O., 2007. Development and elimination of endbulb synapses in the chick cochlear nucleus. J Neurosci. 27, 808-817.

Lu, T. and Trussell, L. O., 2000. Inhibitory transmission mediated by asynchronous transmitter release. Neuron. 26, 683-694.

Lu, Y., Burger, R. M. and Rubel, E. W., 2005. GABA(B) receptor activation modulates GABA(A) receptor-mediated inhibition in chicken nucleus magnocellularis neurons. J Neurophysiol. 93, 1429-1438.

Lu, Y., Monsivais, P., Tempel, B. L. and Rubel, E. W., 2004. Activity-dependent regulation of the potassium channel subunits Kv1.1 and Kv3.1. J Comp Neurol. 470, 93-106.

Lu, Y. and Rubel, E. W., 2005. Activation of metabotropic glutamate receptors inhibits high-voltage-gated calcium channel currents of chicken nucleus magnocellularis neurons. J Neurophysiol. 93, 1418-1428.

Luo, L., Salunga, R. C., Guo, H., Bittner, A., Joy, K. C., Galindo, J. E., Xiao, H., Rogers, K. E., Wan, J. S., Jackson, M. R. and Erlander, M. G.,

1999. Gene expression profiles of laser-captured adjacent neuronal subtypes. Nat Med. 5, 117-122.

Luoma, J. I. and Zirpel, L., 2008. Deafferentation-induced activation of NFAT (nuclear factor of activated T-cells) in cochlear nucleus neurons during a developmental critical period: a role for NFATc4-dependent apoptosis in the CNS. J Neurosci. 28, 3159-3169.

Lurie, D. I. and Durham, D., 2000. Neuronal death, not axon degeneration, results in significant gliosis within the cochlear nucleus of adult chickens. Hearing Res. 149, 178-188.

Ly, C. V. and Verstreken, P., 2006. Mitochondria at the synapse. Neuroscientist. 12, 291-299.

Macdonald, J. A., Murugesan, N. and Pachter, J. S., 2008. Validation of immuno-laser capture microdissection coupled with quantitative RT-PCR to probe blood-brain barrier gene expression in situ. J Neurosci Methods. 174, 219-226.

Macho, A., Decaudin, D., Castedo, M., Hirsch, T., Susin, S. A., Zamzami, N. and Kroemer, G., 1996. Chloromethyl-X-Rosamine is an aldehyde-fixable potential-sensitive fluorochrome for the detection of early apoptosis. Cytometry. 25, 333-340.

Mangiardi, D. A., McLaughlin-Williamson, K., May, K. E., Messana, E. P., Mountain, D. C. and Cotanche, D. A., 2004. Progression of hair cell ejection and molecular markers of apoptosis in the avian cochlea

following gentamicin treatment. J Comp Neurol. 475, 1-18.

Marshall, J., Dolan, B. M., Garcia, E. P., Sathe, S., Tang, X., Mao, Z. and Blair, L. A., 2003. Calcium channel and NMDA receptor activities differentially regulate nuclear C/EBPbeta levels to control neuronal survival. Neuron. 39, 625-639.

Martin, L. J., 2001. Neuronal cell death in nervous system development, disease, and injury (Review). Int J Mol Med. 7, 455-478.

Martin, L. J., Pan, Y., Price, A. C., Sterling, W., Copeland, N. G., Jenkins, N. A., Price, D. L. and Lee, M. K., 2006. Parkinson's disease alpha-synuclein transgenic mice develop neuronal mitochondrial degeneration and cell death. J Neurosci. 26, 41-50.

Martin, M. R., 1985. Excitatory amino acid pharmacology of the auditory nerve and nucleus magnocellularis of the chicken. Hearing Res. 17, 153-160.

Mattson, M. P., 2000. Apoptosis in neurodegenerative disorders. Nat Rev Mol Cell Biol. 1, 120-129.

Mattson, M. P., 2007. Calcium and neurodegeneration. Aging Cell. 6, 337-350.

May, A. P., Whiteheart, S. W. and Weis, W. I., 2001. Unraveling the mechanism of the vesicle transport ATPase NSF, the N-ethylmaleimide-sensitive factor. J Biol Chem. 276, 21991-21994.

McCarthy, N. J., Whyte, M. K., Gilbert, C. S. and Evan, G. I., 1997. Inhibition

of Ced-3/ICE-related proteases does not prevent cell death induced by oncogenes, DNA damage, or the Bcl-2 homologue Bak. J Cell Biol. 136, 215-227.

Meijer, A. E. F. H. and Vloedman, A. H. T., 1980. The histochemical characterization of the coupling state of skeletal muscle mitochondria. Histochem. 69, 217-232.

Micke, P., Ostman, A., Lundeberg, J. and Ponten, F., 2005. Laser-assisted cell microdissection using the PALM system. Methods Mol Biol. 293, 151-166.

Missiaen, L., Taylor, C. W. and Berridge, M. J., 1991. Spontaneous calcium release from inositol trisphosphate-sensitive calcium stores. Nature. 352, 241-244.

Mitchell, P., 1961. Coupling of phosphorylation to electron and hydrogen transfer by a chemi-osmotic type of mechanism. Nature. 191, 144-148.

Moreno-Gonzalez, G., Lopez-Colome, A. M., Rodriguez, G. and Zarain-Herzberg, A., 2008. Transcription of the chicken Grin1 gene is regulated by the activity of SP3 and NRSF in undifferentiated cells and neurons. Biosci Rep. 28, 177-188.

Morishima, N., Nakanishi, K., Takenouchi, H., Shibata, T. and Yasuhiko, Y., 2002. An endoplasmic reticulum stress-specific caspase cascade in apoptosis. Cytochrome c-independent activation of caspase-9 by caspase-12. J Biol Chem. 277, 34287-34294.

Morris, R. L. and Hollenbeck, P. J., 1993. The regulation of bidirectional mitochondrial transport is coordinated with axonal outgrowth. JCell Science. 104, 917-927.

Mostafapour, S. P., Cochran, S. L., Del Puerto, N. M. and Rubel, E. W., 2000. Patterns of cell death in mouse anteroventral cochlear nucleus neurons after unilateral cochlea removal. J Comp Neurol. 426, 561-571.

Mostafapour, S. P., Lachica, E. A. and Rubel, E. W., 1997. Mitochondrial regulation of calcium in the avian cochlear nucleus. JNeurophysiol. 78, 1928-1934.

Mu, W. and Burt, D. R., 1999. The mouse GABA(A) receptor alpha3 subunit gene and promoter. Brain Res Mol Brain Res. 73, 172-180.

Nachlas, M. M., Tsou, K. C., De Souza, E., Cheng, C. S. and Seligman, A. M., 1957. Cytochemical demonstration of succinic dehydrogenase by the use of a new p-nitrophenyl substituted ditetrazole. J Histochem Cytochem. 5, 420-436.

Nakagawa, T., Zhu, H., Morishima, N., Li, E., Xu, J., Yankner, B. A. and Yuan, J., 2000. Caspase-12 mediates endoplasmic-reticulum-specific apoptosis and cytotoxicity by amyloid-beta. Nature. 403, 98-103.

Nelson, B. D., 1987. Biogenesis of mammalian mitochondria. CurrTopics Bioenerg. 15, 221-272.

Nemeth, E. F., Jackson, H. and Parks, T. N., 1983. Pharmacologic evidence for synaptic transmission mediated by non-N-methyl-D-aspartate receptors in the avian cochlear nucleus. NeurosciLett. 40, 39-44.

Nicholas, A. H. and Hyson, R. L., 2004. Group I and II metabotropic glutamate receptors are necessary for the activity-dependent regulation of ribosomes in chick auditory neurons. Brain Res. 1014, 110-119.

Nicholas, A. H. and Hyson, R. L., 2006. Afferent regulation of oxidative stress in the chick cochlear nucleus. Neuroscience. 140, 1359-1368.

Nicholls, D. G., 2008. Oxidative stress and energy crises in neuronal dysfunction. Ann N Y Acad Sci. 1147, 53-60.

Nicholls, D. G. and Budd, S. L., 2000. Mitochondria and neuronal survival. Physiol Rev. 80, 315-360.

Nicholson, D. W. and Neupert, W., 1988. Synthesis and assembly of mitochondrial proteins. Protein Transfer and Organelle Biogenesis. Academic Press, New York, pp. 677-746.

Nishikawa, T., Edelstein, D., Du, X. L., Yamagishi, S., Matsumura, T., Kaneda, Y., Yorek, M. A., Beebe, D., Oates, P. J., Hammes, H. P., Giardino, I. and Brownlee, M., 2000. Normalizing mitochondrial superoxide production blocks three pathways of hyperglycaemic damage. Nature. 404, 787-790.

Nishimura, H., Sakagami, H., Uezu, A., Fukunaga, K., Watanabe, M. and Kondo, H., 2003. Cloning, characterization and expression of two alternatively splicing isoforms of Ca2+/calmodulin-dependent protein kinase I gamma in the rat brain. J Neurochem. 85, 1216-1227.

Ohinata, Y., Miller, J. M., Altschuler, R. A. and Schacht, J., 2000. Intense noise induces formation of vasoactive lipid peroxidation products in the cochlea. Brain Res. 878, 163-173.

Oppenheim, R. W., 1991. Cell death during development of the nervous system. AnnuRevNeurosci. 14, 453-501.

Orrenius, S., Gogvadze, V. and Zhivotovsky, B., 2007. Mitochondrial oxidative stress: implications for cell death. Annu Rev Pharmacol Toxicol. 47, 143-183.

Orrenius, S., Zhivotovsky, B. and Nicotera, P., 2003. Regulation of cell death: the calcium-apoptosis link. Nat Rev Mol Cell Biol. 4, 552-565.

Overly, C. C., Rieff, H. I. and Hollenbeck, P. J., 1996. Organelle motility and metabolism in axons vs dendrites of cultured hippocampal neurons. J Cell Sci. 109 (Pt 5), 971-980.

Ozawa, T., Tanaka, M., Suzuki, H. and Nishikimi, M., 1987. Structure and function of mitochondria: Their organization and disorders. Brain Dev. 9, 76-81.

Park, D. L., Girod, D. A. and Durham, D., 1999. Tonotopic changes in 2-deoxyglucose activity in chick cochlear nucleus during hair cell loss and regeneration. Hearing Res. 138, 45-55.

Parks, T. N., 1981. Changes in the length and organization of nucleus laminaris dendrites after unilateral otocyst ablation in chick embryos. JCompNeurol. 202, 47-57.

Parks, T. N. and Rubel, E. W., 1978. Organization and development of the brain stem auditory nuclei of the chicken: primary afferent projections. J Comp Neurol. 180, 439-448.

Pfeiffer, D. R., Gunter, T. E., Eliseev, R., Broekemeier, K. M. and Gunter, K. K., 2001. Release of Ca2+ from mitochondria via the saturable mechanisms and the permeability transition. IUBMB Life. 52, 205-212.

Piccini, M., Vitelli, F., Bruttini, M., Pober, B. R., Jonsson, J. J., Villanova, M., Zollo, M., Borsani, G., Ballabio, A. and Renieri, A., 1998. FACL4, a new gene encoding long-chain acyl-CoA synthetase 4, is deleted in a family with Alport syndrome, elliptocytosis, and mental retardation. Genomics. 47, 350-358.

Pinton, P., Giorgi, C., Siviero, R., Zecchini, E. and Rizzuto, R., 2008. Calcium and apoptosis: ER-mitochondria Ca2+ transfer in the control of apoptosis. Oncogene. 27, 6407-6418.

Poole, A. M. and Penny, D., 2007. Evaluating hypotheses for the origin of eukaryotes. Bioessays. 29, 74-84.

Poot, M., Zhang, Y. Z., Kramer, J. A., Wells, K. S., Jones, L. J., Hanzel, D. K., Lugade, A. G., Singer, V. L. and Haugland, R. P., 1996. Analysis of mitochondrial morphology and function with novel fixable fluorescent stains. J Histochem Cytochem. 44, 1363-1372.

Pope, S., Land, J. M. and Heales, S. J., 2008. Oxidative stress and mitochondrial dysfunction in neurodegeneration; cardiolipin a critical target? Biochim Biophys Acta. 1777, 794-799.

Raff, M. C., Barres, B. A., Burne, J. F., Coles, H. S., Ishizaki, Y. and Jacobson, M. D., 1993. Programmed cell death and the control of cell survival: Lessons from the nervous system. Science. 262, 695-700.

Reichmann, H. and Wildenauer, D., 1991. Quantitative succinate dehydrogenase analysis in normal and ragged-red muscle fibers. Histochemistry. 96, 251-253.

Reznick, R. M. and Shulman, G. I., 2006. The role of AMP-activated protein kinase in mitochondrial biogenesis. J Physiol. 574, 33-39.

Richardson, B. E. and Durham, D., 1990. Blood flow changes in chicken brain stem auditory nuclei following cochlea removal. Hearing Res. 46, 53-62.

Rimessi, A., Giorgi, C., Pinton, P. and Rizzuto, R., 2008. The versatility of mitochondrial calcium signals: from stimulation of cell metabolism to induction of cell death. Biochim Biophys Acta. 1777, 808-816.

Rivner, M. H., Shamsnia, M., Swift, T. R., Trefz, J., Roesel, R. A., Carter, A. L., Yanamura, W. and Hommes, F. A., 1989. Kearns-Sayre syndrome and complex II deficiency. Neurology. 39, 693-696.

Rizzuto, R., Pinton, P., Carrington, W., Fay, F. S., Fogarty, K. E., Lifshitz, L. M., Tuft, R. A. and Pozzan, T., 1998. Close contacts with the endoplasmic reticulum as determinants of mitochondrial Ca2+ responses. Science. 280, 1763-1766.

Rizzuto, R., Pinton, P., Ferrari, D., Chami, M., Szabadkai, G., Magalhaes, P. J., Di Virgilio, F. and Pozzan, T., 2003. Calcium and apoptosis: facts and hypotheses. Oncogene. 22, 8619-8627.

Roberts, E., Charboneau, L., Espina, V., Liotta, L., Petricoin, E. and Dreher, K., 2004. Application of Laser Capture Microdissection and Protein Microarray Technologies in the Molecular Analysis of Airway Injury Following Pollution Particulate Exposure. Journal of Toxicology and Environmental Health, Part A. 67, 851-861.

Roth, K. A., Kuan, C., Haydar, T. F., D'Sa-Eipper, C., Shindler, K. S., Zheng, T. S., Kuida, K., Flavell, R. A. and Rakic, P., 2000. Epistatic and independent functions of caspase-3 and Bcl-X(L) in developmental programmed cell death. Proc Natl Acad Sci U S A. 97, 466-471.

Rubel, E. W., Falk, P. M., Canady, K. S. and Steward, O., 1991. A cellular mechanism underlying activity-dependent transneuronal degeneration:

Rapid but reversible destruction of neuronal ribosomes. Brain Dysfunction. 4, 55-74.

Rubel, E. W. and Fritzsch, B., 2002. Auditory system development: primary auditory neurons and their targets. Annu Rev Neurosci. 25, 51-101.

Rubel, E. W., Hyson, R. L. and Durham, D., 1990. Afferent regulation of neurons in the brain stem auditory system. J Neurobiol. 21, 169-196.

Rubel, E. W. and Parks, T. N., 1975. Organization and development of brain stem auditory nuclei of the chicken: Tonotopic organization of N. magnocellularis and N. laminaris. JCompNeurol. 164, 411-434.

Rubel, E. W. and Parks, T. N., 1988. Organization and development of the avian brain-stem auditory system. In: Edelman, G. M. et al. (Eds.), Auditory Function. John Wiley and Sons, New York, pp. 3-92.

Ryals, B. M. and Rubel, E. W., 1982. Patterns of hair cell loss in chick basilar papilla after intense auditory stimulation: Frequency organization. Acta Otolaryngol. 93, 205-210.

Ryals, B. M. and Rubel, E. W., 1988. Hair cell regeneration after acoustic trauma in adult coturnix quail. Science. 240, 1774-1776.

Ryals, B. M., Stalford, M. D., Lambert, P. R. and Westbrook, E. W., 1995. Recovery of noise-induced changes in the dark cells of the quail tegmentum vasculosum. Hearing Res. 83, 51-61.

Safieddine, S. and Wenthold, R. J., 1997. The glutamate receptor subunit delta1 is highly expressed in hair cells of the auditory and vestibular systems. J Neurosci. 17, 7523-7531.

Saiki, T., Kawai, T., Morita, K., Ohta, M., Saito, T., Rokutan, K. and Ban, N., 2008. Identification of marker genes for differential diagnosis of chronic fatigue syndrome. Mol Med. 14, 599-607.

Sakahira, H., Enari, M. and Nagata, S., 1998. Cleavage of CAD inhibitor in CAD activation and DNA degradation during apoptosis. Nature. 391, 96-99.

Samejima, K., Tone, S., Kottke, T. J., Enari, M., Sakahira, H., Cooke, C. A., Durrieu, F., Martins, L. M., Nagata, S., Kaufmann, S. H. and Earnshaw, W. C., 1998. Transition from caspase-dependent to caspase-independent mechanisms at the onset of apoptotic execution. J Cell Biol. 143, 225-239.

Sander, T., Hildmann, T., Kretz, R., Furst, R., Sailer, U., Bauer, G., Schmitz, B., Beck-Mannagetta, G., Wienker, T. F. and Janz, D., 1997. Allelic association of juvenile absence epilepsy with a GluR5 kainate receptor gene (GRIK1) polymorphism. Am J Med Genet. 74, 416-421.

Saraste, M., 1999. Oxidative phosphorylation at the fin de siecle. Science. 283, 1488-1493.

Saunders, J. C., Adler, H. J. and Pugliano, F. A., 1992. The structural and functional aspects of hair cell regeneration in the chick as a result of exposure to intense sound. ExpNeurol. 115, 13-17.

Scheffler, I. E., 2001. Mitochondria make a come back. Adv Drug Deliv Rev. 49, 3-26.

Schinder, A. F., Olson, E. C., Spitzer, N. C. and Montal, M., 1996. Mitochondrial dysfunction is a primary event in glutamate neurotoxicity. JNeurosci. 16, 6125-6133.

Schroeder, A., Mueller, O., Stocker, S., Salowsky, R., Leiber, M., Gassmann, M., Lightfoot, S., Menzel, W., Granzow, M. and Ragg, T., 2006. The RIN: an RNA integrity number for assigning integrity values to RNA measurements. BMC Mol Biol. 7, 3.

Schutze, K., Becker, I., Becker, K. F., Thalhammer, S., Stark, R., Heckl, W. M., Bohm, M. and Posl, H., 1997. Cut out or poke in--the key to the world of single genes: laser micromanipulation as a valuable tool on the look-out for the origin of disease. Genet Anal. 14, 1-8.

Schutze, K., Posl, H. and Lahr, G., 1998. Laser micromanipulation systems as universal tools in cellular and molecular biology and in medicine. Cell Mol Biol (Noisy-le-grand). 44, 735-746.

Scorrano, L., Oakes, S. A., Opferman, J. T., Cheng, E. H., Sorcinelli, M. D., Pozzan, T. and Korsmeyer, S. J., 2003. BAX and BAK regulation of

endoplasmic reticulum Ca2+: a control point for apoptosis. Science. 300, 135-139.

Sekido, R. and Lovell-Badge, R., 2007. Mechanisms of gonadal morphogenesis are not conserved between chick and mouse. Dev Biol. 302, 132-142.

Shibata, H., Joo, A., Fujii, Y., Tani, A., Makino, C., Hirata, N., Kikuta, R., Ninomiya, H., Tashiro, N. and Fukumaki, Y., 2001. Association study of polymorphisms in the GluR5 kainate receptor gene (GRIK1) with schizophrenia. Psychiatr Genet. 11, 139-144.

Shiva, S. and Darley-Usmar, V. M., 2003. Control of the nitric oxide-cytochrome c oxidase signaling pathway under pathological and physiological conditions. IUBMB Life. 55, 585-590.

Slee, E. A., Harte, M. T., Kluck, R. M., Wolf, B. B., Casiano, C. A., Newmeyer, D. D., Wang, H. G., Reed, J. C., Nicholson, D. W., Alnemri, E. S., Green, D. R. and Martin, S. J., 1999. Ordering the cytochrome c-initiated caspase cascade: hierarchical activation of caspases-2, -3, -6, -7, -8, and -10 in a caspase-9-dependent manner. J Cell Biol. 144, 281-292.

Smittkamp, S. E., Girod, D. A. and Durham, D., 2005. Role of cochlear integrity in cochlear nucleus glucose metabolism and neuron number after cochlea removal in aging broiler chickens. Hear Res. 204, 48-59.

Smittkamp, S. E., Park, D. L., Girod, D. A. and Durham, D., 2003. Effects of age and cochlear damage on the metabolic activity of the avian cochlear nucleus. Hear Res. 175, 101-111.

Someya, S., Yamasoba, T., Weindruch, R., Prolla, T. A. and Tanokura, M., 2006. Caloric restriction suppresses apoptotic cell death in the mammalian cochlea and leads to prevention of presbycusis. Neurobiol Aging.

Squire, L. R., Bloom, F. E., McConnell, S. K., Roberts, J. L., Spitzer, N. C. and Zigmond, M. J., 2003. Fundamental Neuroscience, Second Edition. 699-726.

Steel, K. P. and Kros, C. J., 2001. A genetic approach to understanding auditory function. Nat Genet. 27, 143-149.

Steward, O. and Rubel, E. W., 1985. Afferent influences on brain stem auditory nuclei of the chicken: cessation of amino acid incorporation as an antecedent to age-dependent transneuronal degeneration. J Comp Neurol. 231, 385-395.

Stewart, V. C. and Heales, S. J., 2003. Nitric oxide-induced mitochondrial dysfunction: implications for neurodegeneration. Free Radic Biol Med. 34, 287-303.

Stone, S. J. and Vance, J. E., 2000. Phosphatidylserine synthase-1 and -2 are localized to mitochondria-associated membranes. J Biol Chem. 275, 34534-34540.

Strehler, E. E. and Zacharias, D. A., 2001. Role of alternative splicing in generating isoform diversity among plasma membrane calcium pumps. Physiol Rev. 81, 21-50.

Stryer, L., 1995. Biochemistry Fourth Edition. 443-556.

Sun, X. M., MacFarlane, M., Zhuang, J., Wolf, B. B., Green, D. R. and Cohen, G. M., 1999. Distinct caspase cascades are initiated in receptor-mediated and chemical-induced apoptosis. J Biol Chem. 274, 5053-5060.

Susin, S. A., Lorenzo, H. K., Zamzami, N., Marzo, I., Snow, B. E., Brothers, G. M., Mangion, J., Jacotot, E., Costantini, P., Loeffler, M., Larochette, N., Goodlett, D. R., Aebersold, R., Siderovski, D. P., Penninger, J. M. and Kroemer, G., 1999. Molecular characterization of mitochondrial apoptosis-inducing factor. Nature. 397, 441-446.

Syka, J., 2002. Plastic changes in the central auditory system after hearing loss, restoration of function, and during learning. Physiol Rev. 82, 601-636.

Szabadkai, G. and Rizzuto, R., 2007. Chaperones as parts of organelle networks. Adv Exp Med Biol. 594, 64-77.

Takemoto-Kimura, S., Ageta-Ishihara, N., Nonaka, M., Adachi-Morishima, A., Mano, T., Okamura, M., Fujii, H., Fuse, T., Hoshino, M., Suzuki, S., Kojima, M., Mishina, M., Okuno, H. and Bito, H., 2007. Regulation of

dendritogenesis via a lipid-raft-associated Ca2+/calmodulin-dependent protein kinase CLICK-III/CaMKIgamma. Neuron. 54, 755-770.

Tang, Y. Z. and Carr, C. E., 2004. Development of NMDA R1 expression in chicken auditory brainstem. Hear Res. 191, 79-89.

Tang, Y. Z. and Carr, C. E., 2007. Development of N-methyl-D-aspartate receptor subunits in avian auditory brainstem. J Comp Neurol. 502, 400-413.

Taylor, R. W., Birch-Machin, M. A., Schaefer, J., Taylor, L., Shakir, R., Ackrell, B. A., Cochran, B., Bindoff, L. A., Jackson, M. J., Griffiths, P. and Turnbull, D. M., 1996. Deficiency of complex II of the mitochondrial respiratory chain in late-onset optic atrophy and ataxia. Ann Neurol. 39, 224-232.

Tempel, B. L. and Shilling, D. J., 2007. The plasma membrane calcium ATPase and disease. Subcell Biochem. 45, 365-383.

Torchinsky, C., Messana, E. P., Arsura, M. and Cotanche, D. A., 1999. Regulation of p27Kip1 during gentamicin mediated hair cell death. J Neurocytol. 28, 913-924.

Tovar, J., Leon-Avila, G., Sanchez, L. B., Sutak, R., Tachezy, J., van der Giezen, M., Hernandez, M., Muller, M. and Lucocq, J. M., 2003. Mitochondrial remnant organelles of Giardia function in iron-sulphur protein maturation. Nature. 426, 172-176.

Truman, J. W., 1984. Cell death in invertebrate nervous systems. AnnuRevNeurosci. 7, 171-188.

Turrens, J. F., 2003. Mitochondrial formation of reactive oxygen species. J Physiol. 552, 335-344.

Tzagoloff, A. and Myers, A. M., 1986. Genetics of mitochondrial biogenesis. AnnuRevBiochem. 55, 249-285.

van der Giezen, M. and Tovar, J., 2005. Degenerate mitochondria. EMBO Rep. 6, 525-530.

Vance, J. E., 1990. Phospholipid synthesis in a membrane fraction associated with mitochondria. J Biol Chem. 265, 7248-7256.

Vila, M. and Przedborski, S., 2003. Targeting programmed cell death in neurodegenerative diseases. Nat Rev Neurosci. 4, 365-375.

Vladutiu, G. D. and Heffner, R. R., 2000. Succinate dehydrogenase deficiency. Arch Pathol Lab Med. 124, 1755-1758.

Wadia, J. S., Chalmers-Redman, R. M. E., Ju, W. J. H., Carlile, G. W., Phillips, J. L., Fraser, A. D. and Tatton, W. G., 1998. Mitochondrial membrane potential and nuclear changes in apoptosis caused by serum and nerve growth factor withdrawal: Time course and modification by (-)-Deprenyl. JNeurosci. 18, 932-947.

White, R. J. and Reynolds, I. J., 1996. Mitochondrial depolarization in glutamate-stimulated neurons: An early signal specific to excitotoxin exposure. JNeurosci. 16, 5688-5697.

Whiteheart, S. W. and Matveeva, E. A., 2004. Multiple binding proteins suggest diverse functions for the N-ethylmaleimide sensitive factor. J Struct Biol. 146, 32-43.

Wilkins, H. R., Presson, J. C., Popper, A. N., Ryals, B. M. and Dooling, R. J., 2001. Hair cell death in a hearing-deficient canary. J Assoc Res Otolaryngol. 2, 79-86.

Wilkinson, B. L., Elam, J. S., Fadool, D. A. and Hyson, R. L., 2003. Afferent regulation of cytochrome-c and active caspase-9 in the avian cochlear nucleus. Neuroscience. 120, 1071-1079.

Wilkinson, B. L., Sadler, K. A. and Hyson, R. L., 2002. Rapid deafferentation-induced upregulation of bcl-2 mRNA in the chick cochlear nucleus. Brain Res Mol Brain Res. 99, 67-74.

Woo, M., Hakem, R., Soengas, M. S., Duncan, G. S., Shahinian, A., Kagi, D., Hakem, A., McCurrach, M., Khoo, W., Kaufman, S. A., Senaldi, G., Howard, T., Lowe, S. W. and Mak, T. W., 1998. Essential contribution of caspase 3/CPP32 to apoptosis and its associated nuclear changes. Genes Dev. 12, 806-819.

Wong-Riley, M., 1979. Changes in the visual system of monocularly sutured or enucleated cats demonstrable with cytochrome oxidase histochemistry. Brain Res. 171, 11-28.

Wong-Riley, M. T. T., 1989. Cytochrome oxidase: An endogenous metabolic marker for neuronal activity. TINS. 12, 94-101.

Wong-Riley, M., Tripathi, S. C., Trusk, T. C. and Hoppe, D. A., 1989. Effect of retinal impulse blockage on cytochrome oxidase-rich zones in the macaque striate cortex: I. Quantitative electron-microscopic (EM) analysis of neurons. VisNeurosci. 2, 483-497.

Wong-Riley, M. T. T., Walsh, S. M., Leake-Jones, P. A. and Merzenich, M. M., 1981. Maintenance of neuronal activity by electrical stimulation of unilaterally deafened cats demonstrable with cytochrome oxidase technique. AnnOtol. 90, Supp.82, 30-32.

Wyllie, A. H., Kerr, J. F. and Currie, A. R., 1980. Cell death: the significance of apoptosis. Int Rev Cytol. 68, 251-306.

Xiang, J., Chao, D. T. and Korsmeyer, S. J., 1996. BAX-induced cell death may not require interleukin 1B-converting enzyme-like proteases. ProcNatlAcadSciUSA. 93, 14559-14563.

Yuan, J. and Horvitz, H. R., 1990. The caenorhabditis elegans genes ced-3 and ced-4 act cell autonomously to cause programmed cell death. DevBiol. 138, 33-41.

Yuan, J. and Yankner, B. A., 2000. Apoptosis in the nervous system. Nature. 407, 802-809.

Zeviani, M., 2004. Mitochondrial disorders. Suppl Clin Neurophysiol. 57, 304-312.

Zhou, N. and Parks, T. N., 1992a. Developmental changes in the effects of drugs acting at NMDA or non-NMDA receptors on synaptic

transmission in the chick cochlear nucleus (nuc. magnocellularis). DevBrRes. 67, 145-152.

Zhou, N. and Parks, T. N., 1992b. Y-D-glutamylaminomethyl sulfonic acid (GAMS) distinguishes subtypes of glutamate receptor in the chick cochlear nucleus (nuc. magnocellularis). Hearing Res. 60, 20-26.

Zhang, A., Wu, Y., Lai, H. W. L. and Yew, D. T., 2004. Apoptosis-A Brief Review. Neuroembryology. 5, 47-59.

Zirpel, L., Janowiak, M. A., Taylor, D. A. and Parks, T. N., 2000a. Developmental changes in metabotropic glutamate receptor-mediated calcium homeostasis. J Comp Neurol. 421, 95-106.

Zirpel, L., Janowiak, M. A., Veltri, C. A. and Parks, T. N., 2000b. AMPA receptor-mediated, calcium-dependent CREB phosphorylation in a subpopulation of auditory neurons surviving activity deprivation. J Neurosci. 20, 6267-6275.

Zirpel, L., Lachica, E. A. and Lippe, W. R., 1995. Deafferentation increases the intracellular calcium of cochlear nucleus neurons in the embryonic chick. J Neurophysiol. 74, 1355-1357.

Zirpel, L., Lippe, W. R. and Rubel, E. W., 1998. Activity-dependent regulation of [Ca2+]i in avian cochlear nucleus neurons: Roles of protein kinases A and C and relation to cell death. JNeurophysiol. 79, 2288-2302.

Zirpel, L., Nathanson, N. M., Rubel, E. W. and Hyson, R. L., 1994. Glutamate-stimulated phosphotidylinositol metabolism in the avian cochlear nucleus. NeurosciLett. 168, 163-166.

Zirpel, L. and Rubel, E. W., 1996. Eighth nerve activity regulates intracellular calcium concentration of avian cochlear nucleus neurons via a metabotropic glutamate receptor. J Neurophysiol. 76, 4127-4139.